Science & Technology Facilities Council

Analysis of GOME-2 level-1b data quality and degradation effects on operational ozone profile retrievals

Visiting Scientist - Final Report

FINAL VERSION 1.2

Prepared by
Georgina Miles[1], Richard Siddans[1], Olaf Tuinder[2], Barry Latter[1]

[1]STFC
Rutherford Appleton Laboratory
Chilton, Didcot OX11 0QX, U.K.

[2]Royal Netherlands Meteorological Institute (KNMI)
Wilhelminalaan 10
NL-3732 GK De Bilt
Netherlands

O3MSAF VS/AS project

19 November 2012

Contents

1 Introduction....4
2 OPERA Band 1 Offset....5
2.1 OPERA Band 1 Offset dependencies....5
2.1.1 Analogy to RAL algorithm retrieval of leakage current....10
3 Scan angle dependence in retrieved ozone for RAL and OPERA schemes....11
3.1.1 Global comparison of tropospheric ozone....12
3.1.2 Zonal Mean comparison of ozone profiles....14
3.1.3 Sonde Comparisons....16
3.2 OPERA and RAL spectral fit residuals....18
3.2.1 RAL fit residual trends....19
3.2.2 OPERA fit residual trends....22
4 Prototype Algorithms from RAL Ozone Profile Retrieval Scheme....27
4.1 Introduction....27
4.2 Slit function retrieval and Band 2 wavelength registration....27
4.3 Degradation Correction....30
4.4 GOME-2 Noise Model....34
5 Transfer of Prototype Modules....38
5.1 Slit Function Retrieval....38
5.1.1 Scan angle dependency of retrieved ozone profiles....41
5.2 Degradation Correction....42
5.2.1 Scan angle dependency of retrieved ozone profiles....43
5.3 GOME-2 Noise Model....44
5.3.1 Scan angle dependency of retrieved ozone profiles....46
5.4 Raman scattering....46
5.4.1 Scan angle dependency of fit residuals and retrieved profiles....49
5.5 Relative impact of prototype modules....50
5.6 Further work to be considered....53
6 Assessment of potential for GOME-2 Chappuis band observations to provide improved tropospheric ozone retrievals....53
6.1 Introduction....53
6.2 Modelling surface reflectance....55
6.3 Retrieval simulations....55
6.4 Real retrievals....59
6.5 Conclusions....73
6.6 Suggestions for further work....73
7 References....74

1 Introduction

Within the framework of the O3MSAF, KNMI produces vertical ozone profiles from Metop (A) data in an operational context for dissemination to end users in Near Real Time (NRT). The scheme used by KNMI is called OPERA, and uses the contiguous wavelength range 265-330 nm (comprising data from GOME-2 bands 1a, 1b and 2b). The scheme fits observed sun-normalised radiances across this entire spectral range to retrieve the ozone profile using the optimal estimation method (OEM).

Over the past 15 years, RAL has developed a distinctly different OEM scheme to retrieve ozone profiles from GOME-1 data [Munro et al., 1998], which has now been adapted for GOME-2, via UK national funding through NERC's National Centre for Earth Observation (NCEO). This was the only physically-based scheme with sensitivity to the troposphere at the time of the last major inter-comparison exercise [Meijer et al., 2006], based on the work of ESA's Ozone Profile Working Group. The RAL scheme has been applied to process all GOME-1 data from 1995 to 2002. The resulting data-set was assimilated in the ECMWF *ERA-40 interim* reanalysis. The scheme was also used as the basis for optimising the GOME-2 instrument and operation for ozone-profile retrieval via the EUMETSAT GOME-2 Error study and its extension [Kerridge 2004].

The scheme differs from KNMI's OPERA scheme in a number of important respects. Most notably, it operates in two steps. First, sun-normalised radiances from 265-307nm are fitted in a manner quite similar to that of OPERA. The resulting ozone profile is then input (as *a priori* information) to a fit of the differential absorption spectrum between 323 and 334nm (formed by taking the logarithm of the sun-normalised radiances and subtracting a low-order polynomial). This allows detailed, temperature-dependent, spectral structure in the Huggins bands to be fitted to a precision close to the photometric noise, a prerequisite for retrieving information on tropospheric ozone.

The ozone profile is the only GOME-2 product that uses wavelengths <310nm. The ozone column and other trace gas columns all use wavelengths >310nm. Furthermore, accurate ozone profiles require very good absolute calibration of the sun-normalised radiances, whereas trace-gas columns (based on DOAS technique) are relatively immune to radiometric calibration errors which vary slowly with wavelength. Since radiances in the relevant spectral range are actually *controlled by the ozone profile*, it is difficult to establish the in-flight spectro-radiometric accuracy other than by application of an ozone profile scheme followed by geophysical validation of the resulting products. Subsequent diagnosis of the character of errors in Level 1 data (and their variation with time) can then be attempted but is far from straightforward. For these reasons, it is expected that the operational scheme can benefit from comparison of OPERA with an independent algorithm (RAL) applied to the common spectral range.

RAL has analysed several GOME-2 ozone profile issues, results of which have been reported at recent Eumetsat conferences, GSAG and at an expert meeting on level 1 issues in 2011. These include:

- Comparison, over a multi-year period, of measured sun-normalised radiances in *Band 1* to radiative transfer simulations based on an ozone climatology, and quantifying apparent across-track and time-dependent Level 1 errors.
- Investigation of fit residuals in *Band 2b*: substantial reductions have been achieved by using measured GOME-2 slit-functions, better wavelength calibration from improved direct-sun spectra, use of state-of-the art ozone absorption cross-sections and improvements to the rotational Raman scattering model.

- Identifying across-track dependent systematic fit residuals.
- Identification of problems with the model being used to estimate noise in band 2.

It is expected that the operational OPERA scheme would benefit from these and other on-going activities to improve the RAL profile scheme.

In this report, the implementation of three prototype modules from RAL the OPERA will be assessed in terms of their impact on both the optimal estimation fit residuals and the retrieved ozone profiles. It is begun with a short assessment of the geophysical dependencies of the offset that is retrieved in Band 1 within OPERA, with a description of the dark current fit which is performed as part of the RAL scheme in order to differentiate them. This is followed by the introduction and description of three RAL prototype modules which could potentially benefit the OPERA scheme. These modules are then individually introduced to OPERA, and their impact is assessed along with suggestions for next steps and further work. In the final part of this report, an assessment of the potential for GOME-2 measurements in the Chappuis bands is undertaken.

2 OPERA Band 1 Offset

OPERA fits an offset in Band 1 as a way to compensate for calibration errors which results in an improved fit of the GOME-2 measurements. This was originally implemented for GOME-1 but it was required for GOME-2 in the same manner when it became apparent that GOME-2 also suffered from degradation. The offset is expressed as a multiple of 1.0E9 photons, which is the 'native' unit of the radiance / irradiance in GOME-2 within OPERA. This offset changes with both time of year/mission and is spatially variable. To better understand the behaviour and dependencies of this offset, it is examined briefly here.

2.1 OPERA Band 1 Offset dependencies

The OPERA Band 1 offset has steadily increased with the lifetime of GOME-2 (on MetOP-A), and is strongly dependent upon latitude/solar zenith angle (SZA), as demonstrated in Figure 1. Its change with time, primarily reflecting the degradation in throughput of the instrument, in addition to an example of its spatial variability is apparent in Figure 2 which shows a map of the Band 1 offset on 25th March 2007. This may be contrasted with the same day in 2010 (Figure 3) when the offset has increased significantly.

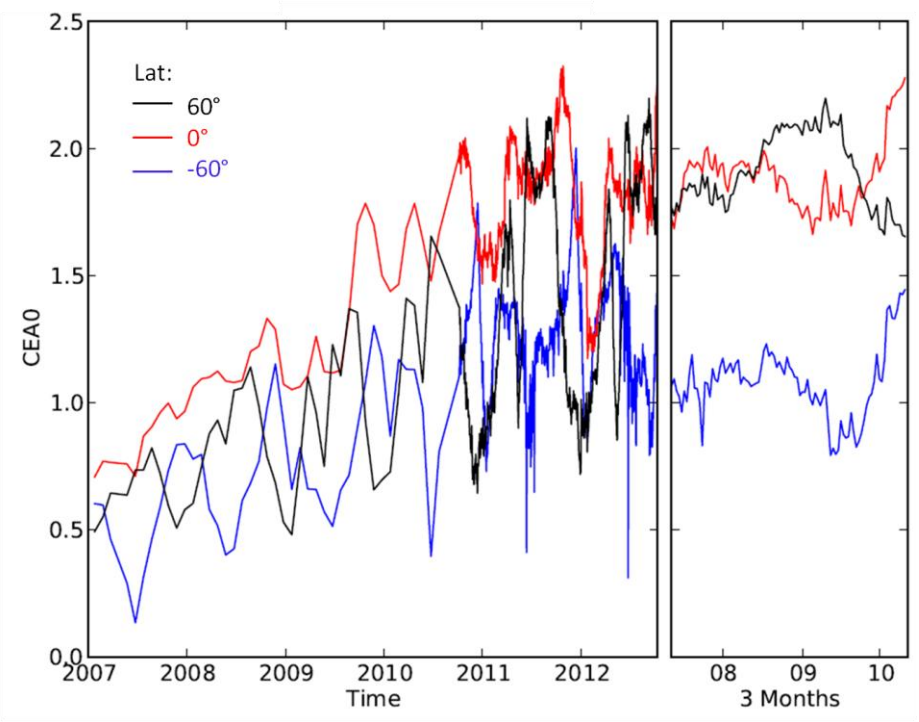

Figure 1: Zonal mean retrieved Band 1 offset (CEA0) from OPERA with time at 3 latitudes. The offset shows a strong solar zenith angle dependence evident and strong seasonal dependence outside the tropics for which the Northern and Southern hemisphere are in anti-phase. Overall the Band 1 offset fit at all latitudes has increased during the lifetime of GOME-2.

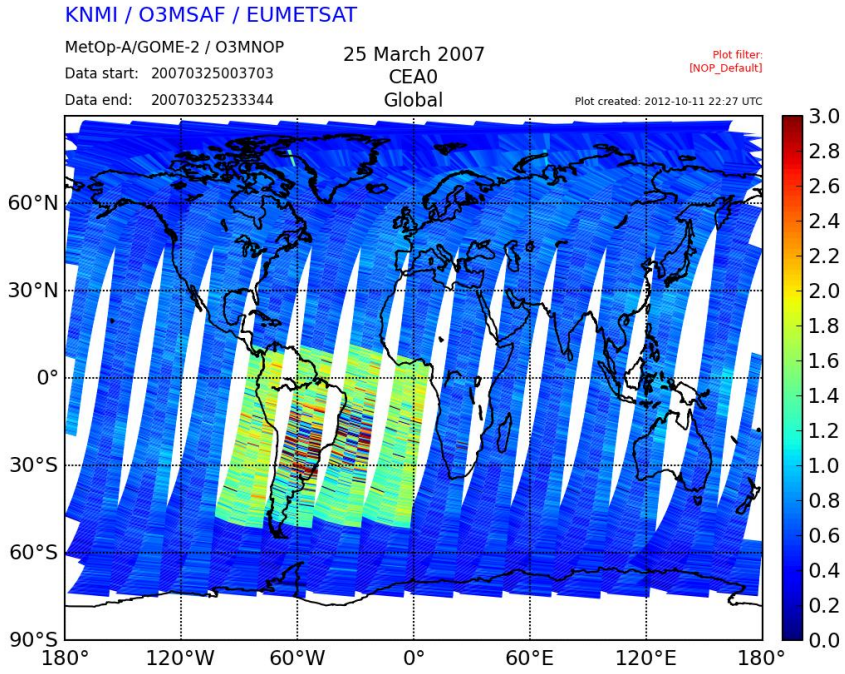

Figure 2: OPERA Retrieved Band 1 offset on 25th March 2007 for the coarse resolution retrieval

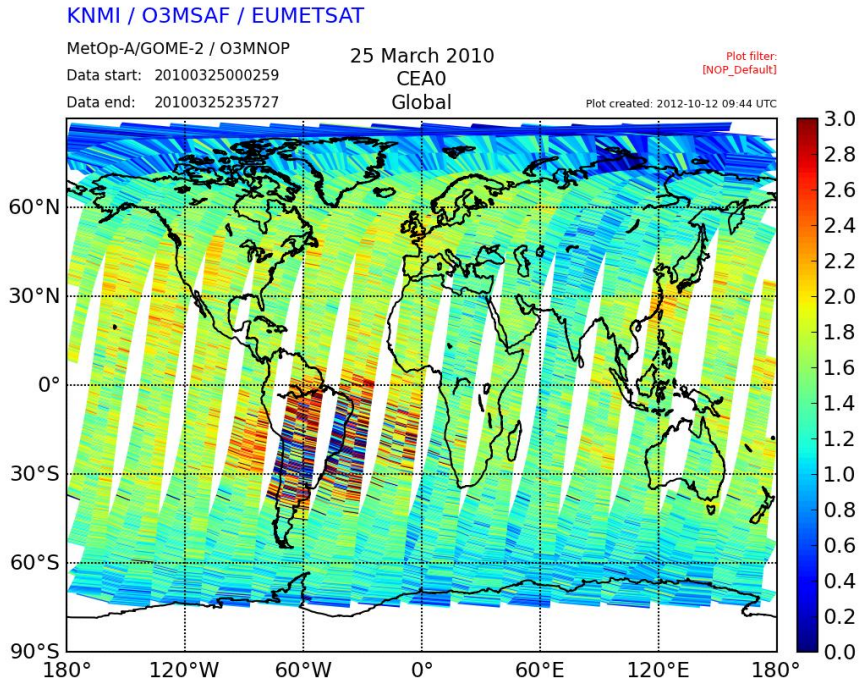

Figure 3: OPERA Retrieved Band 1 Offset on 25th March 2010

It is apparent that the Band 1 offset accounts for a number of measurement or instrument related factors, including the degradation of the instrument but also the leakage current if there are deficiencies in the predicted dark current noise calibration in the Level 1b (Lv1b) measurement. Figure 4 and Figure 5 show the relationship between the OPERA Band 1 offset and a number of geophysical and scene-dependent parameters on 25th March 2008, taken as a specimen date. Some attempt has been made to exclude data from the South Atlantic Anomaly region by screening geographically. The most robust relationship is apparent with SZA, although as implied by Figure 1 this is seasonally dependent. There is a strong relationship between the geometric air mass factor (defined as $\mathrm{AMF_g} = \sec\theta_{LZA} + \sec\theta_{SZA}$ where LZA denotes line-of-sight viewing angle). Both of these relationships show more spread with time as the Band 1 offset increases, as shown in Figure 6, and reflect the fact that the offset becomes considerably noisier. Whilst there is little correlation with cloud parameters in 2007, it increases for both cloud top pressure and cloud fraction until it dominates over solar zenith angle in 2010, which is reflected in the spatial distribution in Figure 3.

Overall it is related to both scene brightness and geometric path length, but scrupulous separation of cloud free and cloudy pixels is required to diagnose its character further. The offset is typically higher in the east pixel than the nadir and west, and in 2010 the offset in the west pixel is higher than both the east and nadir, as shown in Figure 5.

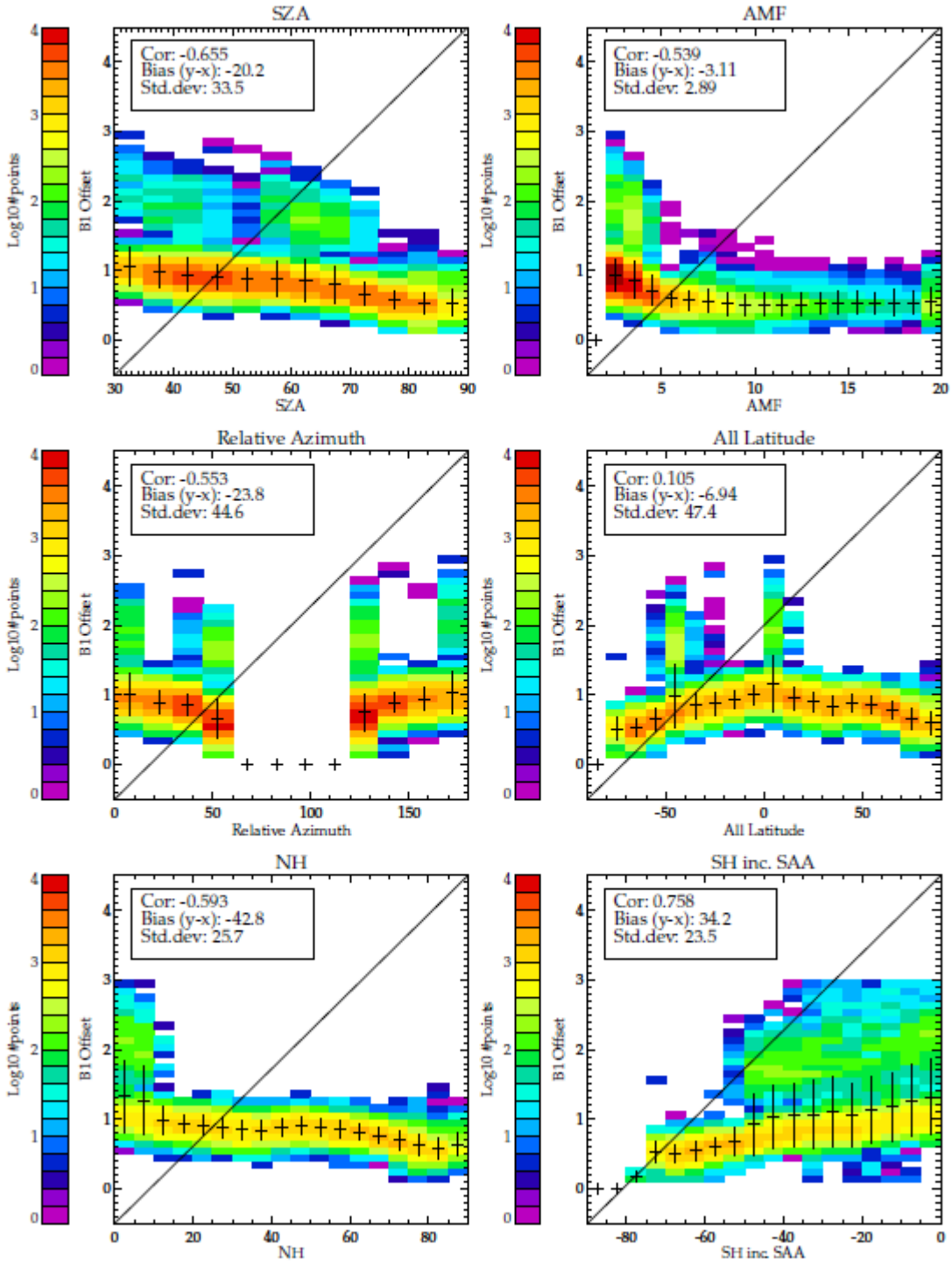

Figure 4: Correlation of OPERA Band 1 offset on 25th March 2008 with a variety of geophysical parameters. AMF denotes geometric air mass factor (see text for details). The clusters off the main sequence predominantly arise from pixels surrounding the South Atlantic Anomaly region, most of which has been screened out by latitude/longitude.

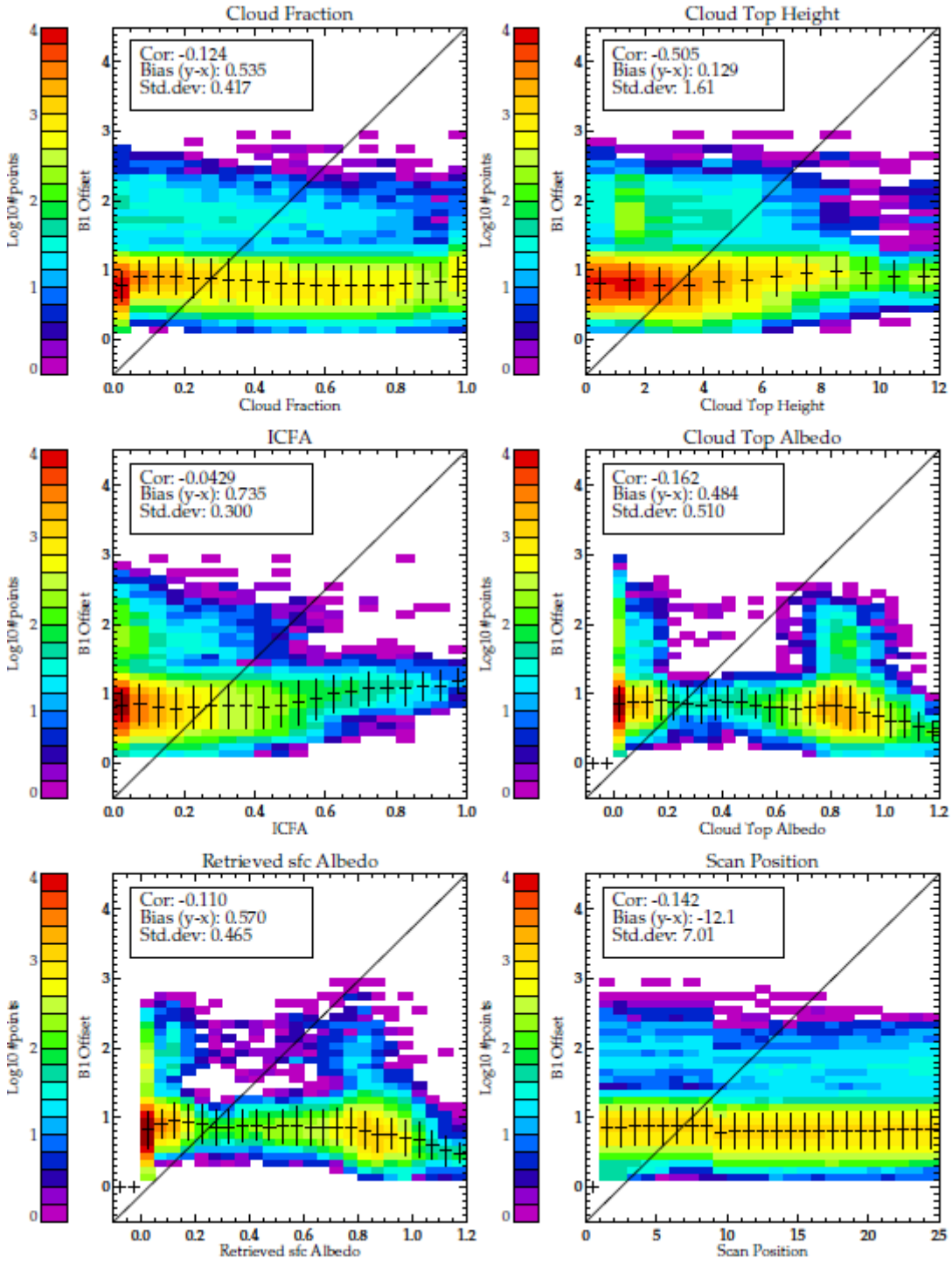

Figure 5: Correlation of OPERA Band 1 offset on 25th March 2008 with cloud fraction (top left), height-equivalent cloud top pressure (in km, top right), retrieved surface albedo (bottom left) and 'ICFA' is a combined cloud top pressure and cloud fraction quantity that weights the cloud fraction by its fractional height in the tropopause. The height is a pressure equivalent altitude assuming hydrostatics.

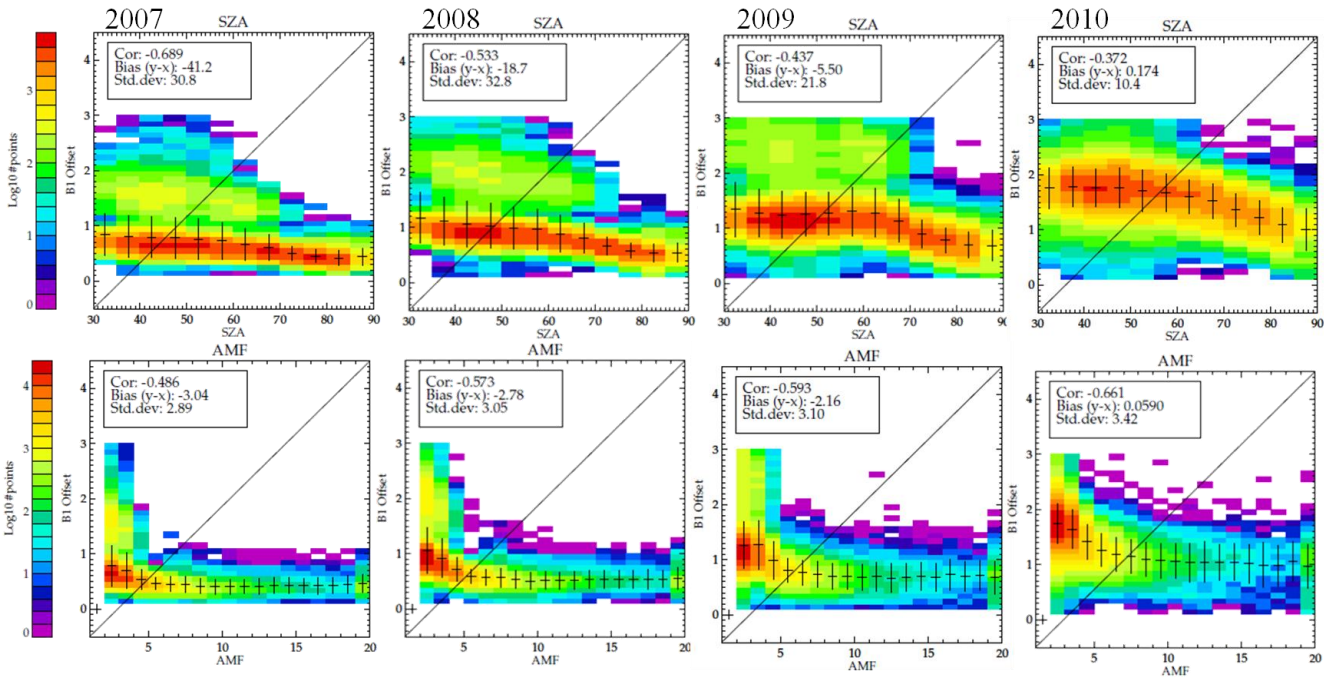

Figure 6: Correlation of OPERA Band 1 offset on 25th March 2008-2010 with SZA (top panels) and geometric Air Mass Factor (bottom panels). Highest correlation shown for SZA and geophysical AMF (dependent upon SZA), and this correlation becomes stronger with time.

2.1.1 Analogy to RAL algorithm retrieval of leakage current

The fit of dark/leakage current (the terms are used interchangeably) is performed within the RAL algorithm in the Band 1 retrieval, and is effectively an offset that is constant for the Band. This is unrelated to the degradation of the instrument, or the degradation correction derived for the RAL scheme.

The leakage current contributes to the noise estimate. The measurement noise is typically proportional to the square root of the total number of electrons recorded by the detector. The leakage current adds to this total, but is only significant when the signal is low. The RAL noise model estimates the number of electrons which have been detected from the calibrated radiance. This is approximate and assumes leakage current estimate was correct in the calibration.

This aspect of the leakage current relating to the noise characterisation is separate and distinct from that which is retrieved in the RAL scheme, which is necessary for the way in which the forward model is designed. In the Band 1 retrieval it is necessary to retrieve an estimate of the leakage or dark current component in order to subtract this from the measurement to achieve a fit in the forward model. The dark current is retrieved in binary units (BU) accounting for the integration time of the pixel. At this point the extraneous electrons that are estimated may arise from a number of sources. Uniform straylight is indistinguishable from the dark current and as a result of this fit its effects are somewhat mitigated. There may be a wavelength dependence to both of these components which will result in small errors where this is not accounted for. The detector pixels used for the Band 1 retrieval have been carefully selected to avoid the influence of Fraunhofer lines which are sensitive to inaccuracies in the estimate of the leakage, the Ring effect and absolute wavelength calibration. [Siddans, 2003] reports that the leakage current (for

GOME) was particularly variable with time (for example due to the influence of the on-board peltier cooler) and contains further discussion of the leakage current fit in the RAL algorithm.

As the OPERA Band 1 offset conflates degradation (a gain term) with leakage-type term, it is not trivial to compare RAL leakage/degradation with it. As opposed to the relationships of the Band 1 offset in the OPERA scheme with geophysical parameters shown, the RAL leakage current shows little correlation with any geophysical or retrieved parameters.

3 Scan angle dependence in retrieved ozone for RAL and OPERA schemes

A scan angle dependence of Level 2 products from GOME-2 has been reported in various forums. It is also evident to varying degrees in the summary plots provided by TEMIS (http://temis.nl/) which report operationally retrieved GOME-2 products.

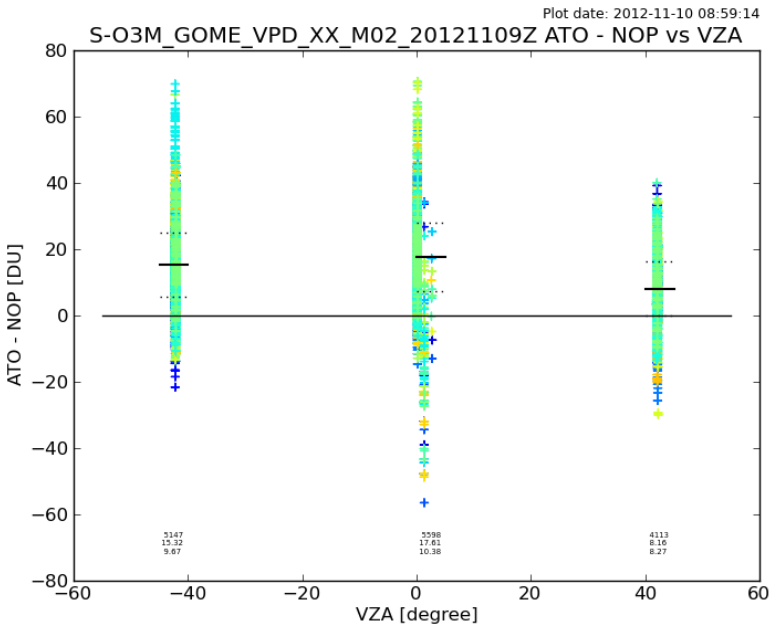

Figure 7: OPERA retrieved total column ozone differenced from assimilated total column ozone product by DLR (http://temis.nl/o3profiles/vpd/gome2/daily/images/)

Figure 7 shows an example of retrieved total ozone column grouped by the east, nadir and west pixels differenced from an assimilated GOME-2 total ozone product derived via a DOAS method [Eskes et al, 2003]. The west pixel typically shows best agreement with this product.

3.1.1 Global comparison of tropospheric ozone

Both OPERA and the RAL ozone profile retrieval schemes characterise the stratospheric and total column ozone to a comparable accuracy. As such, the profiles of each are primarily discussed here in terms of their tropospheric and upper tropospheric/lower stratospheric (UTLS) estimates of ozone sub-columns, and gridded zonal mean profiles where appropriate.

Figure 8 and Figure 9 show a day of retrieved 0-6km ozone sub-column on 25th March 2007 to 2010 for OPERA and the RAL scheme respectively. Also plotted are the a priori sub-columns used in each of the retrievals. For both schemes the priors are very similar. They are both based on the latitude and seasonally dependent climatological profiles based on sondes provided by McPeters et al., (2007). Slight differences arise due to its implementation within the schemes in terms of method of interpolation temporal/spatial and conversion to sub-column layers or number density profiles as the schemes require. Where they differ considerably is in the prior covariance matrix. OPERA takes the standard deviation of the climatology and uses it to directly determine the prior uncertainty for each sub-column. This is typically a small number, particularly in the troposphere, which on the one hand results in very small retrieval errors in that region but on the other can be restrictive in terms of the ability of the retrieval to find a solution any further than this away from the prior. As such, real 'outlying' ozone profiles that occur due to variable atmospheric processes in the troposphere are typically not captured by OPERA, particularly in the lowest retrieval layers.

The RAL scheme sets a minimum prior error limit that is 100% in the troposphere, 30% in the lower stratosphere and 20% above this. Where the prior error as determined by the climatological information is smaller than this it reverts to the relative error limit depending upon the altitude of the retrieval level. A further difference is the precision to which Band 2 is fit in the RAL scheme in order to exploit as much of the tropospheric ozone signal as possible, but it would not be able to do this if the prior constraint were too strict. As such Figure 8 and Figure 9 demonstrate that the RAL scheme typically departs from the a priori significantly more than OPERA in this sub-column. The spatial patterns of tropospheric ozone which are not represented in the a priori but are captured by the RAL scheme have been shown to be robust in comparison with a number of chemistry transport models including TOMCAT [Richards et al., 2012] and MACC.

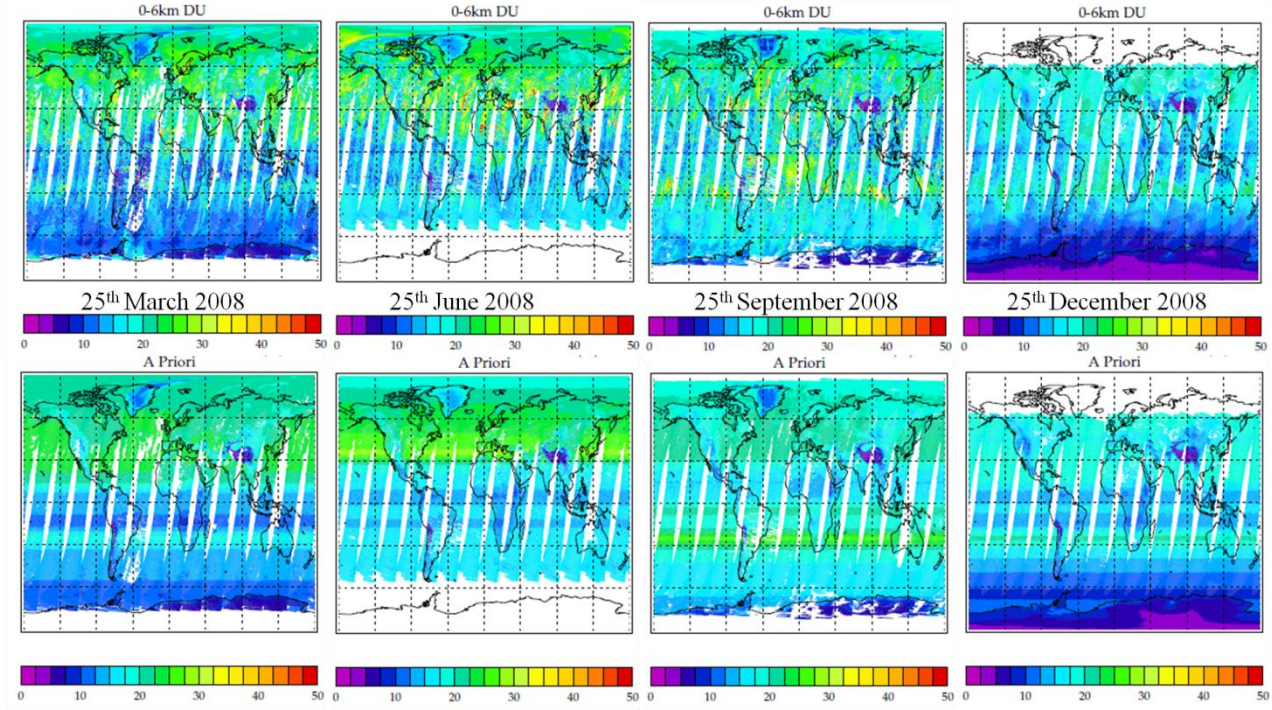

Figure 8: OPERA 0-6 km sub-column maps on 4 days in 2008 on 25th March, June, September and December (top), with the retrieval a priori sub-column given for reference on the bottom row. In this sub-column OPERA demonstrates only a modest departure from the prior.

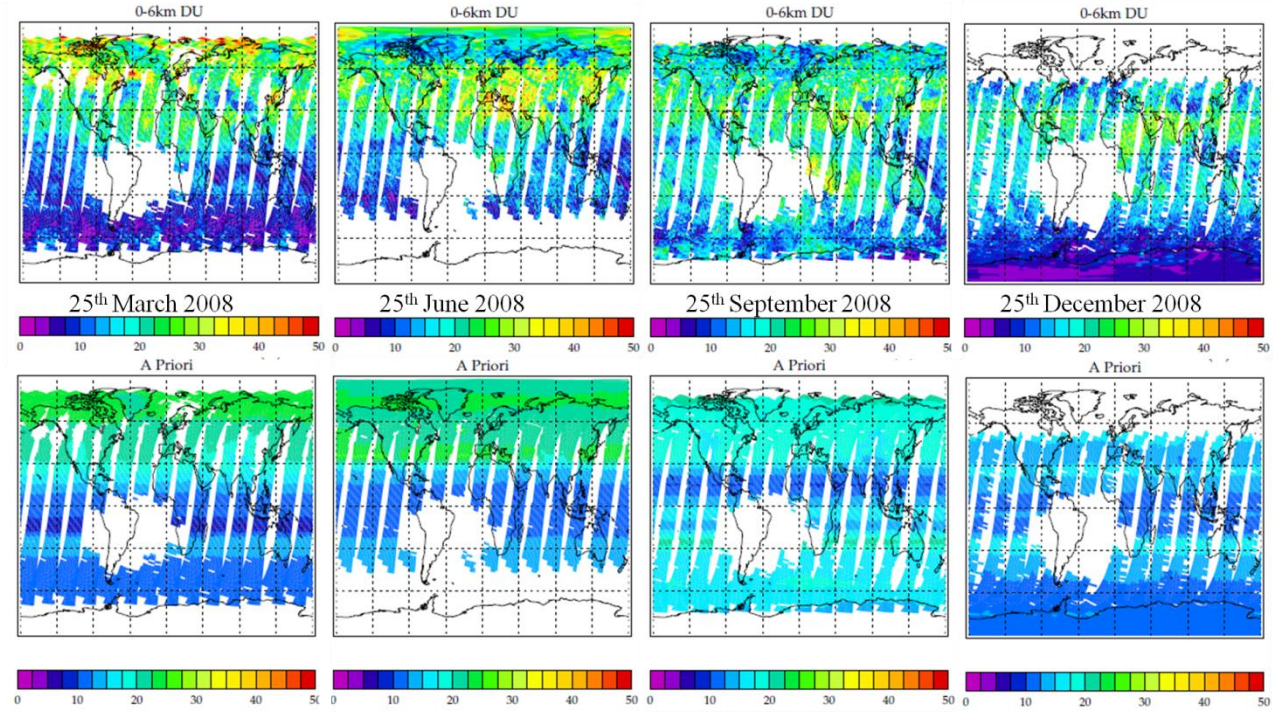

Figure 9: RAL 0-6 km sub-column maps on 4 days in 2008 on 25th March, June, September and December (top), with the retrieval a priori sub-column given for reference on the bottom row. In this sub-column the RAL scheme shows departure from the prior, showing regional enhancements in the Northern Hemisphere and lower ozone values over the tropical and south Pacific in Northern Hemisphere spring and summer.

3.1.2 Zonal Mean comparison of ozone profiles

Figure 10 shows the zonal mean profiles as retrieved by the OPERA scheme and the RAL scheme on their native vertical grids. They show very similar characteristics but in order to draw any meaningful conclusions the OPERA and RAL profiles are interpolated onto a common vertical grid, as in Figure 11.

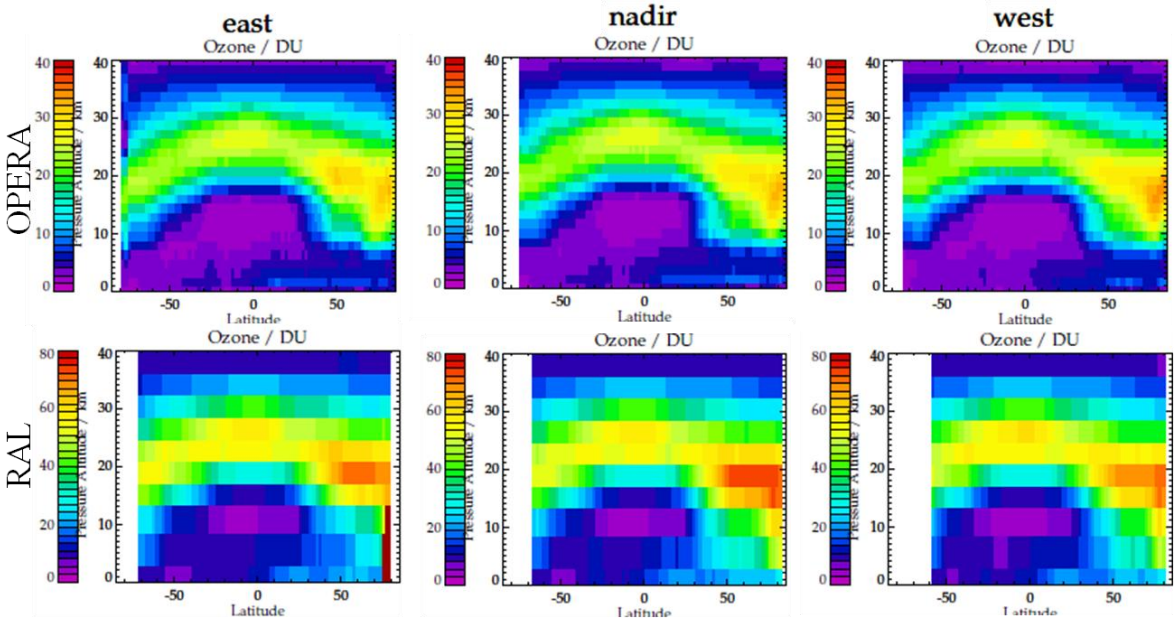

Figure 10: Zonal mean cross sections for OPERA and RAL scheme on 25th March 2008. Note the differing colour scale arising due to different sub-column layers depths used in the respective retrievals.

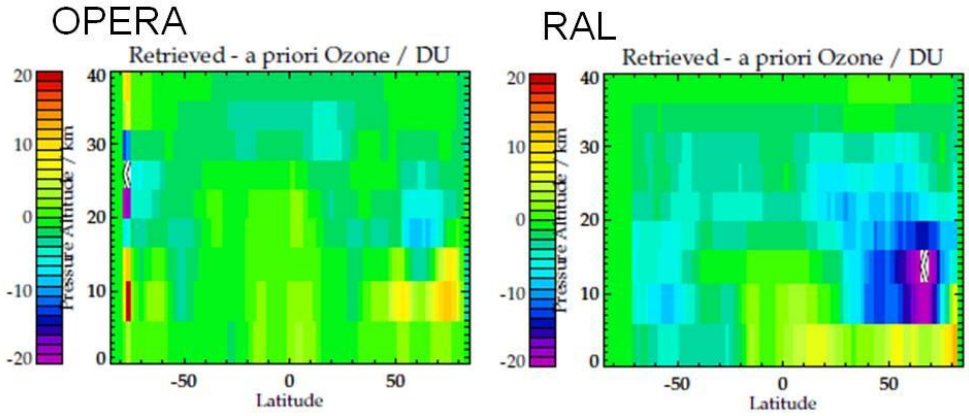

Figure 11: Zonal mean departure from a priori for OPERA and RAL scheme on 25th March 2008, for all pixels.

Figure 12 and Figure 13 show the difference in zonal mean ozone profiles as retrieved by OPERA and the RAL scheme for the 'east' and 'west' pixels with the nadir zonal mean subtracted on 4 days in 2008. East and west pixels as used here are defined as the 8 Band 2 pixel scan positions that are associated with each of the 3 across track Band 1a pixels. The OPERA ozone profiles have been interpolated onto a coarse vertical grid resembling that of the RAL scheme for the purposes of comparison. It is important to note

that the differences from the nadir for each scheme are not relative to each other. The RAL zonal mean demonstrates considerably more departure from the a priori in the troposphere and at other altitudes than the OPERA scheme, as indicated in Figure 12 and Figure 11.

Figure 12 and Figure 13 show that the difference in the zonal mean profiles as retrieved by the east and west pixels differ throughout the year. For both schemes the east and west differences from nadir are very similar in magnitude and meridional structure. On 25th March 2008 in the Northern Hemisphere mid to high latitudes both the RAL and OPERA schemes retrieve lower ozone in the UTLS region. In the west pixel the same effect occurs in the RAL scheme but OPERA retrieves higher ozone relative to the nadir pixels but the absolute difference is smaller. On this date and at this time of year the retrieval of ozone in this particular region of the atmosphere is potentially the most challenging of all circumstances. The total column ozone pole-ward of 50°N is frequently the highest observed both globally and annually at this time of year, and the solar zenith angle is relatively high. The GOME-2 has limited sensitivity to the UTLS region and the tropopause height is highly variable at this latitude and time of year. As such, these departures are not trivial to extricate in their dependence on either measurement factors or limitations of a forward model. That being said, there is a high degree of consistency in the structure of the zonal mean departure from the nadir retrievals for both schemes.

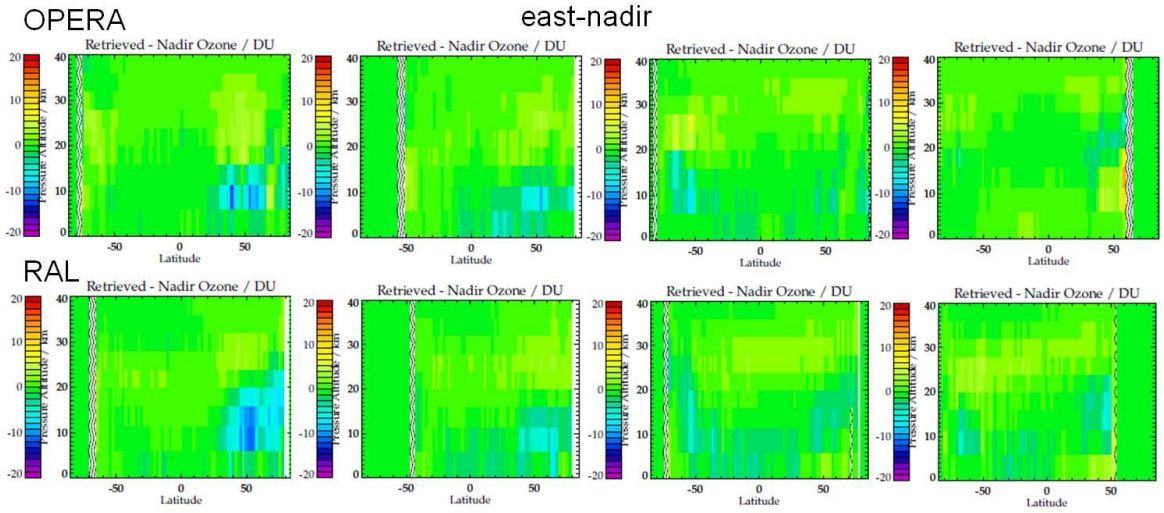

Figure 12: Zonal mean cross sections for OPERA and RAL scheme, Band 2 east and west minus nadir. The dates shown from left to right are 25th March, June, September and December 2008.

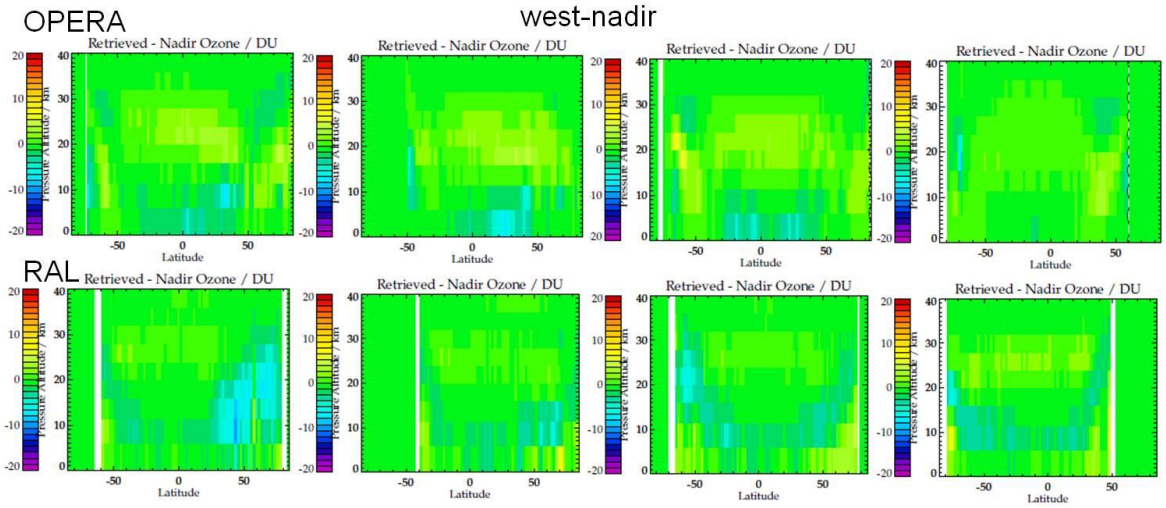

Figure 13: Zonal mean cross sections for OPERA and RAL scheme on 25th March 2008, Band 2 east and west minus nadir. The dates shown from left to right are 25th March, June, September and December 2008.

3.1.3 Sonde Comparisons

Both the OPERA and RAL schemes have been validated or compared with ozone sondes, and examples are shown in Figure 14 and Figure 15 for some tropospheric sub-columns. In general, for OPERA the 0-6km sub-column strongly resembles the prior, but has little scatter. The RAL scheme has a small positive bias with respect to sondes, but does depart from the prior. Comparisons with chemistry transport models indicate that the spatial distribution is well captured in the RAL scheme in this sub-column suggesting that the departures from the prior are real and a result of high precision fitting to the measurement [Richards et al., 2012]. Both schemes have a high degree of scatter with respect to the sonde the 6-12 km region, displaying poorer agreement with sondes than when considering the 0-6km and 0-12km sub-columns. There is a clear physical basis for this relating to both the strictness collocation criteria and the variability in tropopause height relative to the vertical sensitivity of the instrument in this part of the atmosphere. RAL has developed a GOME-2 plus IASI joint that demonstrates significant improvement in this region using the information from IASI which has complementary vertical sensitivity in the IR compared to that of the UV from GOME-2.

There is some indication that the sonde bias for both algorithms is different in the 8 east-most pixels than the nadir and west pixels, and that this difference in bias is more prominent at specific altitudes (namely the lower stratosphere), and this cross track bias changes slightly when averaging kernels are applied to sondes. However, there was not sufficient time to establish this to a level of statistical significance in this study, and so the scan angle dependence of the retrieved products is explored elsewhere in this report.

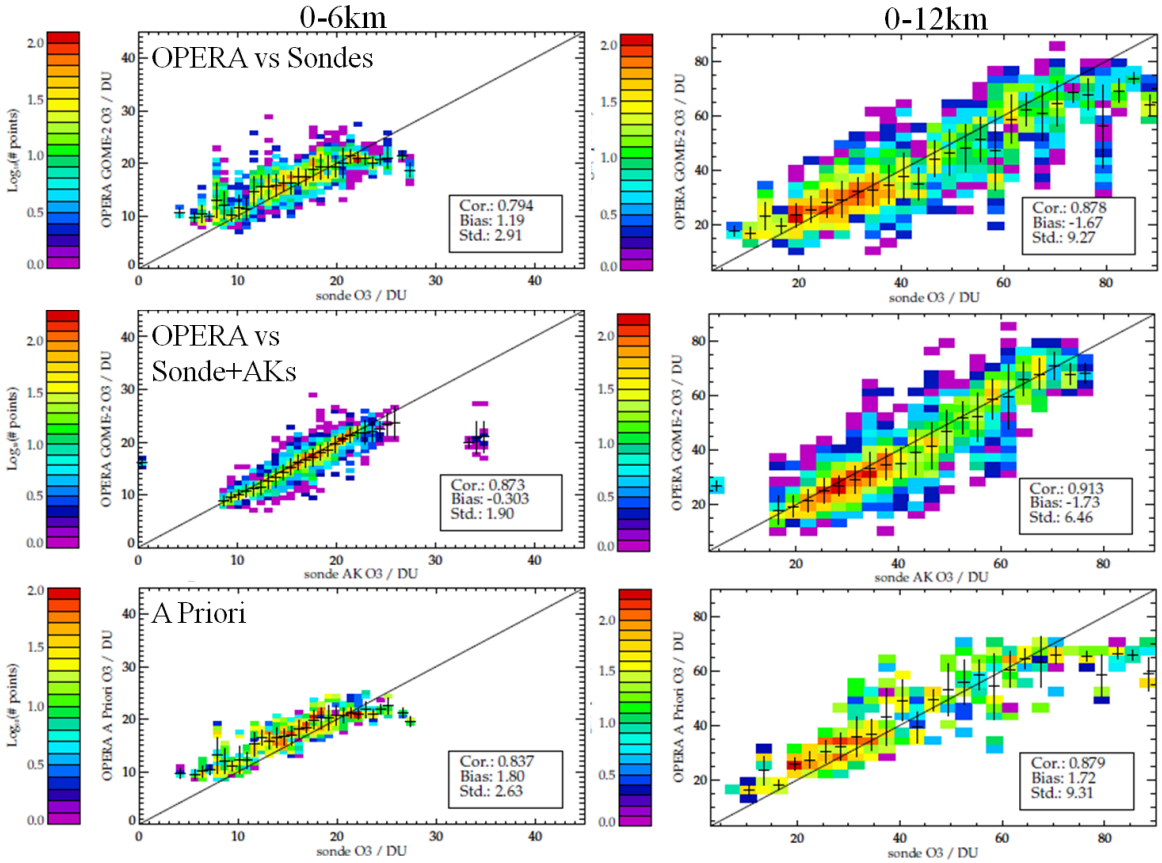

Figure 14: Sonde comparison with OPERA sub-columns for some coincident matches in 2008. The aberrant high sonde+AK values in the 0-6km sub-column sonde comparison are removed when the data is screened for high thick cloud. This is not shown because the screening removes a significant amount of data which lessens the significance of the comparison.

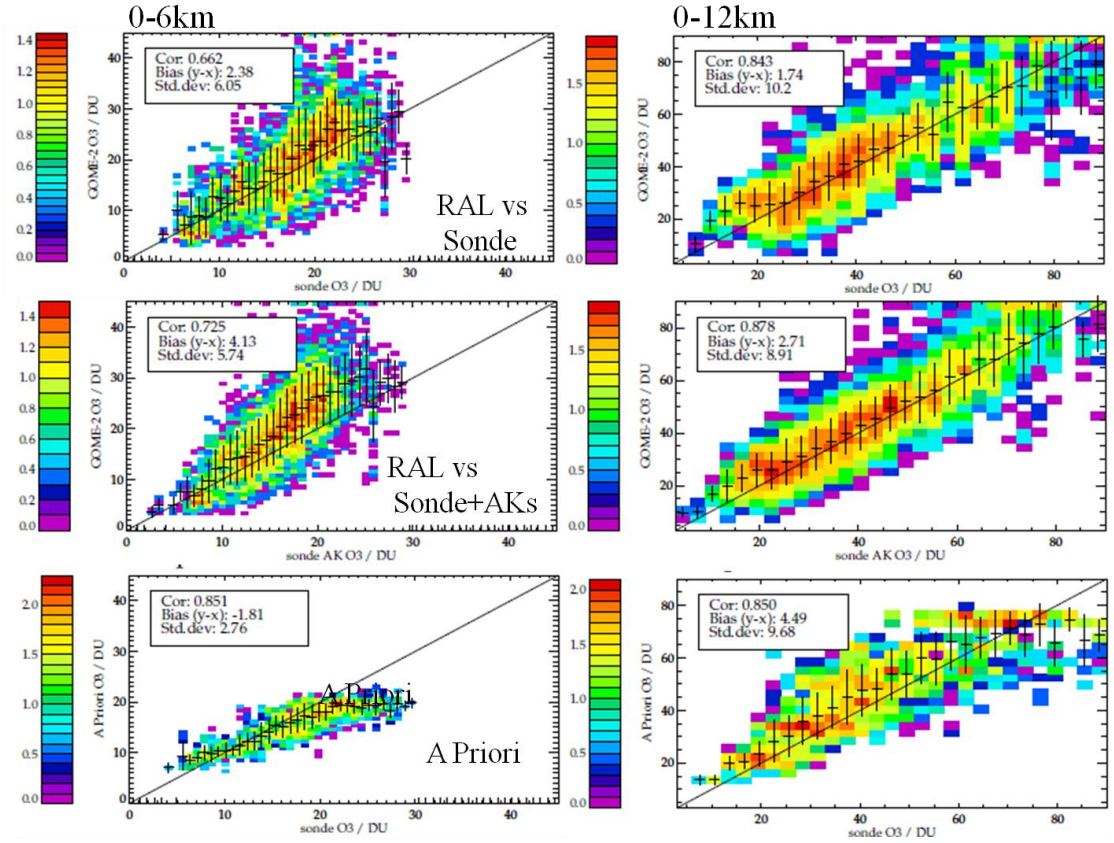

Figure 15: Sonde comparison with RAL sub-columns for some coincident matches in 2008. Correlation with sondes is improved when sondes are convolved with the averaging kernels.

3.2 OPERA and RAL spectral fit residuals

Fit residuals from both algorithms are here defined as the measurement (Y) minus the fit or simulated (F) sun normalised radiance at the point of retrieval convergence (Y-F). They are evaluated as daily means as a function of a selection of geophysical variables that can influence the quality of the fit, interpreted as how small the fit residuals are compared to either the measurement noise or more appropriately the standard deviation of the fit residuals. Mean residuals that are typically larger than the standard deviation indicate that the retrieval is potentially not fitting the measured spectrum to a precision that implies it is using all of the information available in the spectrum. It may also be interpreted as an indication that there are potential improvements that can be made to the forward model.

The OPERA and RAL mean residuals are considerably different, principally because the algorithms function in different ways. OPERA fits one contiguous spectral measurement in a joint retrieval of ozone profiles. RAL, a sequential joint retrieval first conducts a fit in Band 1 that forms a prior for later steps with the intension of characterising stratospheric ozone well before attempting to improve the tropospheric profile. It then performs a surface albedo fit in a small spectral region in Band 2 near to the Huggins ozone bands. Finally, a fit in Band 2 of the differential Huggins structure is performed. The last step of the retrieval includes the fit of the leading principle components of the mean residual which effectively removes them from the fit residual, and as such characteristically fits below the standard deviation of the fit residuals. This is a requirement of the scheme to enable it to exploit the information in the temperature dependent Huggins Bands in order

to retrieve information about tropospheric ozone, where the retrieval is relatively loosely constrained with regards to the *a priori* in comparison to OPERA.

The nature of the measurement noise was changed in later Level 0 to 1processing versions to resemble an estimate of the random noise more appropriate for optimal estimation retrievals. In the interim, RAL has developed a noise model based on the calibration keydata to estimate the random noise, which is commensurate to that provided by EUMETSAT in lv1b product format version 5.3 and above (after January 2012) [O. Tuinder, *Pers. Comm*.]. The impact of this noise model when used in the OPERA retrieval algorithm will be explored in Chapter 5.

In Band 1 both OPERA and the RAL scheme fit comfortably within the measurement noise and standard deviation of the respective fit residuals. This remains the case after the shift in wavelength separation of Band 1a/1b in late 2008 although the mean OPERA residual increases in the spectral region accordingly as shown in Figure 20. For OPERA only the high resolution (B2b pixel basis) fit residuals are assessed here, but they differ little from those from the coarse resolution. Other than examining trends with time, the date used for assessing trends of fit residuals with geophysical variables a specimen date of 25th March 2008, and 2008 is also the year chosen to illustrate the seasonal behaviour of the fit residuals. 2008 is a particularly favourable year for assessing character of the retrieval schemes since the degradation of GOME-2 is not significantly progressed.

Since the relative size of the fit residuals of the two algorithms are so different (particularly in band 2 where the fitting approaches differ significantly) it does not make sense to consider them jointly, and as such they are examined individually. The scales of the figures are selected to be appropriate for residuals from both schemes and are Band dependent.

3.2.1 RAL fit residual trends

Typical fit residuals in Band 1 and 2 from the RAL scheme are shown in Figure 16, as a function of solar zenith angle (SZA). The RAL retrieval does not use any measurement information between 306 and 323nm, or perform retrievals for pixels where the solar zenith angle is greater than 80° due to the relatively poor signal to noise ratio.

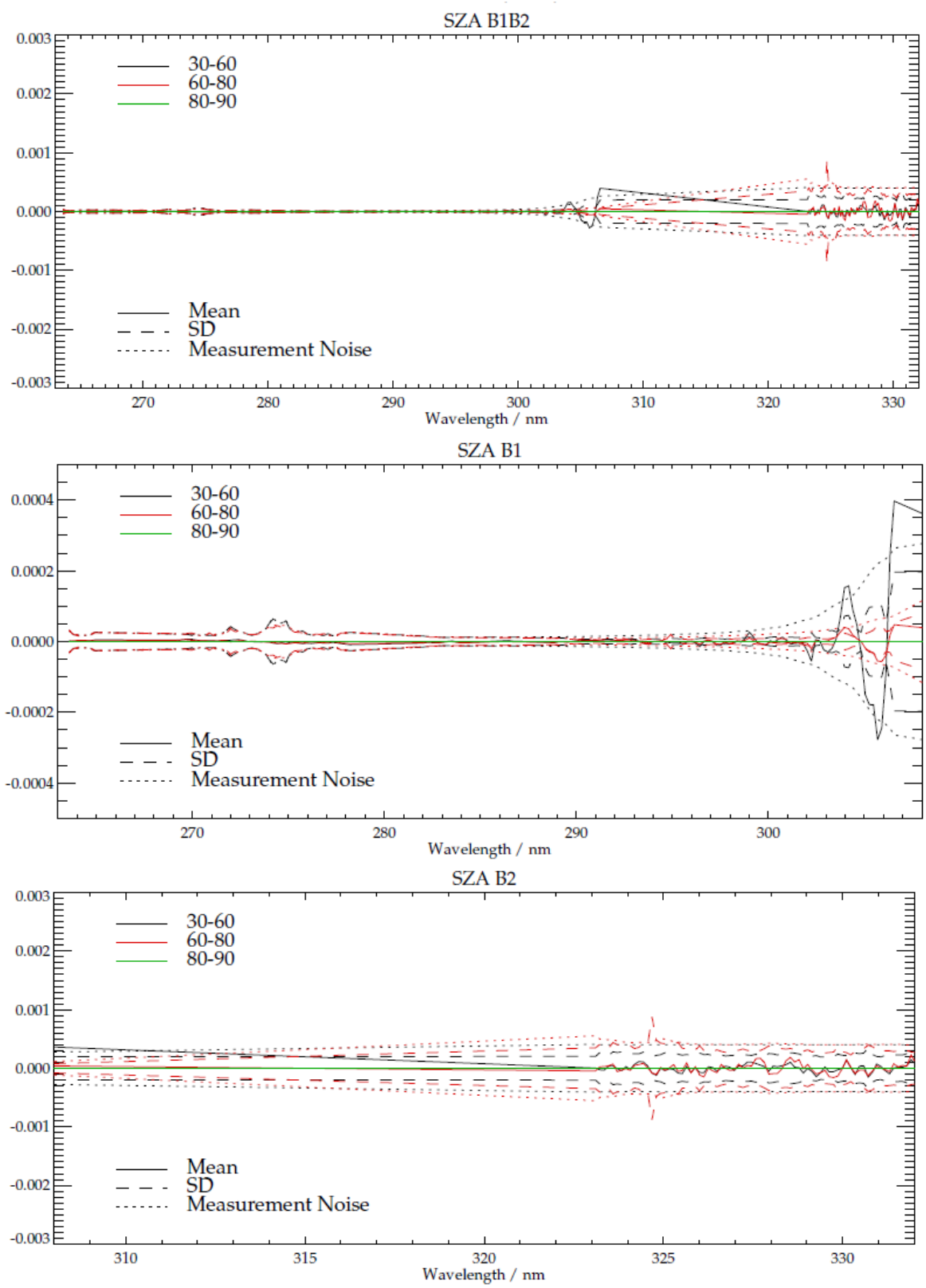

Figure 16: Top: Mean RAL fit residual (measurement minus fit) for 1 day of retrievals (25th March 2008), in both Band 1 and Band 2 to illustrate relative scale. Middle: Band 1 only. Bottom: fit residuals in Band 2 only. The RAL retrieval does not use any measurement information between 306 and 323nm, and is a sequential retrieval using profile retrieval results from Band 1 as a prior for the Band 2 retrieval.

The trend of the RAL fit residuals with time is illustrated by mean residual differences from 25th March 2007 in Figure 17 for the latitude band 30-90°N for the Band 1 and Band 2 fits. In Band 1, the change in Band 1a/b separation is reflected around the separation wavelength implemented at the end of 2008. The quality of the fit above 304nm becomes eroded with time (the fit residuals become larger) which suggests there may be some scope for improving this part of the Band 1 fit in this spectral region. Deficiencies in the fit are somewhat mitigated in the sequential approach since the Huggins bands have some sensitivity to the profile as a whole and may improve upon it.

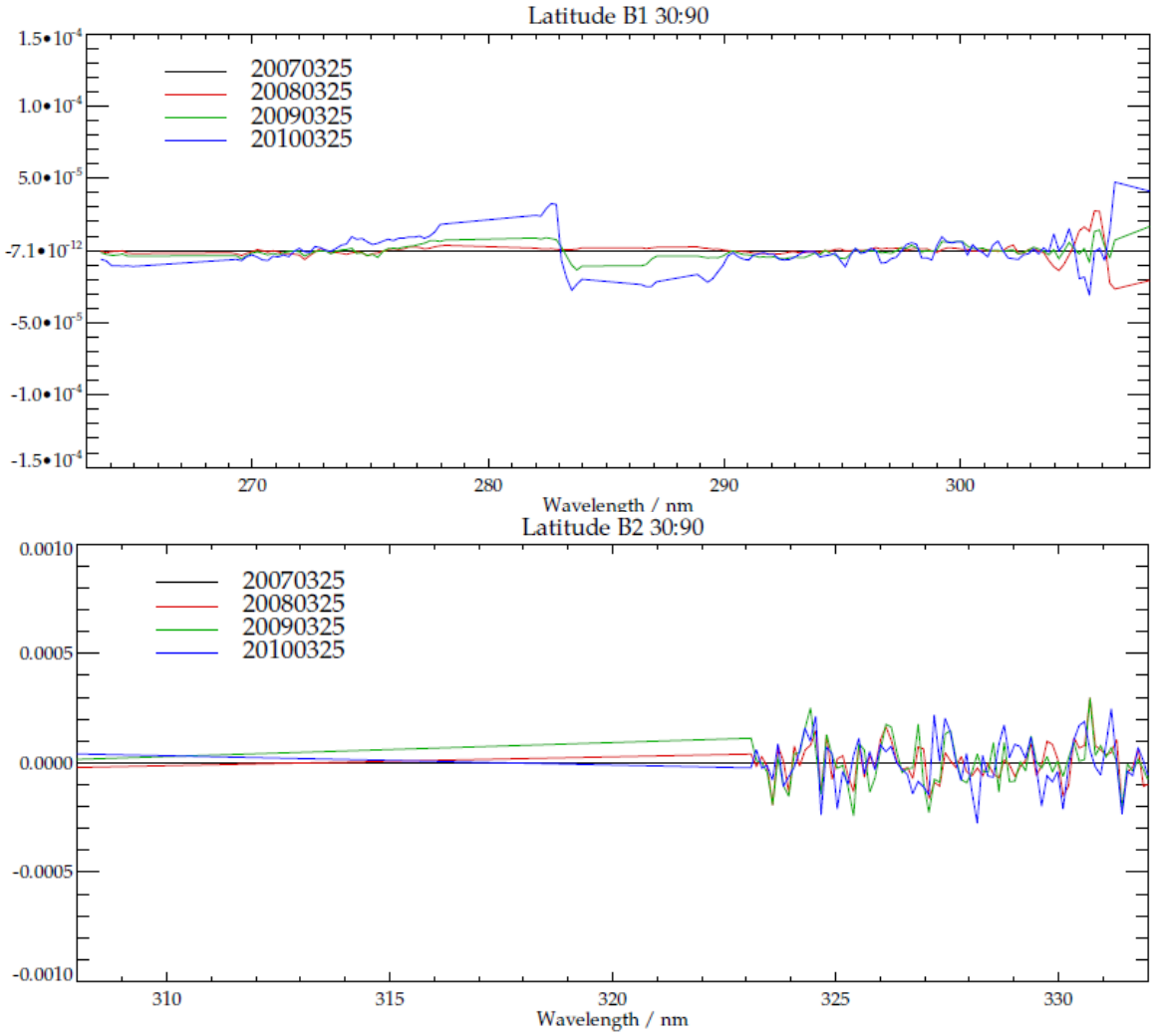

Figure 17: Top: Mean RAL fit residual difference from 2007 on 25th March each year until 2010 for Band 1 (top) and Band 2 (bottom). The difference is defined as the reference year minus the mean residual for each following year.

The impact of this in the RAL scheme is further suppressed by combining the Band 1b pixels such that 8 are averaged for each Band 1a pixel for the Band 1 fit, and 1 Band 1 pixel is used as a prior for up to 8 Band 2 pixels. Whilst this may come at the cost of some spatial information for stratospheric ozone in the fit, the increase in the integration time of the effective co-added measurement results in a lower measurement noise than would otherwise be the case. The measurement is still within the bounds of both the standard deviation and does not exceed the measurement noise. In Band 2 the trend is less straightforward to interpret, since principle components of the mean residual are fit and removed and these themselves have trends associated with them. The principle

components are fit based on a test set of ozone retrievals during 1 year after ozone has been retrieved and as such are designed to be orthogonal to the ozone information in the spectrum, and account for atmospheric, physical and instrument parameters that are otherwise not represented in the forward model and as such un-quantified. Unless a forward model is perfect it is not possible to remove all ozone information in this way however, so there remains the possibility that some or part of the eigenvectors will capture some aspect of zone variability. The physical interpretation of the principle components of the fit residuals or their trend is outside the scope of this report, but both have been examined at RAL.

3.2.2 OPERA fit residual trends

The mean residual shape for OPERA baseline scheme is robust both with time in mission and time of year. Figure 18 shows the OPERA fit residuals for the baseline date of 25th March 2008 as a function of solar zenith angle, for Band 1 and 2. The comparable residuals for the RAL scheme were shown in Figure 16.

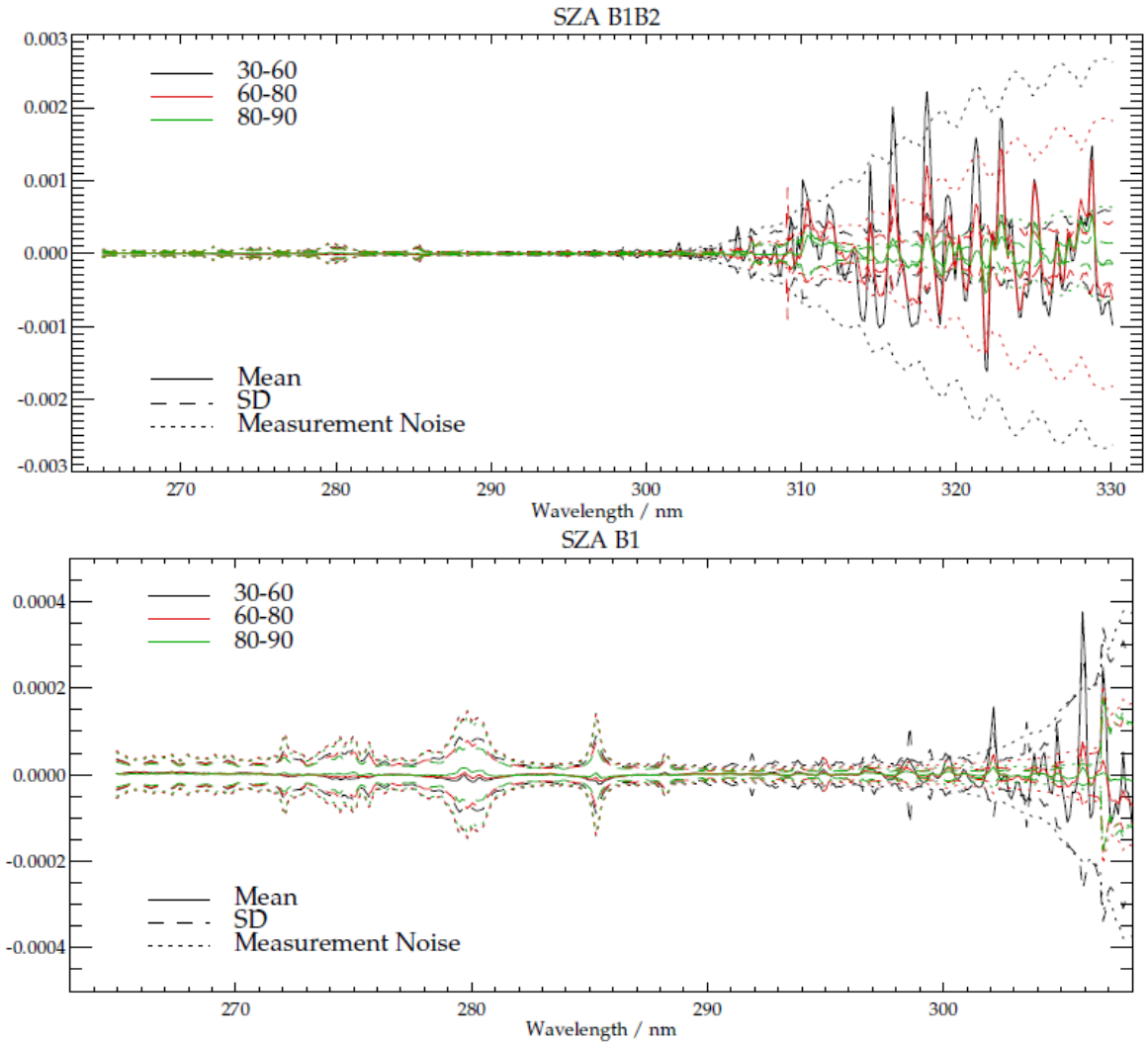

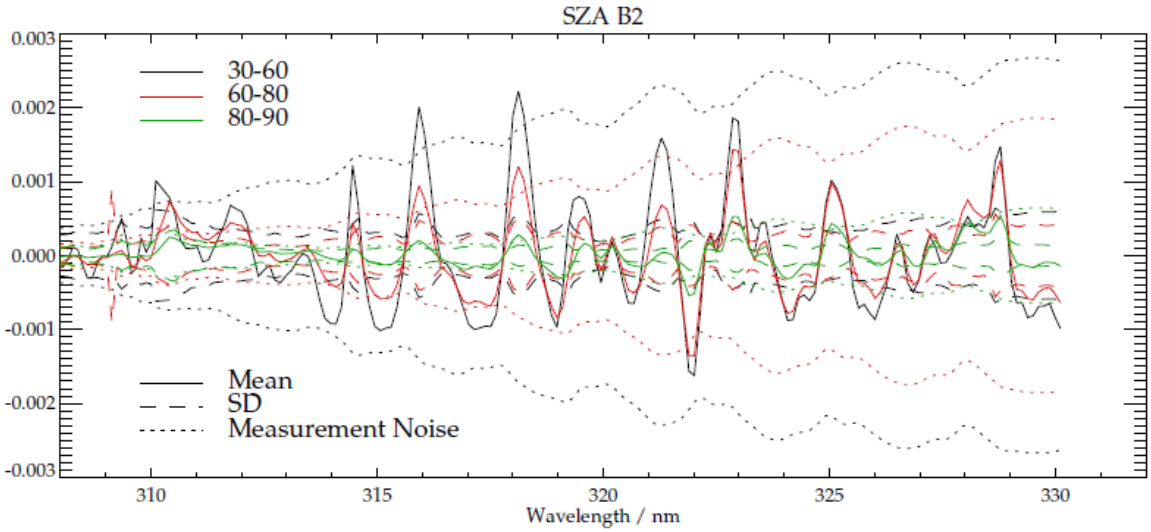

Figure 18: Top: Mean OPERA fit residual (measurement minus fit) for 1 day of retrievals (25th March 2008), in both Band 1 and Band 2 to demonstrate relative scale. Middle: Band 1 only. Bottom: fit residuals in Band 2 only.

Figure 19 shows both the mean residual in Band 2 as a function of Band 2 scan position, but also the difference in the mean fit residual from the nadir fit residual. This illustrates the dependence of the fit residual upon scan position, although it should be noted that the difference from nadir in absolute terms is small when compared to the mean residual itself.

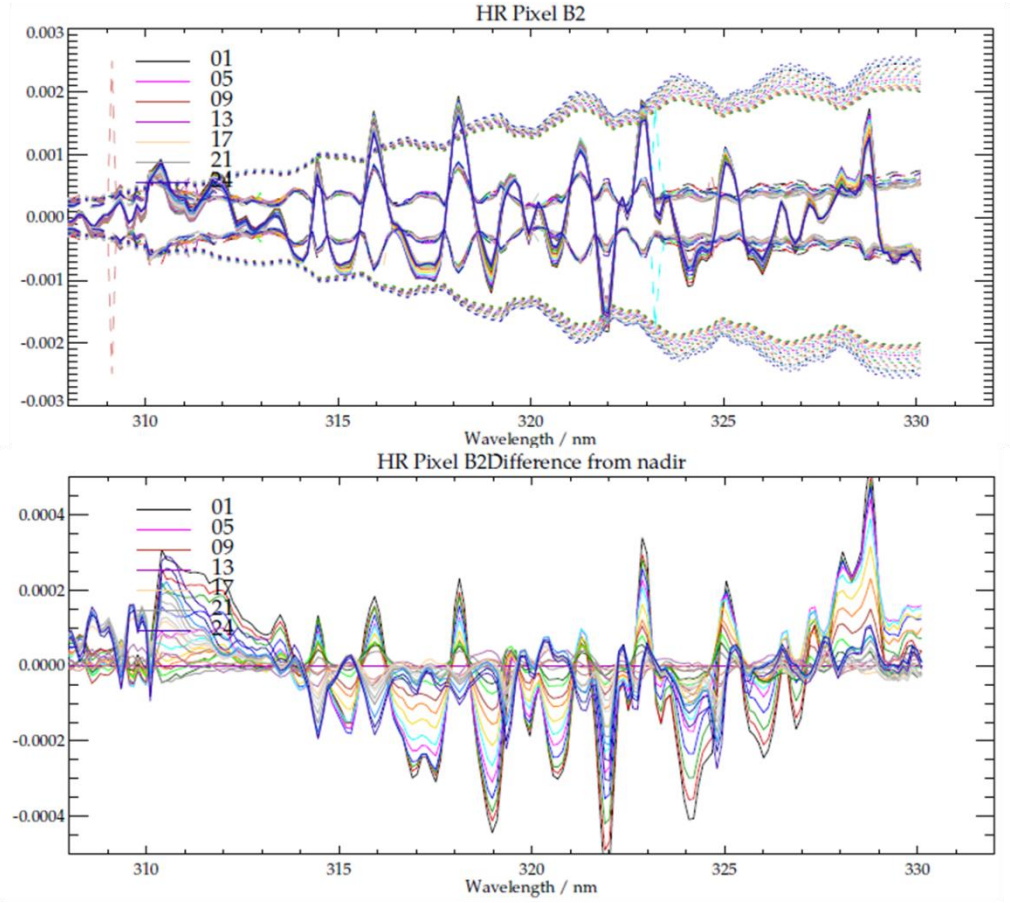

Figure 19: Top: Mean OPERA high resolution (24 across-track pixel) profile retrieval fit residuals over 1 day (25th March 2008). Dotted lines indicate mean measurement noise for a given scan position, dashed lines the standard deviation of the fit residual. Bottom: mean fit residuals differenced from nadir mean fit residual, where pixels 1 to 24 indicate the east to west Band 2 pixels.

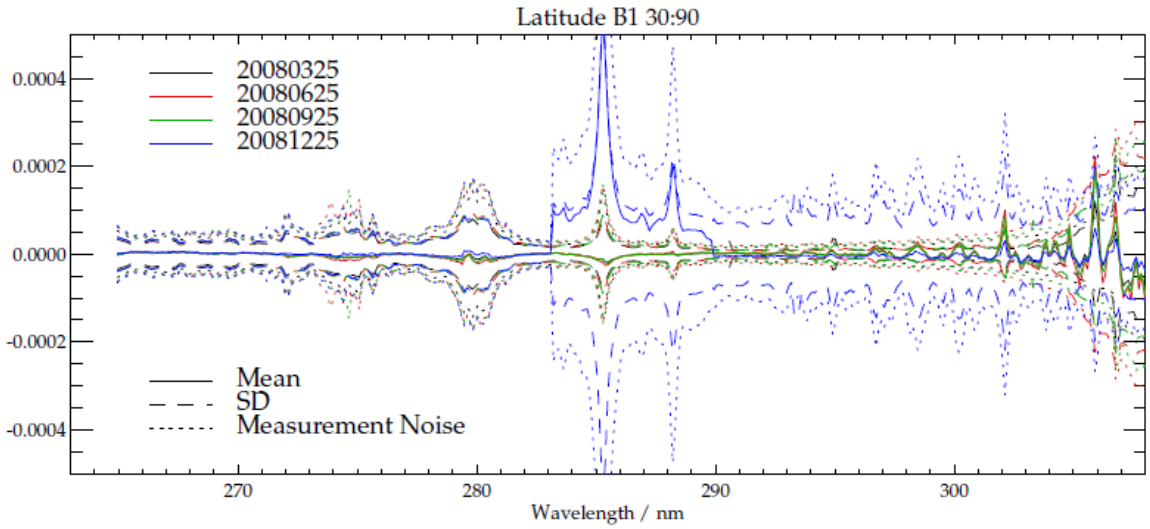

Figure 20: Mean residuals in Band 1a/b for 1 day in March, May, September and December 2008. The change in Band 1a/ separation is evident in December.

The characteristic shape and size of the OPERA mean fit residuals in Band 1 are further illustrated in Figure 20 for 4 days in 2008 that represent residuals in different seasons.

The shape of the mean residuals in Band 1 changes little by latitude band, and only those for the Northern Hemisphere mid to high latitudes are shown. The mean residual shown from December 2008 demonstrates the impact on the fit residuals that results from the change in wavelength of Band 1a/b separation.

Figure 21 demonstrates how the OPERA mean fit residual in Band 2 changes as a function of latitude for dates in different seasons, and they reflect the change in reflectance with latitude/SZA.

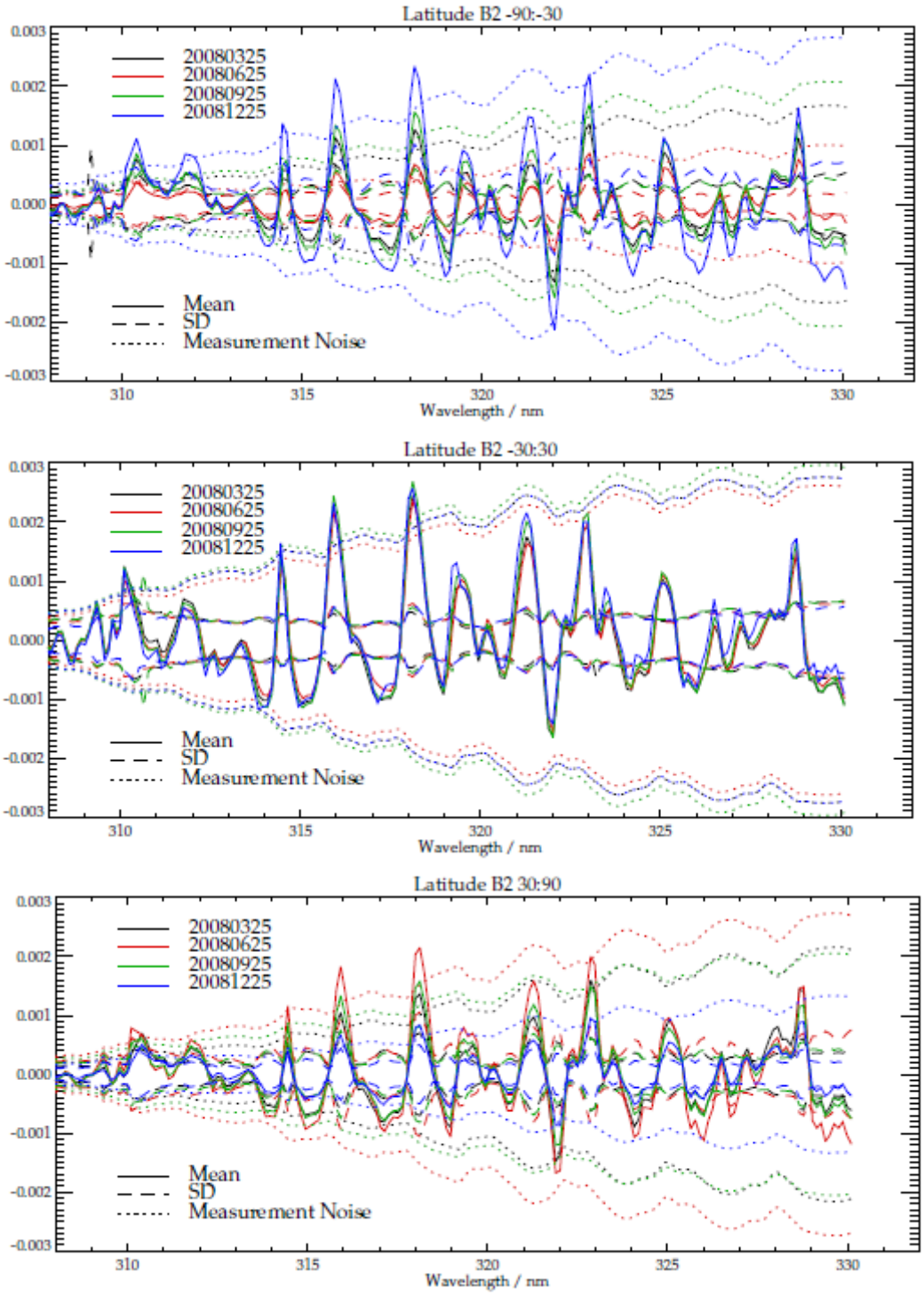

Figure 21: Mean OPERA fit residuals as a function of latitude band (-90:-30, -30:30, 30:90) for 4 differing times of year, on 25th March, June, September and December 2008.

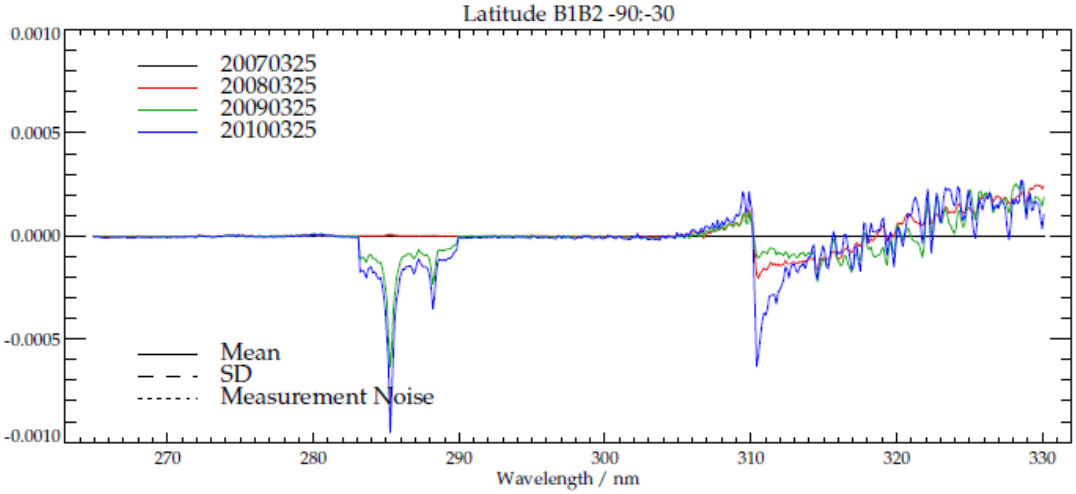

Figure 22: Top: Mean OPERA fit residual with time on 1 day from 2007-2010 on 25th March for Bands 1 and 2 in latitude band -90-30°N.

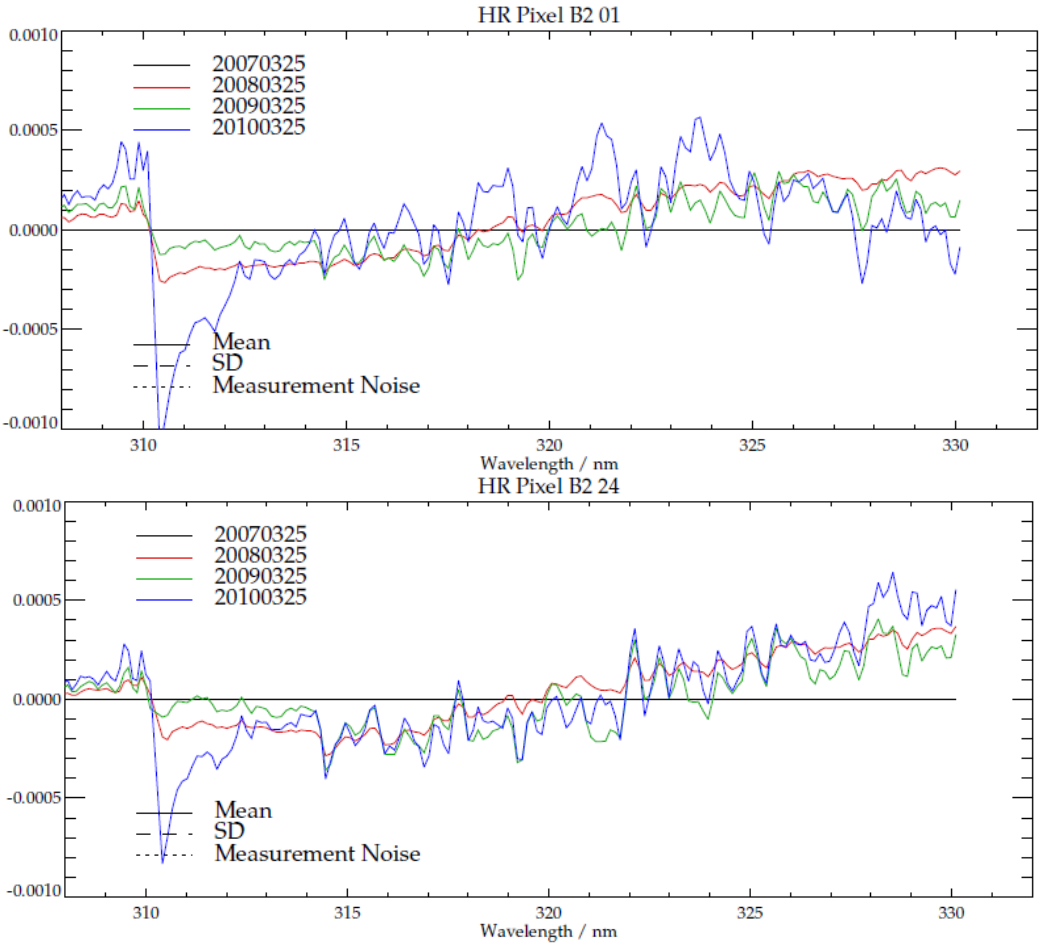

Figure 23: Difference of mean fit residual in Band 2 of the OPERA baseline from 25th March 2007 minus the same date in the following 3 years as a function of scan angle, where 01 (top) indicates retrievals from the east–most scan position and 24 (bottom) the west-most scan position. There are low-order differences in the trend for each extreme scan position.

In Band 2 the OPERA mean residual peaks and troughs are larger than the predicted noise and significantly larger than the standard deviation of the fit residuals (which are taken to reflect the true size of the measurement noise). For the RAL scheme in Band 2 the fit residuals are typically less than both the estimate of the measurement noise (smaller than that used for OPERA baseline) and the standard deviation of the fit residuals.

4 Prototype Algorithms from RAL Ozone Profile Retrieval Scheme

4.1 Introduction

The three prototype modules developed by RAL for test implementation with OPERA are a slit function/wavelength registration OE fit for Band 2, a degradation correction model and a measurement noise model. They are introduced in this section demonstrating the motivation for the modules with a description of how they are derived, implemented and tested in the RAL scheme.

4.2 Slit function retrieval and Band 2 wavelength registration

GOME-2 Level 1b earthshine and direct sun measurements are provided by EUMETSAT with nominal wavelength grids that are calculated during the Level 0-1 processing using on-board calibration information. The precise nominal wavelengths vary as a function of time and with respect to each other, since the direct sun measurement made once daily while the earthshine measurements are continuous. The RAL GOME-2 slit function retrieval algorithm was derived out of an offline process that registered the slit function key data to the measured direct sun spectrum. The RAL scheme is designed to exploit tropospheric ozone information from the fit in the temperature-dependent Huggins Bands as measured in Band 2. In order to do this the absolute calibration of the wavelength to the spectrum is required to a higher accuracy than that given by the derivation of the nominal wavelength in the Lv1b data, as this is reliant on a white light source relatively distant from the spectral features of interest.

The registration of the slit function key data to the measured direct sun spectrum is achieved by fitting a series of polynomials to a high resolution reference solar spectrum convolved with the GOME-2 slit functions using an offline optimal estimation retrieval. Originally 3 Legendre polynomials were used to describe the required gain, offset and shift/squeeze to the slit function nominal wavelengths in order for the simulated spectrum to best match the measured spectrum. The appropriate order of the polynomials was established on a 3-way cost basis where a range of combinations of orders were used respectively and the configuration with consistently the lowest fit cost was deemed most appropriate. The orders of the polynomials found by this method were 5, 5 and 60 for the offset, wavelength registration and gain respectively.

The fit was extended to additionally retrieve a full width half maximum scaling factor for the slit function key data in a given band. Since it is not trivial to anticipate what the spectral variation the in-orbit slit function shape evolution might have, to a first order it is sufficient to retrieve one scaling factor for either the entire band or the spectral region of interest in the ozone retrieval, which may not be identical. Sensitivity studies at RAL have ascertained that the spectral region over which this fit is obtained does indeed lead

to modest differences in the absolute magnitude of the slit function retrieved at a given point in time, but that the trend in the slit function shape is robust by this methodology.

In order to establish that there was sufficient independence in the retrieval of wavelength registration and slit function width, the resultant wavelength registration shifts were examined to establish whether or not they were affected by the slit function retrieval. It was found that the retrieval of the slit function width did not significantly affect the retrieved wavelength registration.

Figure 24 shows the retrieved scaling factor for the slit function width from 2007 to mid 2012. It indicates that the slit functions are effectively narrowing with time. The widths decrease steadily overall until the second throughput test in September 2009 where a sharp narrowing occurs, after which the rate of narrowing decreases. Superimposed on this trend is higher frequency structure relating both to various instrument interruptions and seasonality. This seasonal aspect is highlighted in Figure 25, where the slit function time series from Figure 24 is sub-divided into 1 year periods, de-trended and superposed by removing the annual mean. The origins of this seasonal trend are not obviously apparent. It is possible that they relate to seasonal sun-earth-instrument factors not otherwise accounted for.

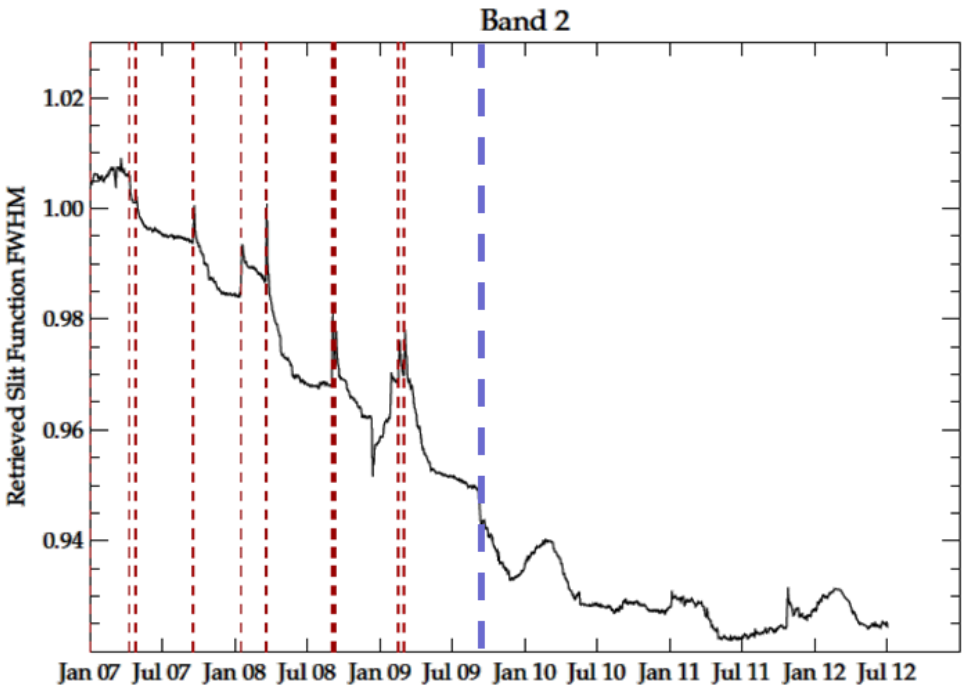

Figure 24: Trend in slit function FWHM. Vertical dashed red lines show interruptions to the throughput from calibration and testing. Vertical dashed purple line shows major interruption to instrument due to last throughput test carried out in September 2009.

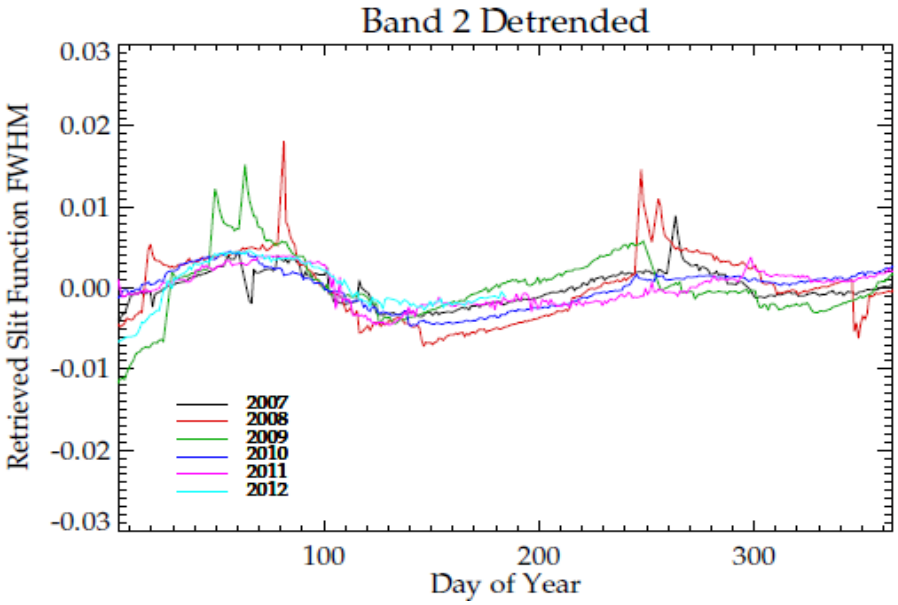

Figure 25: Retrieved slit function FWHM de-trended with annual mean removed to highlight seasonal aspect to slit function shape.

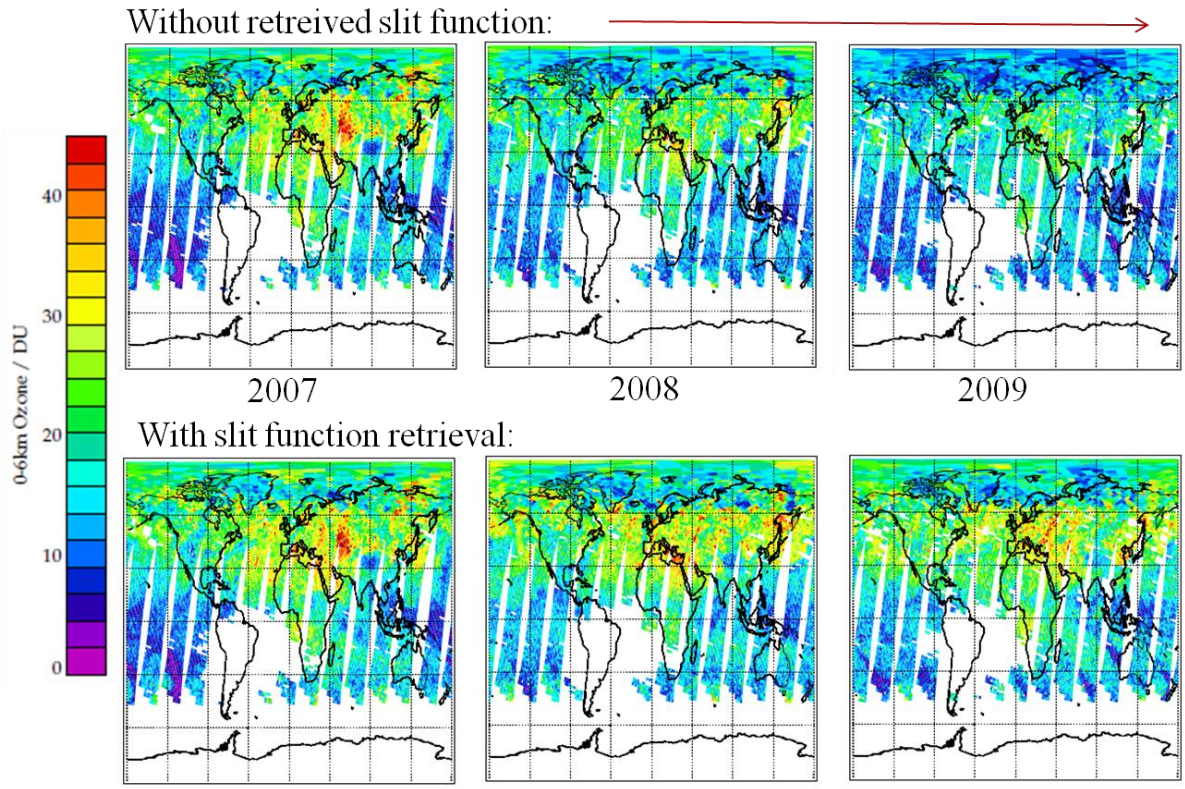

Figure 26: Demonstration of the effect of accounting for the change in slit function width, within the RAL GOME-2 ozone profile algorithm on the 0-6km sub-column for the period 1st June 2007-2009.

Figure 26 demonstrates the impact on the 0-6km sub-column tropospheric ozone from the RAL retrieval if no account is made of the change in the slit function. On 1st June 2007 when the slit function width has changed little from that predicted by the slit function keydata, there is no apparent impact of retrieving the slit function width. On 1st June 2008

and 2009 it becomes increasingly apparent that not retrieving the slit function results in a spurious negative trend in tropospheric ozone. This is highlighted in Figure 27 which shows the 30-day mean bias with respect to ozonesondes in the same sub-column from 2007-2010. Without retrieving the slit function there is an evident negative trend in the bias. When the slit function retrieval is implemented the trend in the bias is removed.

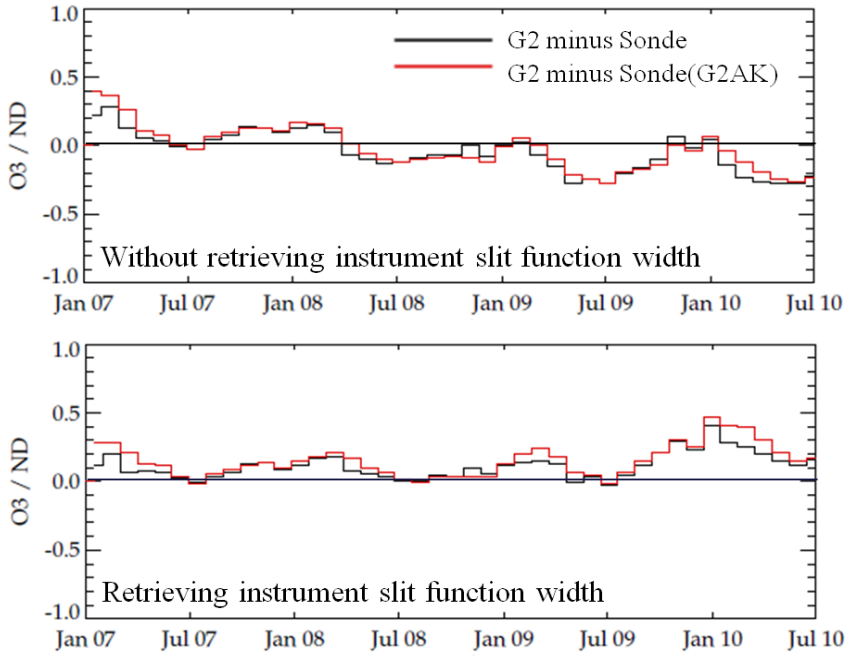

Figure 27: Demonstration of the effect of accounting for the change in slit function width, within the RAL GOME-2 ozone profile algorithm on the 0-6km sub-column bias against ozone sondes as a function of time. Data binned into 30-day means for RAL GOME-2 minus sonde layer mean number density. The top panel shows that without retrieving the slit function the bias has a trend with time. The bottom panel shows a more stable bias when the slit function retrieval is enabled.

4.3 Degradation Correction

The MetOp-A GOME-2 instrument throughput has been degrading since it was first made operational in 2007. The precise mechanism and character of the degradation are not entirely understood, but involve deposition of one or more contaminant substances on the detectors and potentially the instrument optics. The decrease in throughput is wavelength dependent where shorter wavelengths are more strongly affected than the longer wavelengths of the instrument. In absolute terms the throughput decreased by over 60% from 2007 to the end of 2011 at the lowest wavelengths.

The degree to which this effects the retrieval of level 2 products using GOME-2 measurements depends on how they are retrieved. For example, the fitting of a differential spectrum is potentially less affected since both the direct sun and earthshine measurements are degrading together, provided they are degrading in an identical way. It does however reduce the signal to noise with time which affects the precision to which Level 2 products can be known.

In order to account for this, a degradation correction has been derived for the RAL GOME-2 ozone profile retrieval algorithm. The correction is applied in Band 1, where the degradation is largest and the spectrum is fit directly. GOME-2 measurements are

sampled at a rate of 1 day per week over the period where the degradation correction is to be fit. The retrieval algorithm is not permitted to iterate and as such returns a fitted spectrum commensurate with the *a priori* ozone profile using the geophysical parameters of the measurement. The data used is filtered to lie within 30 degrees of the equator to minimise solar zenith angle dependencies, and measurements with a high cloud content or proximity to the South Atlantic Anomaly are removed. The departure of the actual measurement from this no-iteration synthetic spectrum with time is then used to estimate the degradation in an optimal estimate fit of a set of 2 dimensional Legendre polynomials to describe the degradation with both time and as a function of wavelength. A leakage current is also fit in this retrieval such that it may be kept separate from the degradation correction. This is because the leakage current is retrieved as part of the RAL ozone algorithm and not to do so would result in effectively accounting for leakage effects twice. Three separate correction polynomials are retrieved for each of the GOME-2 Band 1a pixel geometries: east, nadir and west. Figure 28 shows the ratio of the prior-simulated spectrum to the measurement for the selected data for each of these scan positions. The east pixel is somewhat distinct from the nadir and west pixels in terms of the nature of the correction required, indicating that it would not be appropriate to use one corrective polynomial for all scan positions in this Band.

The period until the change in Band 1a and Band 1b separation is treated as a distinct period for the purposes of the fit, and the resulting polynomials are joined using a smoothing function. This correction is 'model-based', and as such makes the analysis of trends in ozone more difficult with such a correction.

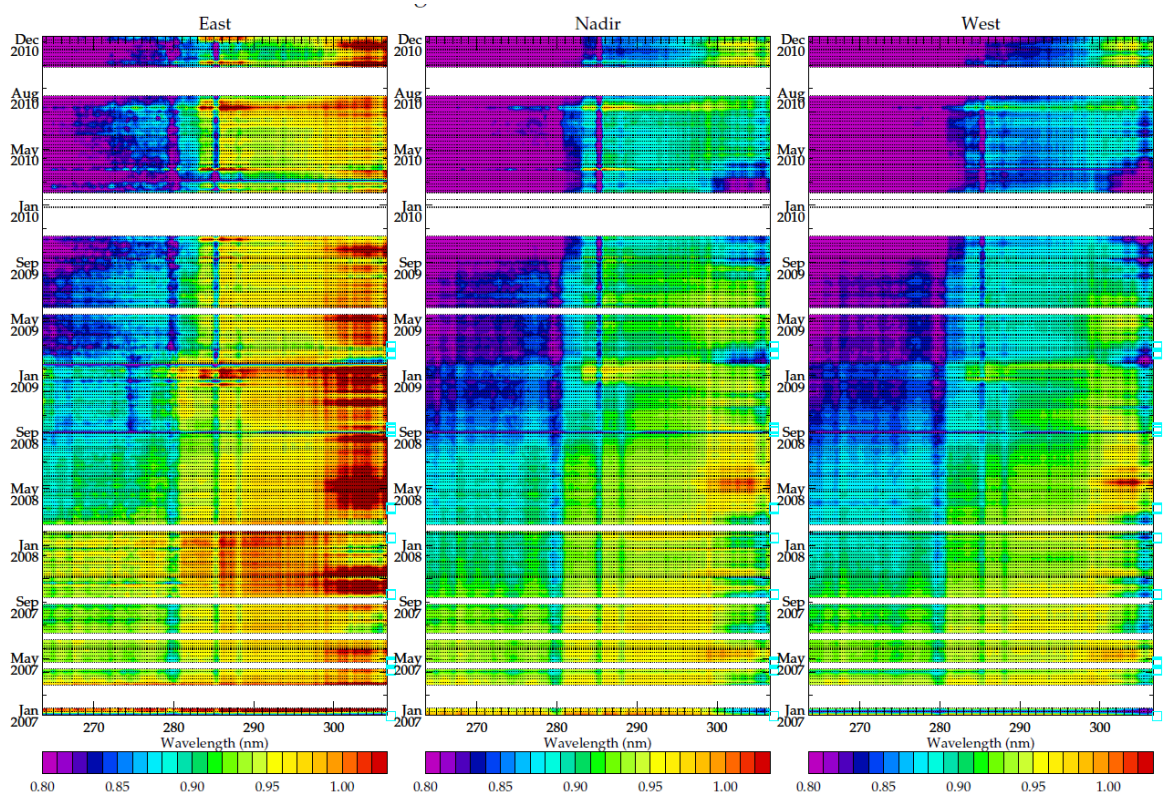

Figure 28: Ratio of a priori-simulated GOME-2 sun normalised radiance to measurement. Narrow dashed horizontal black lines indicate where a GOME-2 measurement was used. White gaps signify absence of data for a short period, associated with non-nominal instrument operation or data unavailability at the British Atmospheric Data Centre at the time of processing.

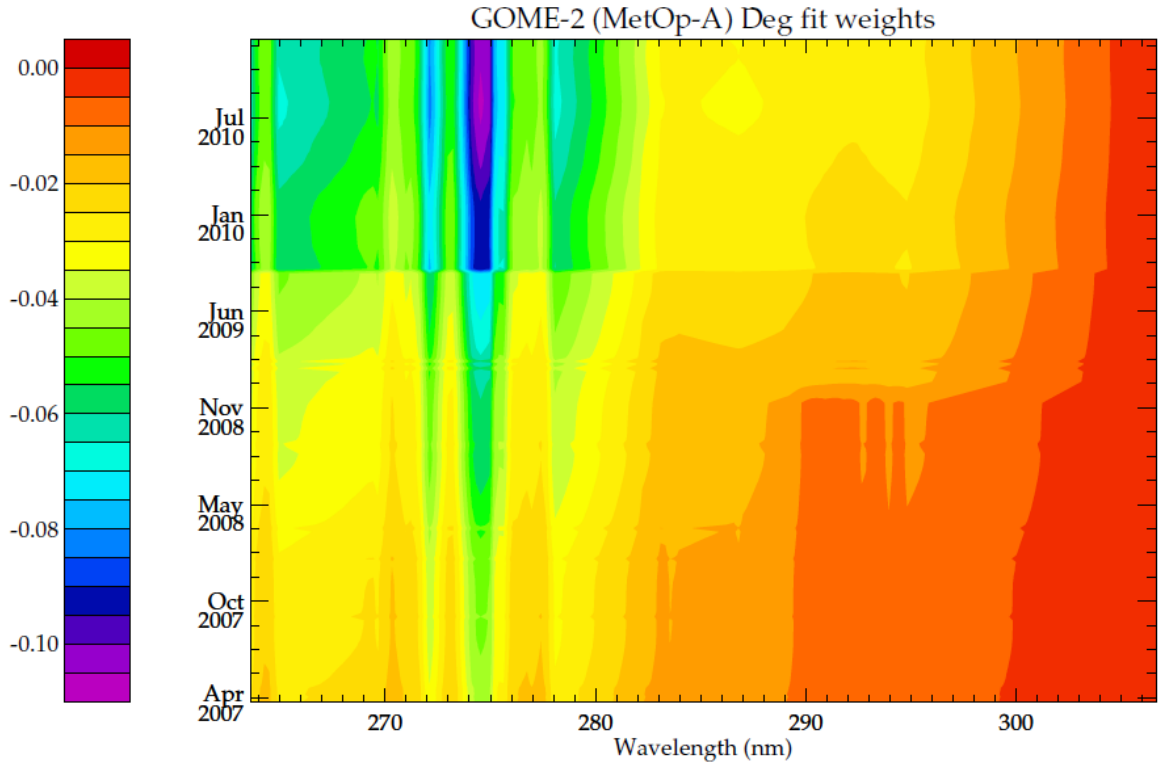

Figure 29: Two dimensional fit polynomial, for nadir B1a pixel. There is a notable discontinuity in September 2009 after second through-put test.

Figure 29 shows an example of the two dimensional polynomial retrieved for the nadir B1a pixel for 2007 to mid-2010 that can be applied to simulated sun-normalised radiance. Whether or not they are applied to simulated radiances within the forward model or on a corrective basis to the measurements themselves is debateable, and pertains to where functionality of a given algorithm will allow it although they will effectively achieve the same thing so long as there is consideration of whether the quantity in question (measurement or simulated radiance) is to be divided or multiplied by the correction in each case. In the RAL scheme the correction is applied to the simulated sun-normalised radiance. Not only is this most appropriate since it is most analogous to how the degradation correction was derived, but it is also most easily implemented here.

The sharp discontinuity apparent after the second throughput test in September 2009 suggests that it may be more suitable to treat the measurements in two distinct phases for the purposes of generating future corrective polynomials.

Figure 30 shows an example of the degradation correction as returned by the degradation correction test module supplied for implementation with OPERA. The impact when these are applied to the measurements is indicated in Figure 31. In absolute terms the correction in mid-2008 (shown) is small, but becomes more significant with time.

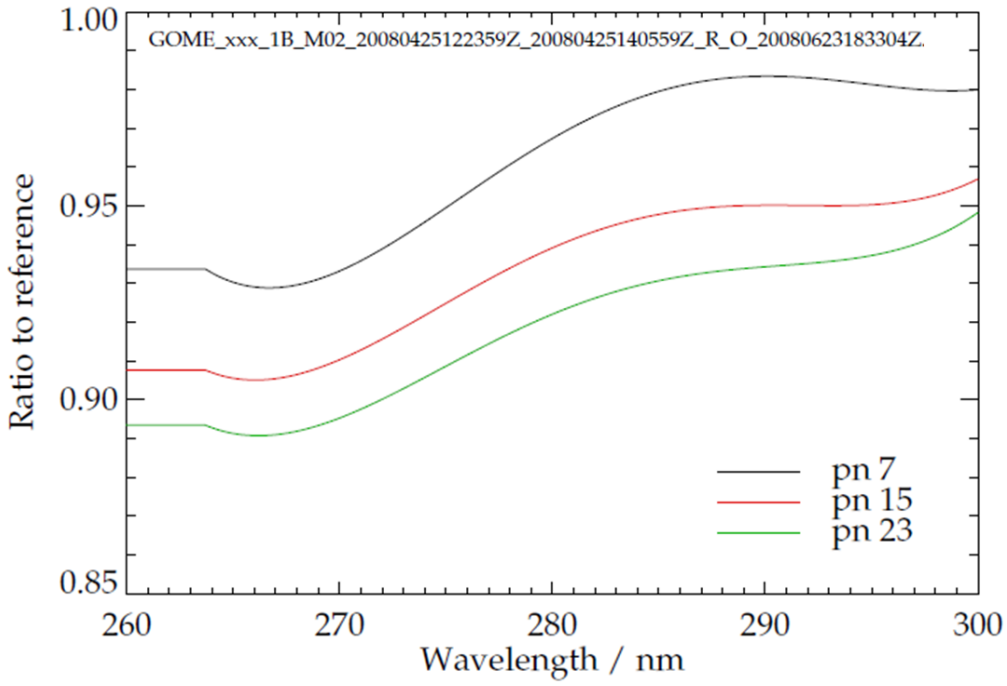

Figure 30: Demonstration of the estimation degradation correction for the first 3 Band 1 pixels of a sample orbit (specified in figure). A separate wavelength-dependent correction factor is derived for each scan position.

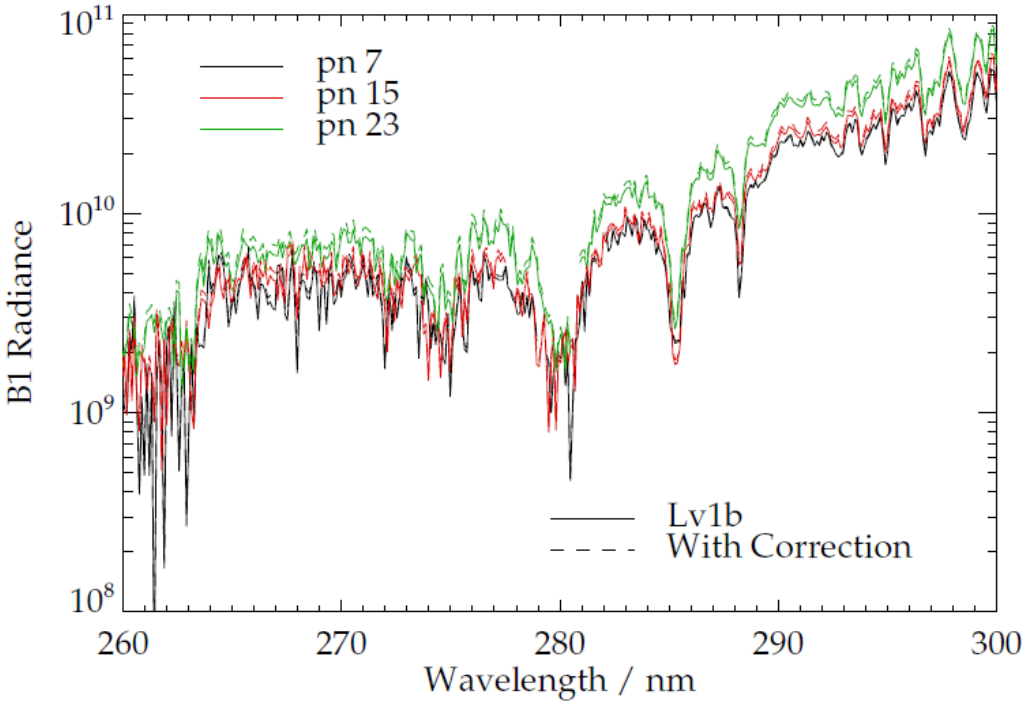

Figure 31: Example of measured radiance before and after correction factor is applied for specimen pixels described in previous figure.

4.4 GOME-2 Noise Model

Optimal estimation retrieval of ozone profiles requires the random noise of the measurement to be quantified. The magnitude of this can be estimated by examining the standard deviation of the difference of the measured spectrum in neighbouring pixel footprints. By this method, it is evident that earlier versions of the noise estimates provided by the level 1b measurement files the noise estimate resembled that of the systematic and random noise components combined, which is inappropriate for the purposes of optimal estimation retrieval. As such, RAL developed a GOME-2 noise model to estimate the random component of the measurement noise. This was initially based on a model derived for the GOME-2 Error Study [Kerridge et al., 2004]. It was further developed to make use of elements of the calibration keydata derived for GOME-2. An accurate estimate of the measurement noise is particularly important where the retrieval is required to fit to the noise level in order to fully exploit all of the information from the measurement. This is particularly the case for the RAL ozone profile retrieval algorithm fit in Band 2 for characterising tropospheric ozone in the region of the Huggins bands.

The noise model estimates the noise as follows. The variables 'RA_ABS_RAD_MAIN' and 'POL_KAPPA' from calibration keydata are used to calculate the Muller Matrix element which gives the radiance response, including scan angle dependence. The variable 'DE_DARK_MAIN' (or *D*) is used to calculate the dark current (σ_d), as shown by:

$$\sigma_d = \sqrt{(DT_i E_{BU})}$$

Equation 1

where T_i is the integration time for a given pixel and E_{BU} the number of electrons per binary unit. The signal in photons, F_e, is given by:

$$F_e = IMT_i E_{BU}$$

Equation 2

where *I* is the measurement intensity and *M* the Muller Matrix element derived from the slit function keydata above. The photon noise is given as:

$$\sigma_s = \sqrt{F_e}$$

Equation 3

The total noise is calculated as:

$$\sigma_t = \sqrt{(\sigma_d^2 + \sigma_s^2 + \sigma_r^2)}$$

Equation 4

where σ_r is the readout noise, a constant with a value of 1700 electrons. The signal to noise ratio is given by:

$$SNR = \frac{F_e}{\sigma_t}$$

Equation 5

In the case where pixels are combined to improve the signal to noise ratio (effectively increasing the integration time of a measurement but with the sacrifice of some spatial resolution) the mean combined pixel radiance is used as the input intensity and the signal to noise is reduced by a factor of 1/√n, where n is the number of pixels combined. Under some conditions (e.g. high latitudes at certain times of year) this can result in an underestimate of the noise. Indeed, this can also result when pixels are not combined.

This is remedied by the introduction of a noise floor of 0.01%. It is conceivable that this can be avoided if the random and some systematic components of this noise estimate were combined more appropriately (i.e. where systematic noise components' error is propagated rather than averaged). This would be desirable since examination of retrieval cost indicates that for most latitudes/solar zenith angles this noise floor is not required and there is potentially more information in the measurements than is being made use of in the RAL fit.

Figure 32 and Figure 33 show the comparative measurement noise as predicted for a single specimen pixel in Bands 1 and 2 respectively. It is apparent that in both channels the RAL noise model predicts a lower estimate than that provided within the level 1b measurement file. Product format version 5.3 and above (from January 2012 onwards and in re-processed data of this version number) contain measurement noise estimates that also resemble the random noise contribution, and as such the RAL GOME-2 noise model is only considered useful in circumstances where the new Lv1b noise estimate is not present.

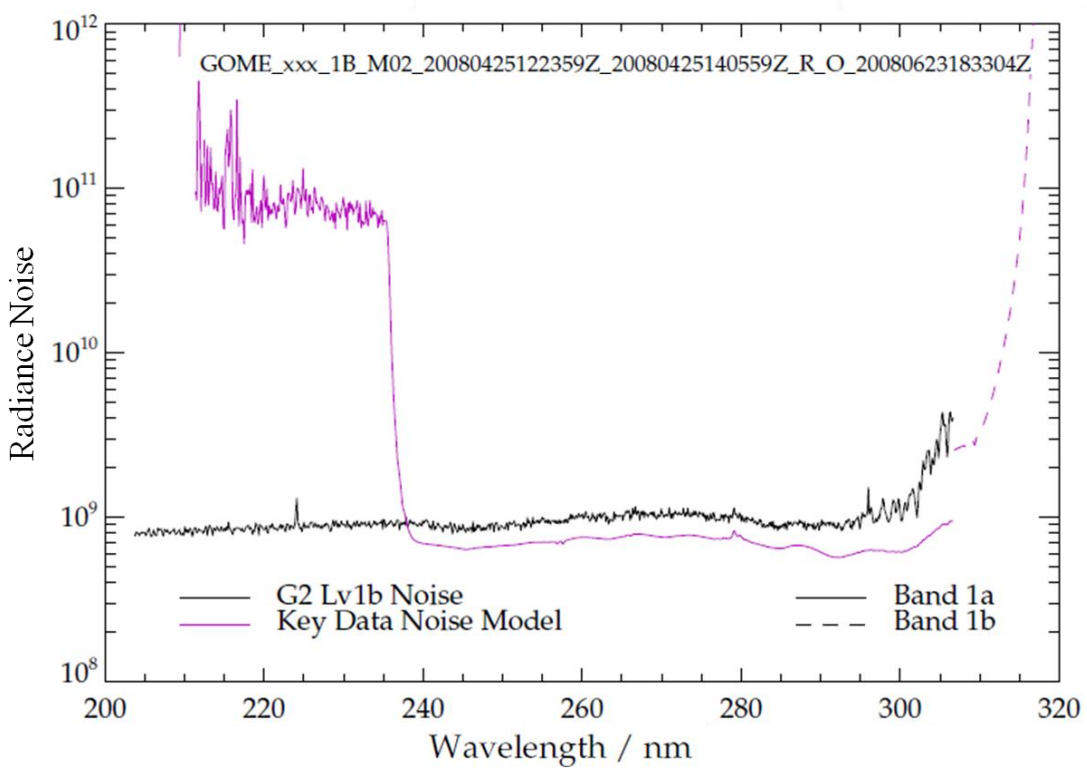

Figure 32: Example of Band 1 earthshine measurement noise as given in GOME-2 Level 1b measurement (prior to product format version 5.3) and that predicted by the RAL GOME-2 noise model (based on calibration key data) for the first pixel in the orbit denoted within the figure.

Figure 34 shows the relationship between both the Lv1b noise and the RAL GOME-2 noise model and the sun-normalised radiance at specimen wavelengths for 1 orbit in April 2008 (as specified in previous figures). The noise model predicts a noise level that is more proportional to the sun-normalised radiance that might be expected from a random noise estimate.

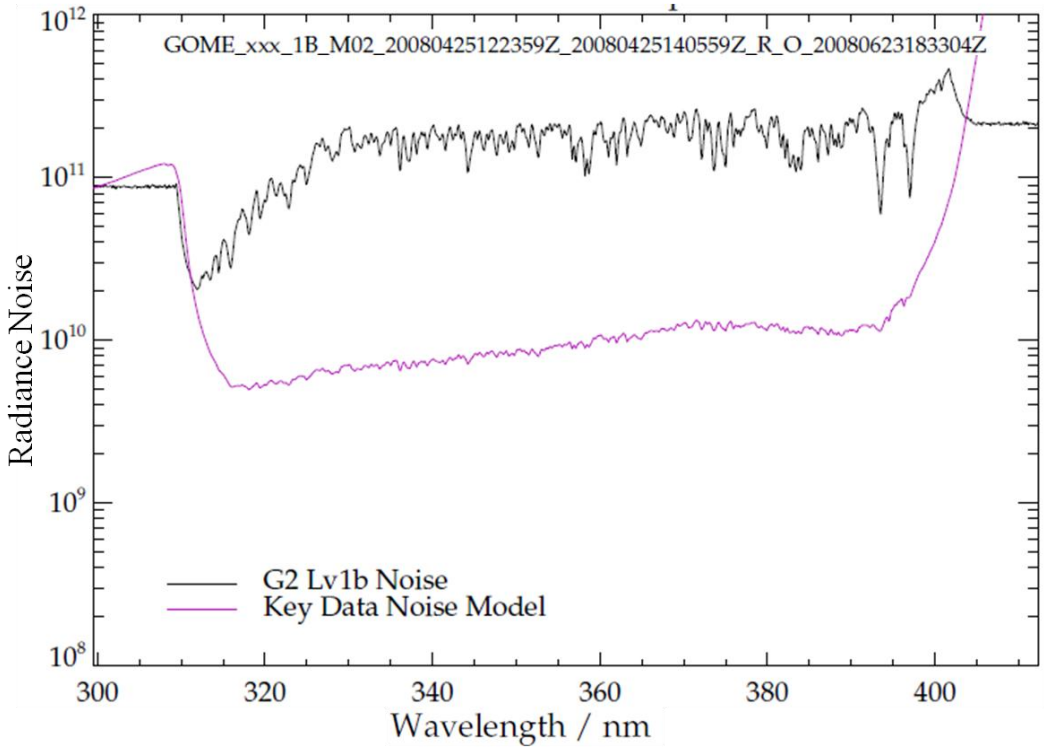

Figure 33: Example of Band 2 earthshine measurement noise as given in GOME-2 Level 1b measurement (prior to product format version 5.3) and that predicted by the RAL GOME-2 noise model (based on calibration key data) for the first pixel in the orbit denoted within the figure.

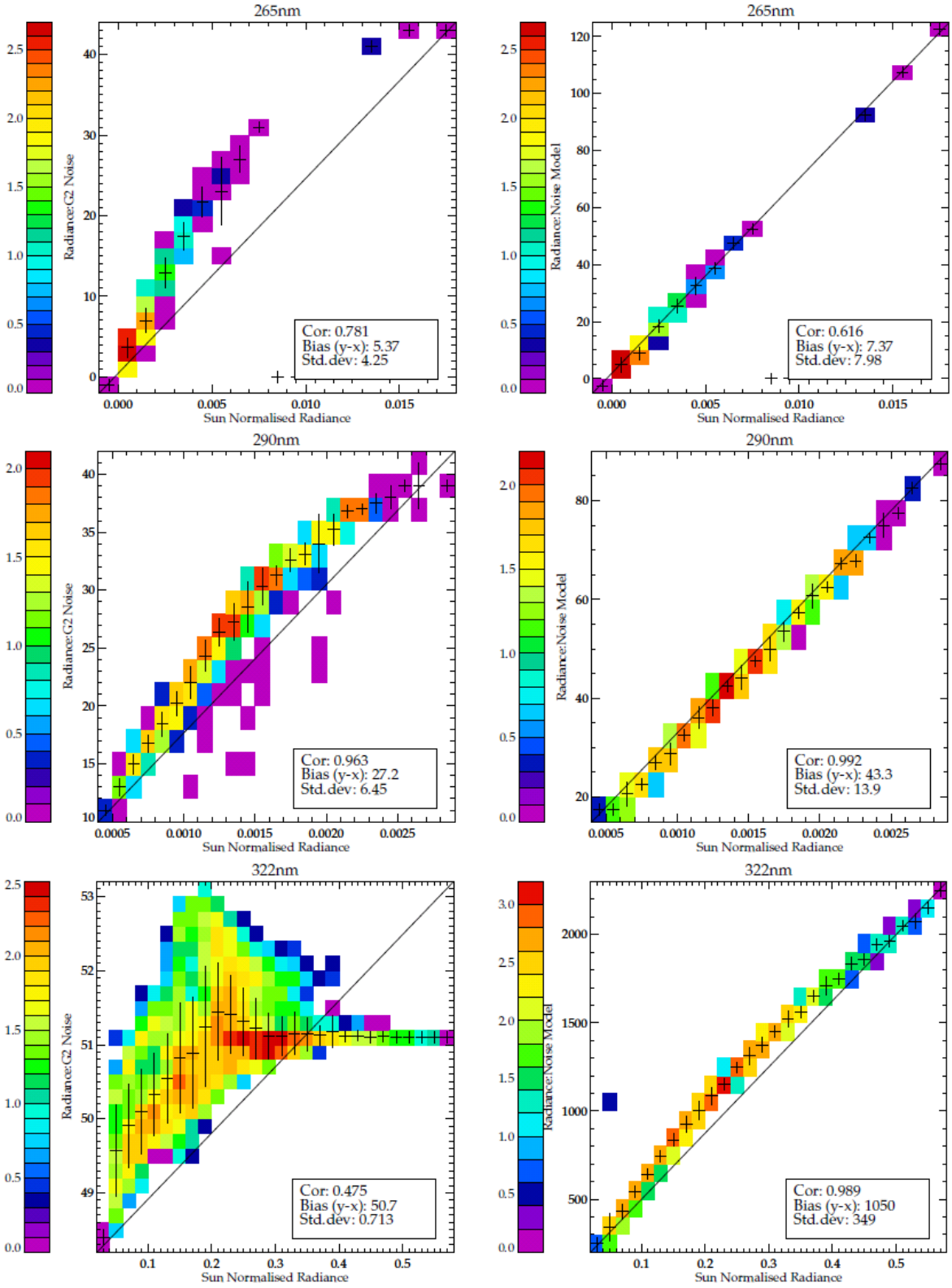

Figure 34: Example of earthshine measurement noise as given in GOME-2 Level 1b measurement (prior to product format version 5.3) and that predicted by the RAL GOME-2 noise model (based on calibration key data) for a specimen orbit (denoted in previous figures). The panels show the correlation of noise with sun normalised radiance at 3 wavelengths in Bands 1 and 2. The panels on the right show the noise from the level1b measurement file, the panels on the left those predicted by the RAL GOME-2 noise model.

5 Transfer of Prototype Modules

The three prototype modules from the RAL GOME-2 ozone profile scheme were successfully transferred to the OPERA scheme. RAL assisted the implementation of the prototypes within OPERA by KNMI. They were variously amended and developed to work in accordance with the different functionality of OPERA as detailed in this chapter. This is followed by a comparison of fit residuals and retrieved ozone profiles when the test modules are used as compared to the baseline without. Finally, some there is some discussion about the outcome of these tests and suggestions for further work.

5.1 Slit Function Retrieval

The implementation of the slit function module within OPERA is achieved via an external function (written and tested in python by Dr Olaf Tuinder) based on the test function delivered by RAL (written in IDL). The function stores output from the slit function retrieval that can be selected for use within the OPERA call. In accordance with its implementation within the RAL scheme, this output is associated with each daily solar reference direct-sun measurement by GOME-2 and is therefore only required to be generated once.

There are some key differences to the way in which the slit function retrieval is implemented in OPERA from that of the RAL scheme, some of which are necessary because the algorithms differ in the way that they operate.

In the RAL scheme, the slit function retrieval, solar and earthshine spectra are referenced according to the index of individual detector pixels. Within OPERA, these are referenced to the nominal wavelengths in the Lv1b data, and change with time. Both of these approaches are considered appropriate for the respective schemes and the relative wavelength registration between solar and earthshine grids are handled internally. As such, the exact parameters derived as part of the slit function retrieval (including the wavelength registration of the slit functions to best match the GOME-2 measurement) may differ slightly between the algorithms.

In the RAL version of the slit function retrieval, the slit function width is represented by a scalar value that is applied across the whole band (or fitting window as appropriate). Upon transfer to KNMI, the opportunity was seized upon to extend this scalar to a wavelength dependent polynomial, allowing the slit function scaling to change across the band. Since the precise nature of the change to the slit functions is unknown, this presented an opportunity to investigate the wavelength dependency of the change across Band 2. This approach also retains the flexibility to fit a single scalar value by setting the order to the Legendre polynomial to zero.

In the KNMI implementation (hereafter also referred to as ‘DISQ’ for the displacement/squeeze function of the output parameters) the slit function retrieval does not converge beyond mid-January 2012. This coincides with the change in specification of the Lv1b measurement noise. This has yet to be tested in the RAL scheme (which does not use its noise model in this fit), but suggest some tuning to the retrieval parameters may be necessary to promote convergence with the new estimate of noise.

KNMI were also able to test the sensitivity of the slit function fit to the order of polynomials described in section 4.2 using the standard deviation of the fit residuals as a measure of how well the measurements were fit, which were in agreement with those proposed by RAL. The small but quantifiable sensitivity of this retrieval to the order of the polynomials

indicates that it would be beneficial to revisit their specification should the module be made part of the operational algorithm.

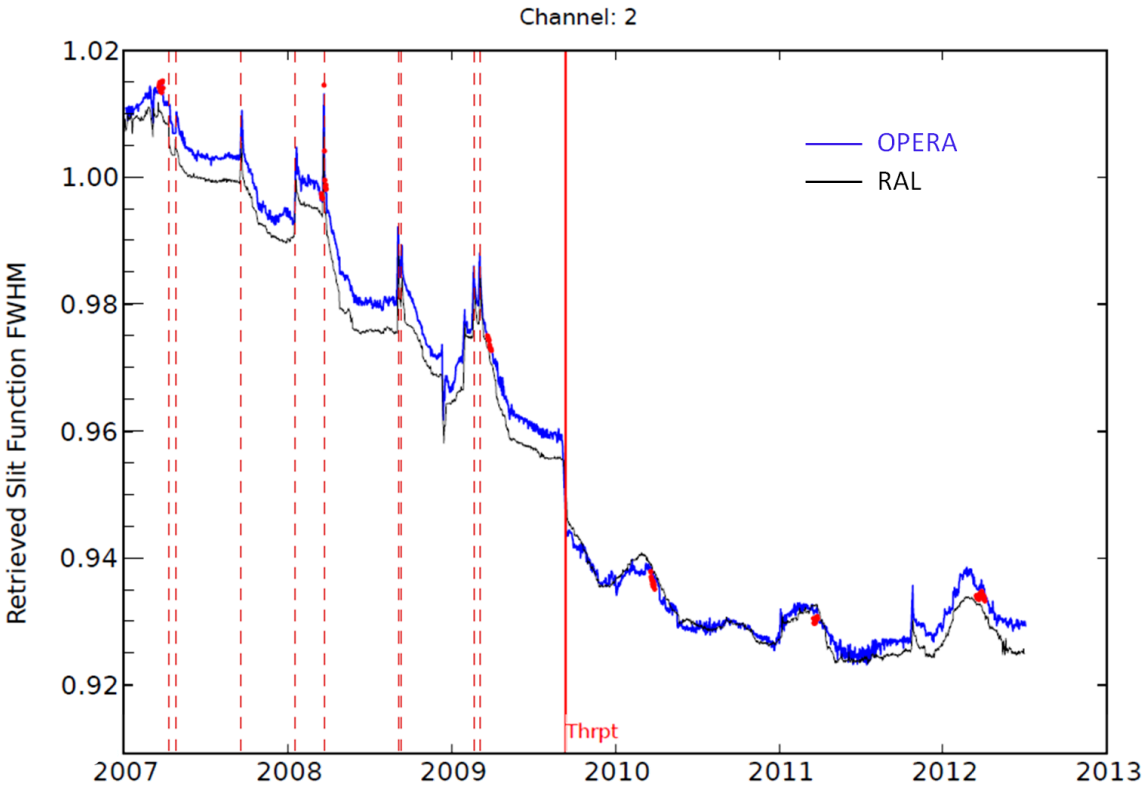

Figure 35: Comparative slit function FWHM scaling factors as derived using slit function retrieval scheme as applied at KNMI and within the RAL scheme. The former has been extended to retrieve a polynomial representing variation of the slit function change across the band, the latter is one factor applied to the spectral region of the retrieval. The mean of the 5th order polynomial FWHM retrieval closely follows the FWHM predicted by fitting one FWHM across the band. Red vertical dashed and solid lines indicate discontinuities in the throughput of the instrument and the second throughput test respectively. The red dots indicate retrieved values when the OPERA slit function retrieval uses a 0th order polynomial to emulate the RAL single scaling factor.

The retrieved slit function scaling factors from the RAL and OPERA schemes are shown in Figure 35. The absolute values differ very slightly between algorithms and it is considered that this mainly relates to the methods of referencing the measurements between the algorithms. The KNMI application of the slit function retrieval is also able to retrieve a slit function polynomial for Band 1, as shown in Figure 36. This not used in the application with OPERA for the purposes of this work, nor is it used in the RAL scheme. This is because both schemes fit the spectrum in Band 1 to a high precision and the fit is therefore less dependent on the absolute wavelength registration to the measurement, but more reliant on the absolute radiometric calibration of the instrument (in part addressed by the other modules). It is notable that the KNMI fit in Band 1 predicts a marginally steeper narrowing of the slit function width than shown for Band 2, but less sensitivity to thermal or seasonal sources that impact Band 2.

Figure 36: Slit function FWHM scaling factors as derived using slit function retrieval scheme in Band 1. The mean slit function scaling factor predicted by a polynomial across the fitting window of band 1 is shown. The red vertical line indicates the second instrument throughput test that led to a sharp narrowing of the slit function width in Band 1. The red dots indicate retrieved values when the OPERA slit function retrieval uses a 0^{th} order polynomial to emulate the RAL single scaling factor.

The impacts of the wavelength displacement and slit function width polynomials on the OPERA mean fit residuals are relatively small, and only evident in certain conditions. The likelihood of this was anticipated firstly because the fit precision that OPERA achieves in Band 2 (where this RAL module is applied) is characteristically larger than the measurement error or the standard deviation of the fit residuals which imposes a limit to the amount of information that can be exploited from GOME-2 measurement in the Huggins Bands. A further reason why the impact of the wavelength re-registration and slit function width correction may be limited is due to the way the OPERA retrieval simulates measurements, which differs slightly from the RAL scheme for which it was designed.

Within OPERA, the measured solar spectrum from the measured solar grid is interpolated to the earthshine grid using a convolved high resolution solar reference spectrum. The same high resolution solar reference spectrum is used to calculate a simulated solar spectrum using a convolution with the slit function. The final output of the spectrum of OPERA is on the measured earthshine grid, which is stable along an orbit but drifts with time.

The slit function retrieval and wavelength registration polynomial are optimally fit using only solar data, using the direct sun grid. There is no complementary transform of this for the newly interpolated high resolution simulation in the forward model, there is a

possibility that this might either obscure the effects of both the wavelength registration polynomial and thusly the retrieved nominal wavelength of the retrieved slit functions or introduce spurious attributes to the convolved simulated spectra. It was envisioned that either fully investigating or altering this aspect of OPERA functionality beyond the scope of this project, but could be considered in the event that OPERA fit residuals are sufficiently optimised in the region of the Huggins Bands as to make such subtle enhancements productive.

Although the impact of DISQ is small, it becomes stronger with time and does change the fit residuals and retrieved ozone under some conditions as shown in Figure 37 for 25th March 2010. Very little impact is apparent in 2007, with a steady increase amounting to up to ±3 DU integrated over the tropospheric column in places in 2010.

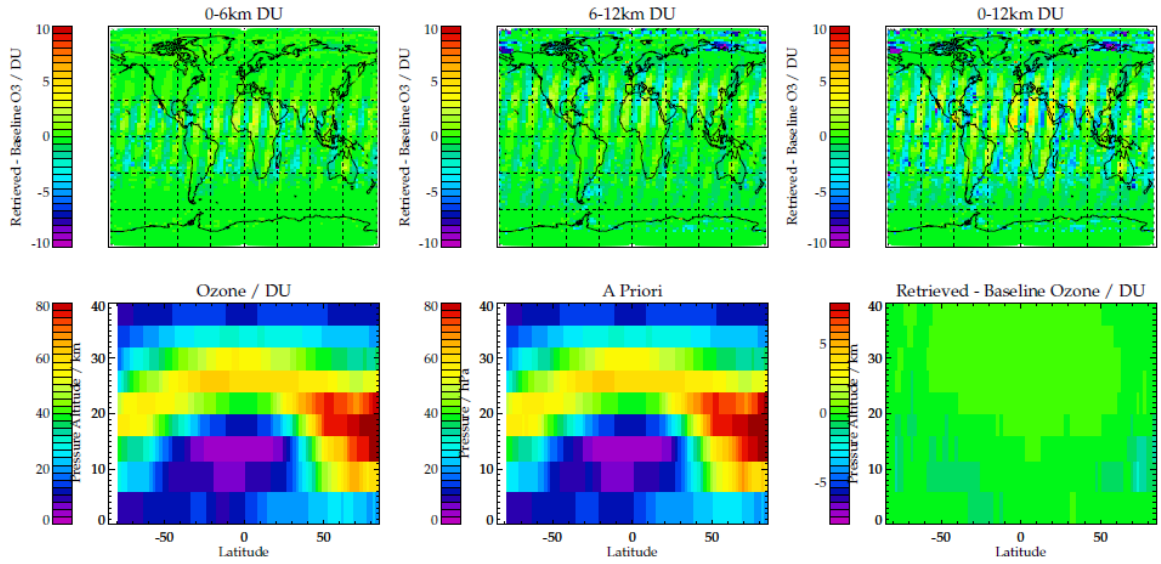

Figure 37: The top row shows sub-column maps of retrieved tropospheric ozone when DISQ is switched on, minus that retrieved by the baseline retrieval on 25th March 2010, showing differences of ±7DU in places over the tropospheric column. The bottom row shows the zonal mean retrieved ozone profiles, a priori and retrieved minus baseline zonal mean for this date degraded onto a coarse vertical resolution in order to highlight differences in retrieved ozone by summing them over a deeper layer. The east-west opposing dependency evident in the top right panel is somewhat nullified in the zonal mean profile shown in the bottom right.

The effect of DISQ is scan angle dependent, and becomes stronger with time, although this is the case for all of the modules and is conflated with the trend in the baseline residuals also. As such it is discussed in full in Section 5.5.

5.1.1 Scan angle dependency of retrieved ozone profiles

Figure 38 demonstrates how much more DISQ impacts retrieved tropospheric ozone in 2010 than in 2007. Over the 0-12km tropospheric sub-column this amounts to up to ±7DU, or 25% of a typical tropospheric sub-column amount.

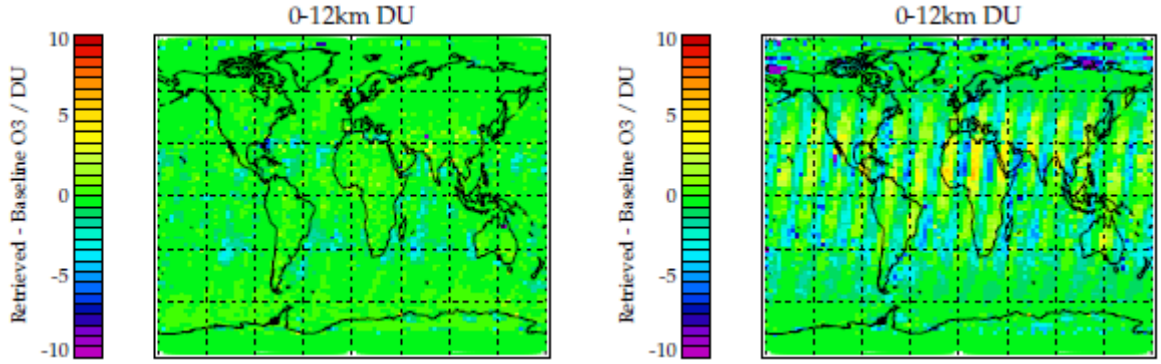

25th March 2007 **25th March 2010**

Figure 38: Tropospheric sub-column (0-12km) retrieved with DISQ implemented minus the baseline for 25th March 2007 and 2010 demonstrating the more significant impact of the change in slit function with time.

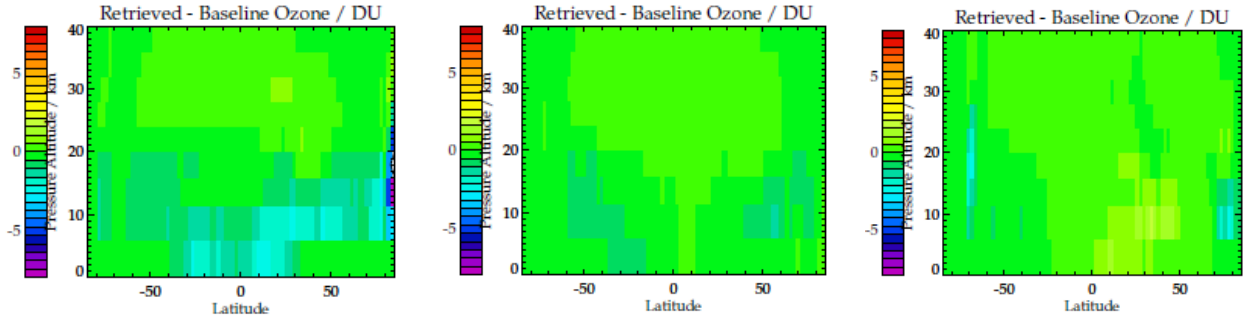

East **Nadir** **West**

Figure 39: Zonal mean cross section of ozone profiles retrieved with DISQ implemented minus the baseline zonal mean on 25th March 2010.

As shown in Figure 39 when compared to the baseline zonal mean cross section, the retrieval with DISQ implemented retrieves 2-3DU less over the 0-6 and 6-12km sub-columns in the tropics and midlatitudes. In the west pixels from 0-40°N DISQ retrieves 1-2DU more ozone over the 0-6 and 6-12km sub-columns on average. The impact of this module requires further testing against ozonesondes to establish whether the implementation of the slit function retrieval improves sonde agreement.

5.2 Degradation Correction

When implemented in OPERA the impact of the degradation correction becomes more prominent with time in accordance with increase in the predicted degradation. The meridional and vertical structure to the change in retrieved ozone profiles is shown in the bottom right plot of Figure 40. In general, the correction leads to more ozone retrieved in the stratosphere (most evident in the tropics on the date/time of year shown) and less ozone retrieved in the tropical troposphere, although this pattern is dependent upon scan angle. The change in total column is almost balanced by this opposing vertical change in ozone.

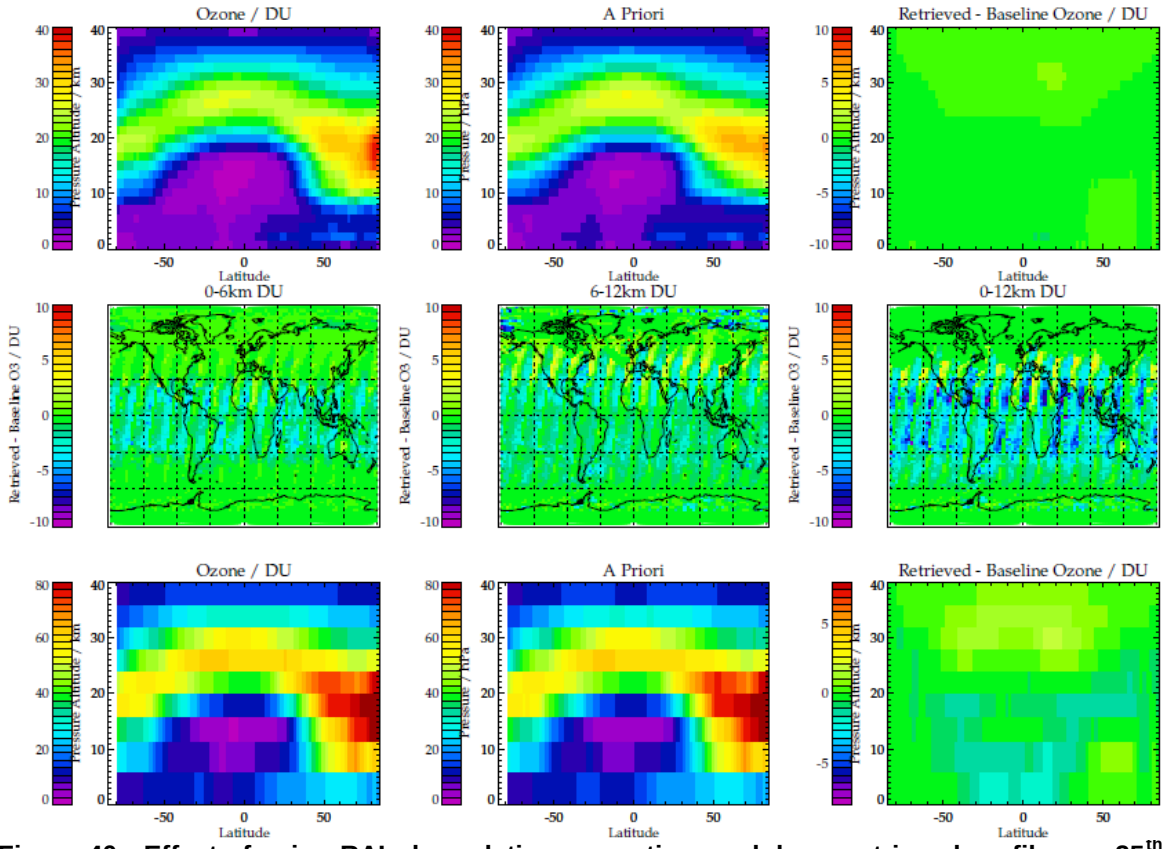

Figure 40: Effect of using RAL degradation correction module on retrieved profiles on 25th March 2010. The top row shows the retrieved ozone, a priori and difference of retrieved profile from the baseline retrieval (left to right) on OPERA vertical grid. The middle row shows this difference spatially when considering the tropospheric sub-columns 0-6 km, 6-12 km and 0-12 km (left to right). The bottom row is analogous to the top row but with the vertical resolution degraded to show the significance of retrieved sub-column differences.

There is little apparent change to the spectral residuals from the baseline but its relative impact is discussed in the context of the other prototype modules in section 5.5.

5.2.1 Scan angle dependency of retrieved ozone profiles

The zonal mean difference from the baseline for the east, nadir and west pixel retrievals is shown in Figure 41. While all three broadly show similar meridional patterns the west pixel shows an increase in mid to upper tropospheric ozone retrieved in the northern hemisphere midlatitudes. The impact of this module requires further testing against ozonesondes to ensure the degradation correction improves sonde agreement.

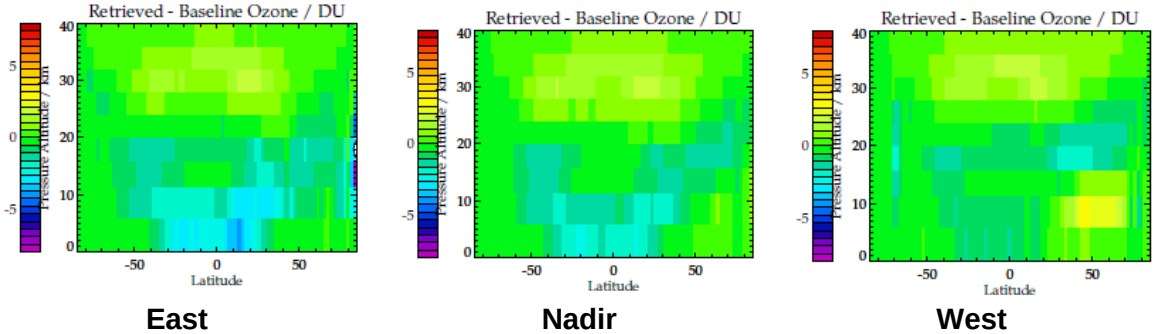

Figure 41: Zonal mean cross section of ozone profiles retrieved with the degradation correction implemented minus the baseline zonal mean on 25th March 2010.

5.3 GOME-2 Noise Model

It is evident from Figure 42 that the mean measurement noise as predicted by the RAL GOME-2 noise model is significantly smaller than that provided in the Lv1b data, more resembling a random noise estimate appropriate for optimal estimation retrievals than the full systematic and random components. Figure 42 shows the mean residuals as a function of SZA for the baseline case and where the RAL GOME-2 noise model is implemented. There is little change in the absolute magnitude of the mean residuals although the standard deviation in Band 2 is marginally narrowed.

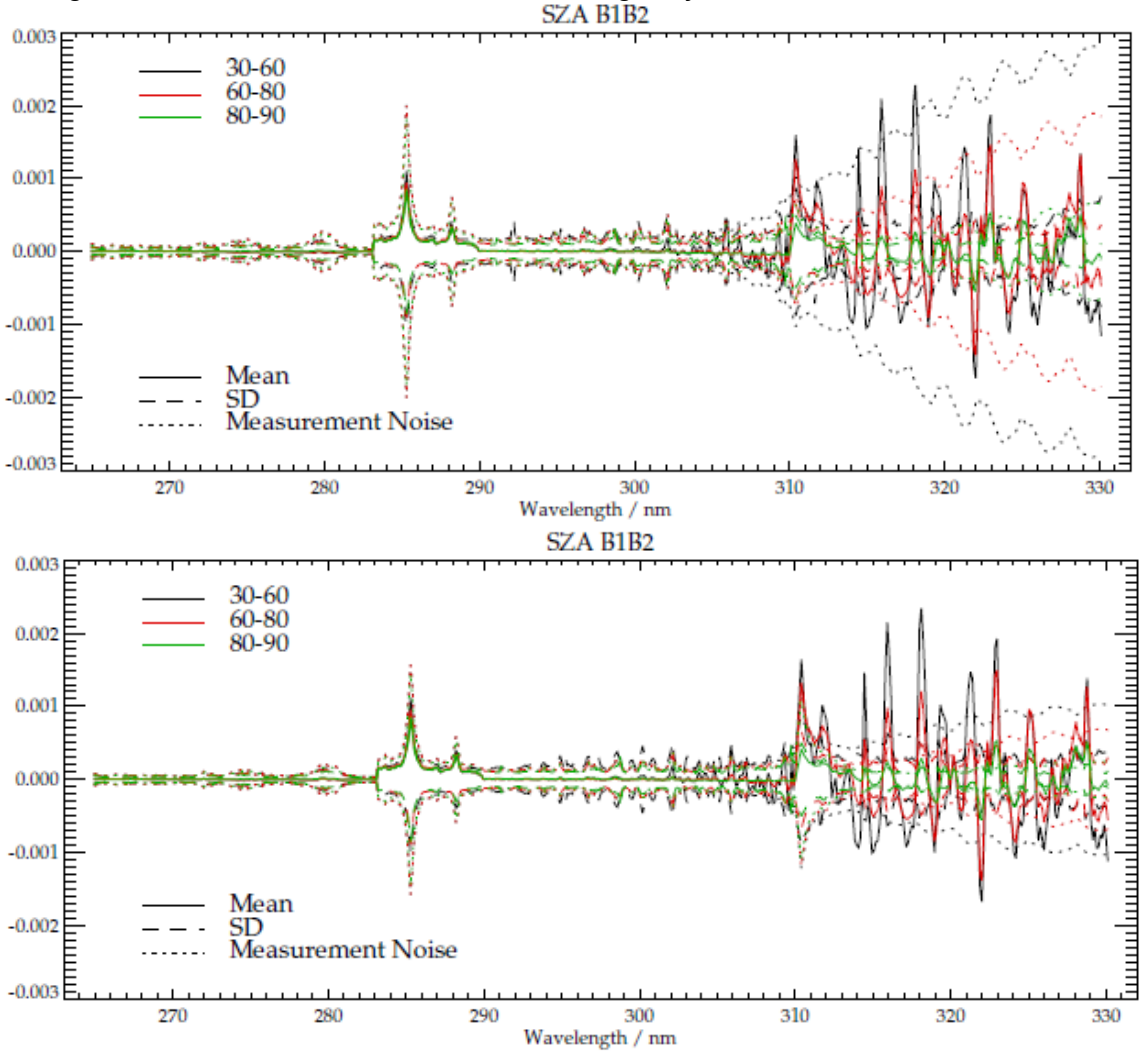

Figure 42: Mean residuals for 25th March 2010 as a function of solar zenith angle (top) and when RAL GOME-2 noise model used (bottom). The measurement noise in Band 2 is significantly smaller.

While there is only limited change to the mean fit residuals from the use of the noise model, the retrieved ozone changes significantly. Figure 43 shows the impact of the implementation of the noise model on retrieved tropospheric ozone for 25th March 2007-2010. In 2007 an increase in ozone in the troposphere is retrieved almost globally. In 2008 this pattern is less well defined, and by 2010 a decrease in tropospheric ozone is retrieved with the exception of some highly localised features of tropospheric enhancement. The impact elsewhere in the profile is shown in Figure 44, which shows the zonal mean cross section for each day. The structure is broadly the same with an

increase in ozone above 16km and a decrease below, although 2007 stands out with significantly less ozone retrieved between 16 and 24km.

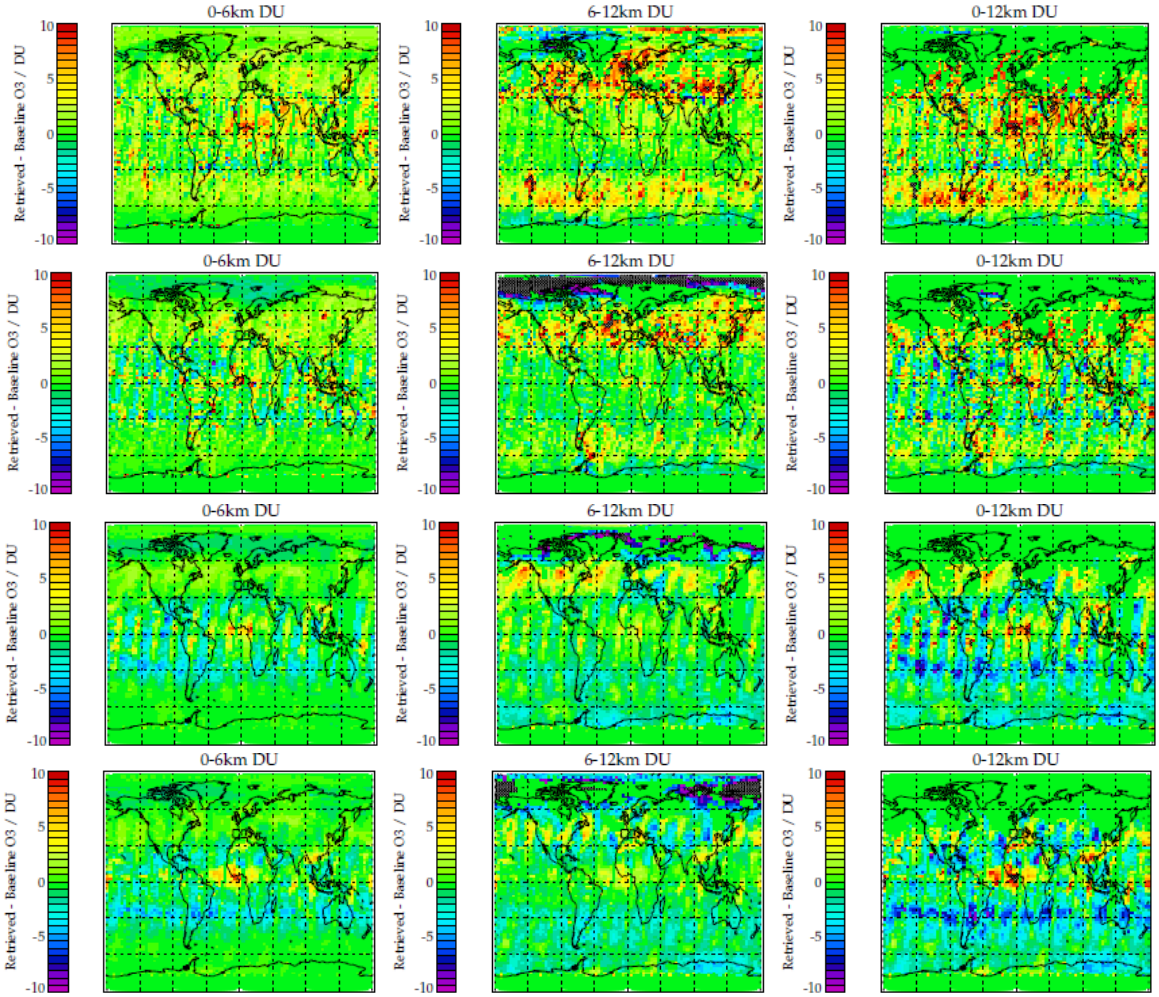

Figure 43: Impact of RAL noise model on OPERA retrieved tropospheric sub-columns (left to right 0-6km, 6-12km adn 0-12km) shown as retrieved minus baseline on 25th March 2007 to 2010 (top to bottom). Red indicates an increase in retrieved ozone, blue indicates a decrease. Black high latitude values (e.g. second row, middle panel) result from an increase in retrievals that fail to converge with the new noise.

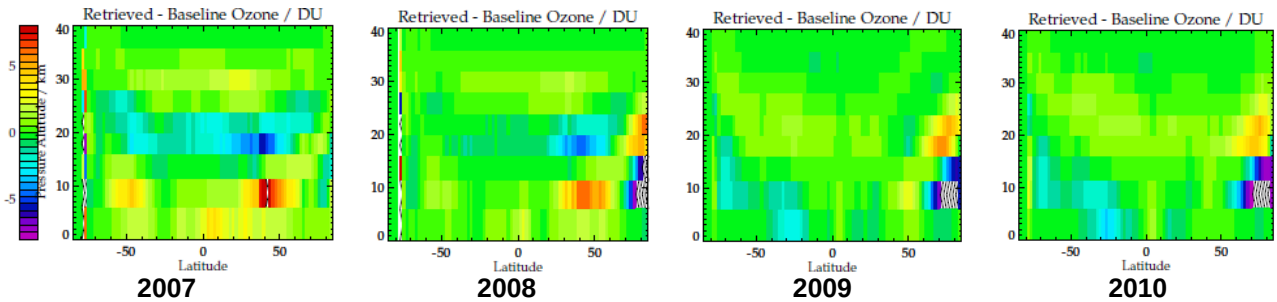

Figure 44: Impact of noise model on the zonal mean profiles (retrieved minus baseline) for 25th March 2007-2010. Cross-hatching indicates the colour scale has been exceeded.

This change in the impact on stratospheric ozone may be related to the degradation of the instrument, and further work should test the impact of multiple modules (the noise model and the degradation correction) used on conjunction.

5.3.1 Scan angle dependency of retrieved ozone profiles

Figure 45 shows the difference in the impact of the noise model over the baseline OPERA retrieval. The predominant difference occurs in the tropospheric ozone in the tropical and southern latitudes.

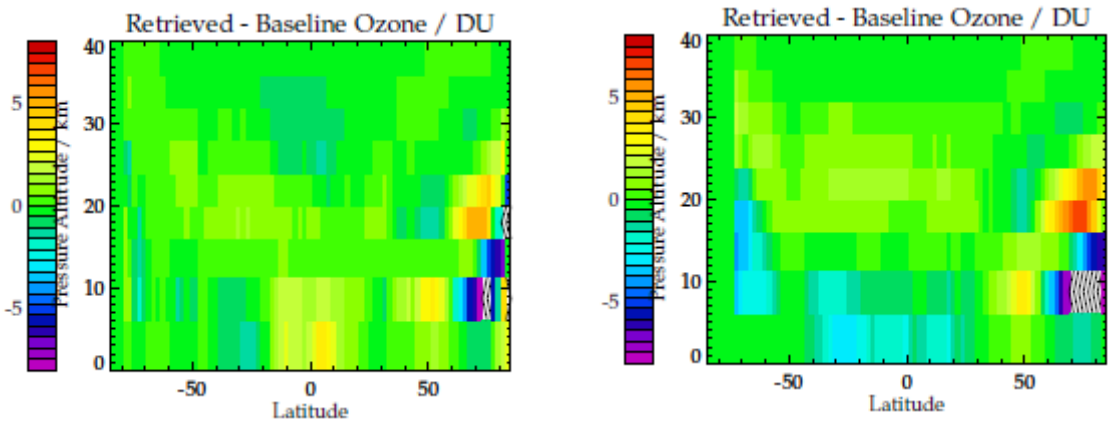

Figure 45: Difference in retrieve ozone in east and west pixels minus the baseline for the east and west pixels when the noise model is used. The OPERA vertical sub-columns have been made coarse to highlight absolute sub-column differences.

Further work should involve testing the impact of the noise model (in conjunction with other modules tested here) against sondes to investigate how the bias with respect to sondes is affected.

5.4 Raman scattering

As part of this project, a brief assessment is made of the impact of switching on existing (but computationally demanding) Raman scattering module within OPERA, alongside the assessment of the impact of the RAL prototype modules.

The Raman scattering module was written by Dr Johan de Haan at KNMI. It calculates a Raman contribution as follows. For each wavelength a radiative transfer calculation each for Rayleigh and Cabannes cross sections is performed. Then the sun normalised radiance for these two runs are subtracted for each wavelength to calculate the Raman contribution. This contribution is multiplied with a high resolution Ring Spectrum. Then a convolution with Raman lines is performed. Afterwards the two components (original Cabannes and newly convolved Raman) are brought together to form the new SNR. In the last step the viewing and solar geometry is taken into account.

The impact of the Raman scattering module predominantly affects the fit in Band 2, and shown in Figure 46. With the module switched on the size of the mean residuals becomes similar to that of the standard deviation of the fit residuals, indicating a

significant improvement of the spectral fitting. Furthermore, the standard deviation has also decreased. The fit residuals remain circa 5 times larger than those of the RAL scheme in the region of the Huggins bands, but considering that OPERA does not characterise the impact of non-modelled artefacts contributing to the mean residuals in Band 2 (as the RAL scheme does) this implies a profound improvement.

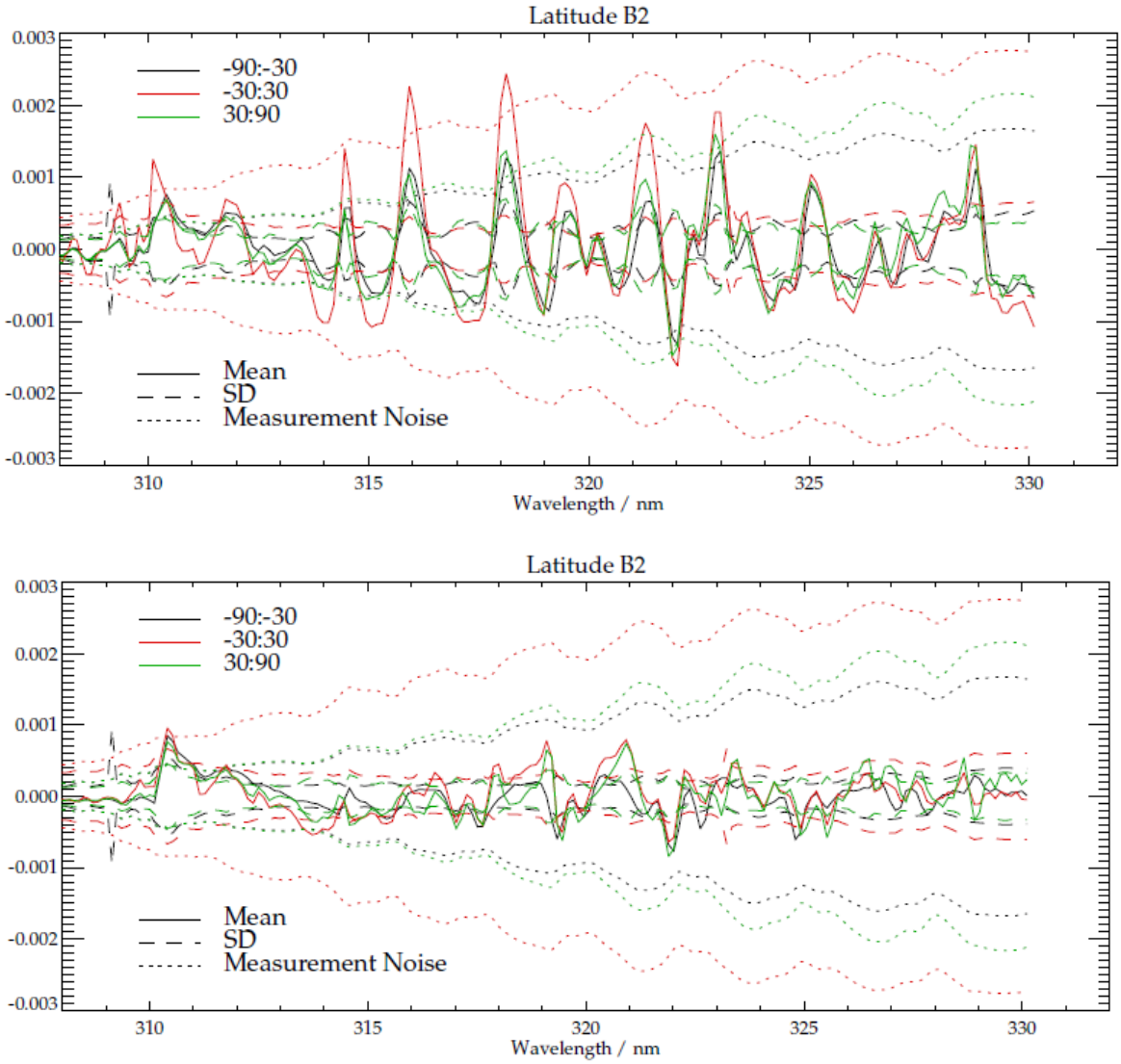

Figure 46: Mean sun-normalised radiance fit residuals in Band 2 as a function of wavelength and latitude – effect of implementing Raman scattering process in OPERA FM (25th March 2008). Both the mean residual and SD of fit residuals in Band 2 become significantly smaller.

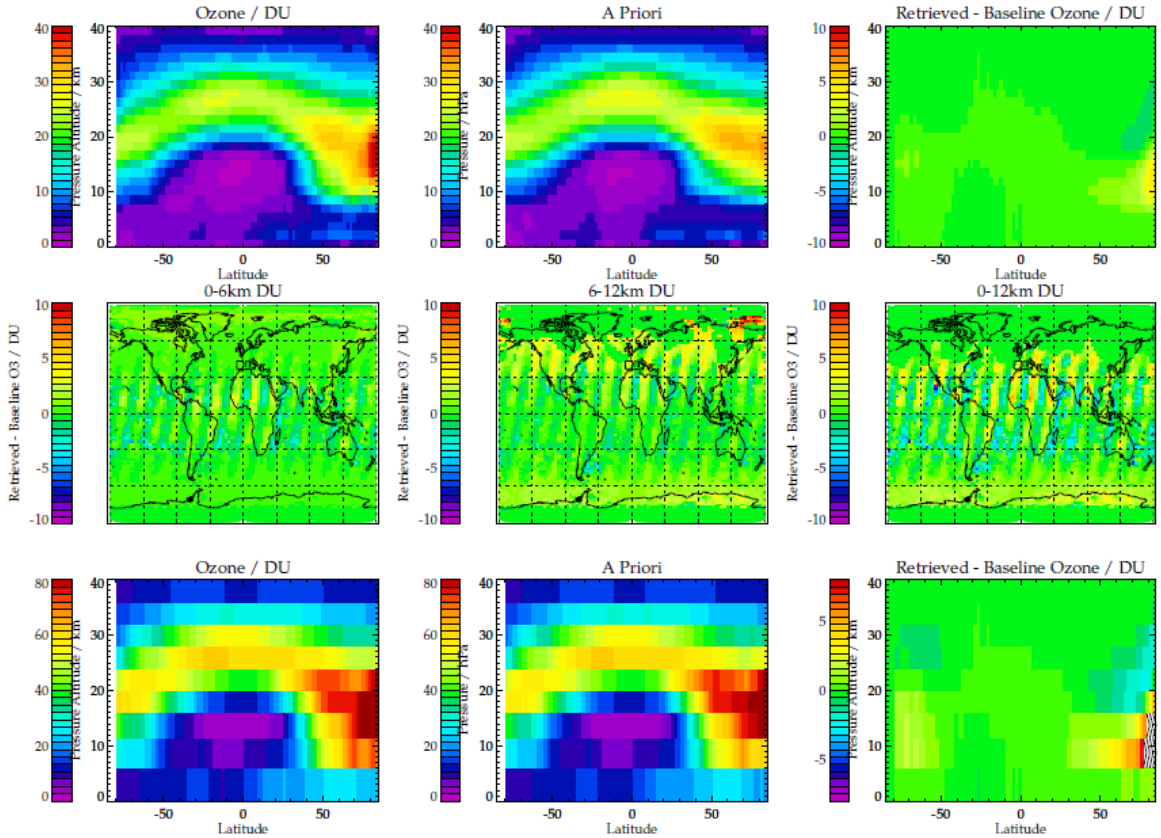

Figure 47: Effect of using full OPERA Raman scattering code on retrieved profiles on 25th March 2010. The top row shows the retrieved ozone, a priori and difference of retrieved profile from the baseline retrieval (left to right) on OPERA vertical grid. The middle row shows this difference spatially when considering the tropospheric sub-columns 0-6 km, 6-12 km and 0-12 km (left to right). The bottom row is analogous to the top row but with the vertical resolution degraded to show the significance of retrieved sub-column differences.

The impact of the Raman scattering module to the baseline retrieval by OPERA in March 2008 is characterised by an increase in ozone at high latitudes between 6 and 16km, and a decrease between 16 and 30km (although this is only at high latitudes and may be seasonally dependent) as shown in Figure 47. The impact on the tropospheric ozone increases with time. In March 2007 the difference in the departure from the prior is almost negligible (except at high northern latitudes) and is greatest in 2010. Lower ozone is retrieved at the lowest altitude (0-6km) in the tropics in 2007 and 2008, but this is only the case for the east pixels in subsequent years (as shown in Figure 48 for 2010). This behaviour with time may be related to the degradation of the instrument and as highlighted previously for the noise model subsequent testing of this module should be done in conjunction with other modules including the degradation correction and noise model.

As part of the work done at KNMI to generate this data, Dr Olaf Tuinder was able increase the speed of this function considerably which make it potentially viable for operational use.

5.4.1 Scan angle dependency of fit residuals and retrieved profiles

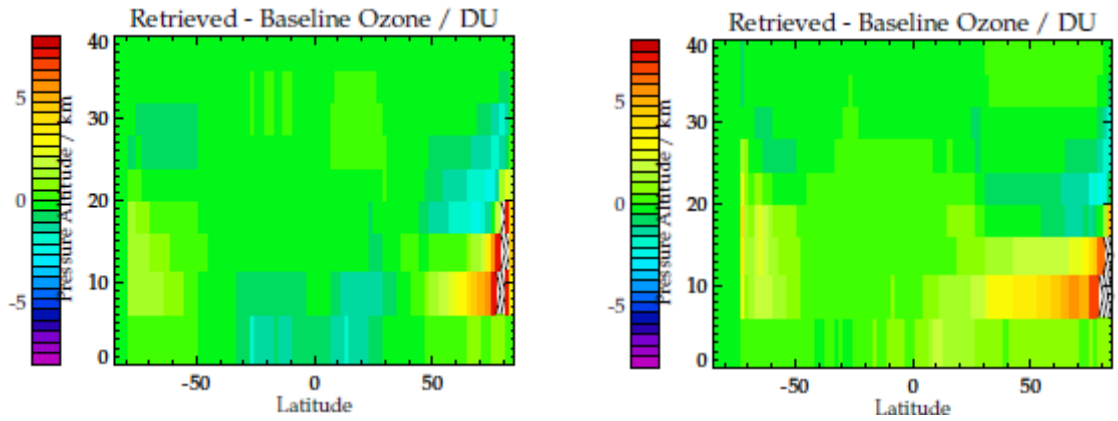

Figure 48: Difference in retrieve ozone in east and west pixels minus the baseline for the east and west pixels on 25th March 2010 when the impact is most significant. The OPERA vertical sub-columns have been made coarse to highlight absolute sub-column differences.

The overall decrease in the magnitude of the mean residuals in Band 2 is accompanied with a change in shape (the peaks and troughs) which is also reflected in the cross-track mean residuals for each Band 2 pixel. Figure 49 shows the difference from nadir of these mean residuals. The difference in the shape and overall size of the west pixels from the nadir changes very little. Most impact is seen for the eastern pixels (denoted by the lowest numbers indicated in Figure 49), and little impact is observed below 313nm. Both of these may be anticipated due to the higher degree of Raman scattering in the east-ward pixels that results from the sun-earth-instrument geometry. Improvements to the representation of the Raman scattering cross section are more likely to impact such pixels.

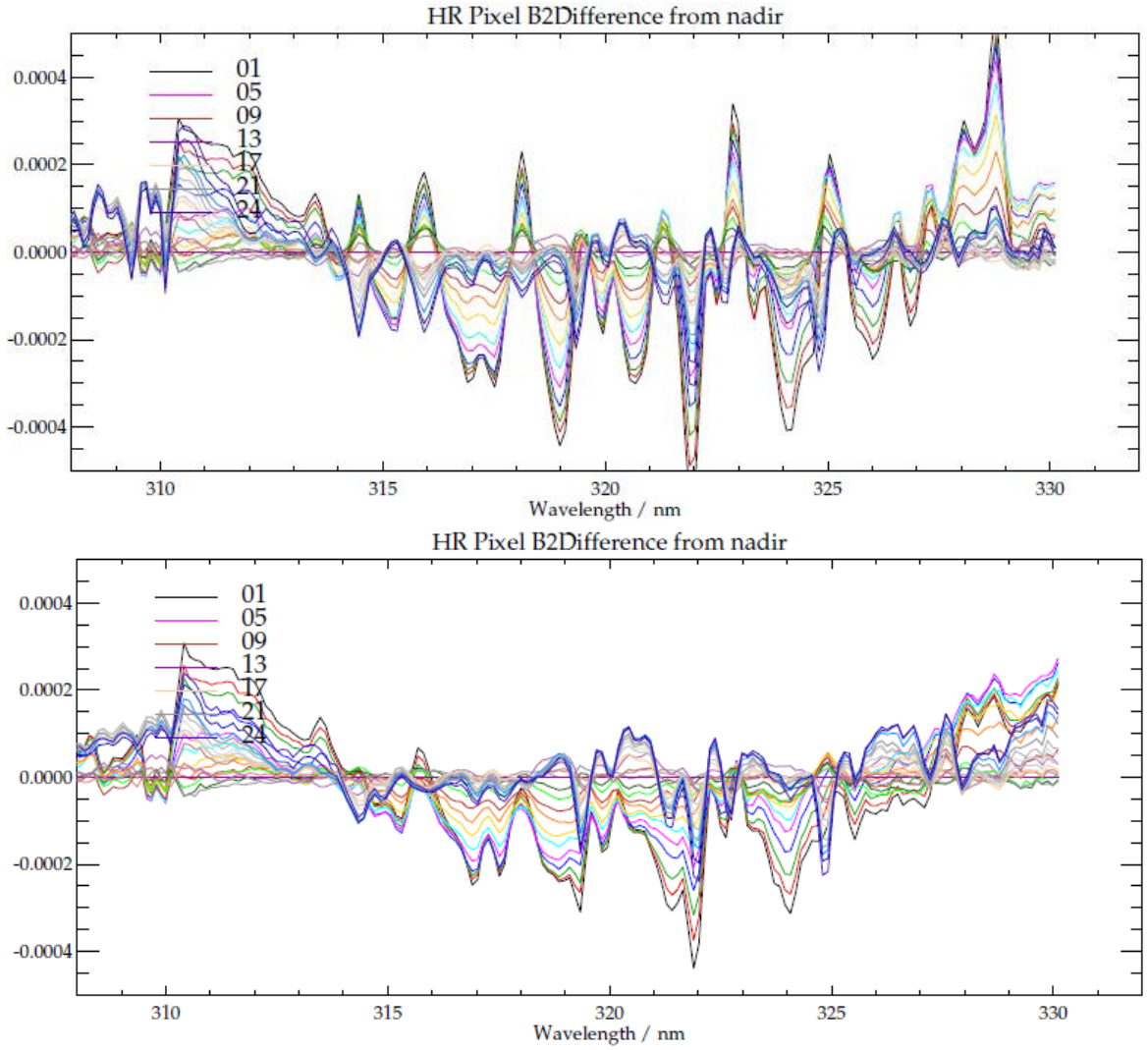

Figure 49: Mean sun-normalised radiance fit residuals in Band 2 as a function of cross-track position differenced from that of nadir scan position from baseline (top) and the effect of implementing Raman scattering process (bottom) in OPERA FM on 25th March 2008.

5.5 Relative impact of prototype modules

Figure 50 and Figure 51 show the retrieved minus the baseline mean residual for 25th March 2007 and 2010 for each of the modules (noise model, degradation correction, DISQ and the Raman scattering). The module that has the most significant impact on the size of the fit residuals is that of the Raman scattering. The impact of the RAL modules on the fit residuals is small in 2007, as is their general impact on retrieved ozone for the most part, but both increase in amplitude with time. Figure 50 shows the mean residuals for the extreme eastern Band 2 across track pixel, and Figure 51 the western most. As shown in Figure 23 there is a trend in the mean fit residual from 2007 to 2010, and this trend is scan angle dependent. This is reflected in the shape of the difference of the mean fit residuals derived from module fits from the baseline but make their overall shape shape more difficult to interpret.

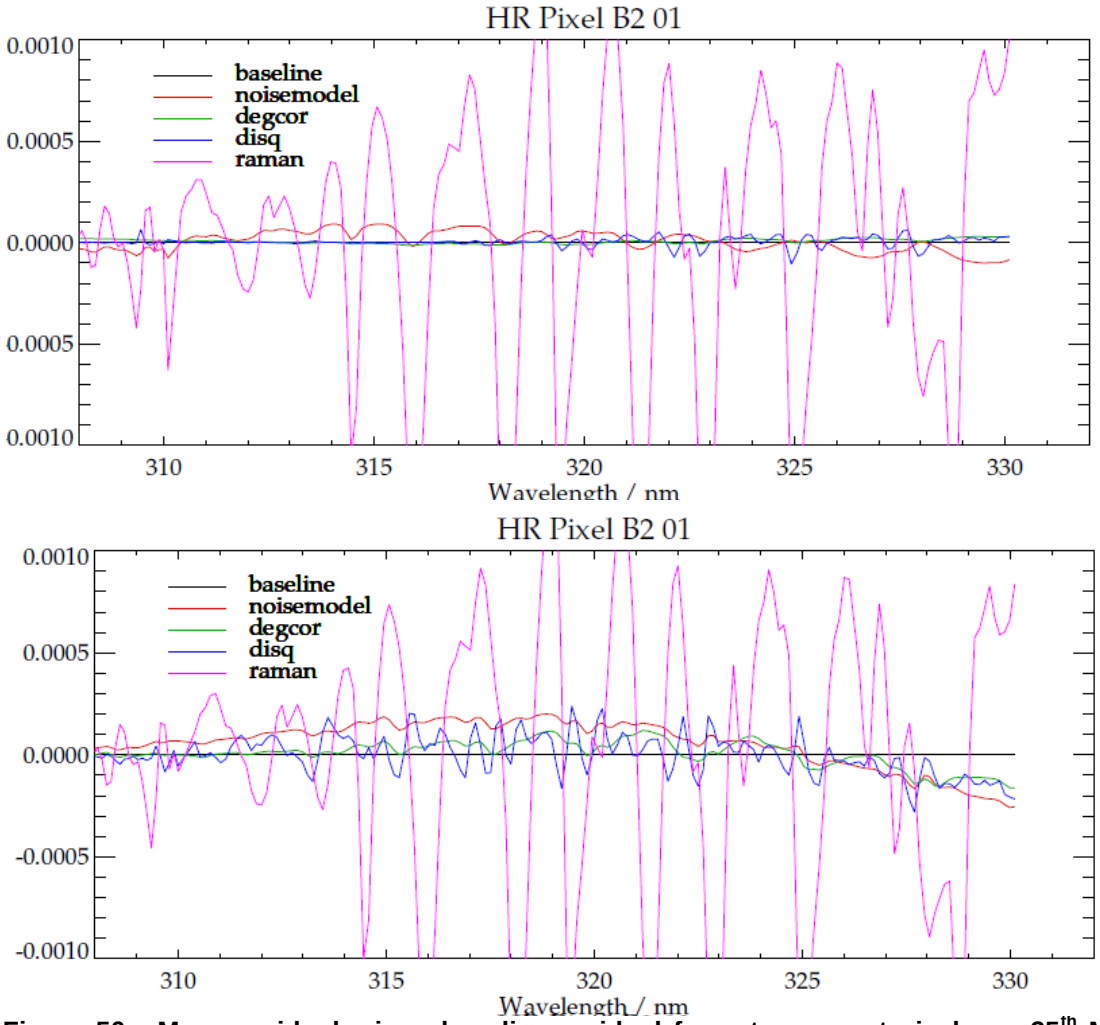

Figure 50: Mean residual minus baseline residual for extreme east pixels on 25th March 2007 (top) and 2010 (bottom). The effects on the mean residuals from the Raman scattering model are most significant. Those resulting from the RAL modules are small in 2007.

The impact of some of the test modules on the retrieved profiles can on occasion be of opposing sign (e.g. Figure 45 and Figure 48 which show the impact of the noise model and Raman scattering respectively). Many of these mechanisms will have inter-related influences on the retrieval and as such must be tested in conjunction. It is a necessary step however to have tested each module individually to ascertain the nature of their impact. The modules with the most significant impact on retrieved tropospheric ozone were the noise model and the degradation correction. The Raman scattering had most impact where most Raman scattering events occur – in the eastern side of the swath and with large total ozone slant columns as observed in northern hemisphere spring. The impact of the slit function retrieval and wavelength registration (DISQ) was small in 2007 but became notable in 2010, with opposing effects on retrieved tropospheric ozone in the east and west pixels but still with little impact in the nadir. Also by 2010 the amplitude of difference to the mean fit residual is second only to the Raman scattering module.

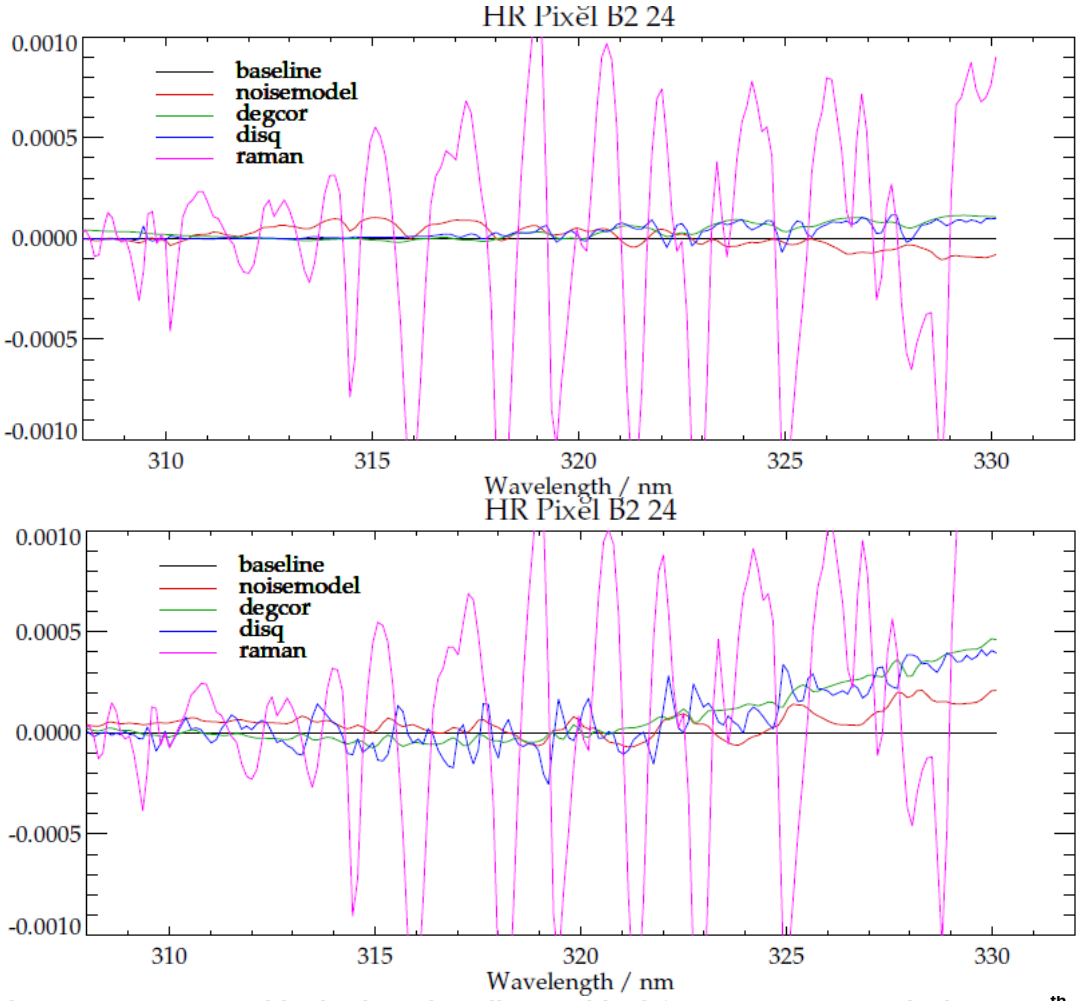

Figure 51: Mean residual minus baseline residual for extreme wast pixels on 25th March 2007 (top) and 2010 (bottom). The effects on the mean residuals from the Raman scattering model are most significant. Those resulting from the RAL modules are small in 2007, but increase with time.

5.6 Further work to be considered

It is generally recommended that all four modules examined in this report are individually tested against ozonesonde profiles to quantify their impact and determine whether or not they improve sonde agreement, both in the troposphere and stratosphere. There was not sufficient time remaining in this project for these OPERA runs to be either completed or examined. Based on the performance against sondes they could be considered for inclusion in the Operational scheme.

It is further recommended that these modules are evaluated in combination since some aspects of their function may be enhanced or suppressed depending upon each other. At this point further testing of the scheme performance against sondes would be desirable.

Extending the prototype runs (in combination) over multiple days in the year to capture the impact upon seasonal changes in ozone globally should be done to ensure the effects of the modules are understood both spatially and with time.

It is also suggested that once the fit residuals in Band 2 have been reduced (such as with the Raman scattering code and additionally the RAL modules), that a study is performed into relaxing the prior error in the troposphere and lower stratosphere to enable the retrieval to potentially make use of more information from the troposphere. Consideration would have to be given to ensuring that the rate of convergence is not adversely impacted, that oscillations do not begin to feature in the retrieved profiles (which could be suppressed with regularisation) and that the computation time for OPERA does not become non-compliant with the operational demands. Should all of these things be achieved, it is likely that the total information content and tropospheric profile/product from OPERA could improve significantly.

6 Assessment of potential for GOME-2 Chappuis band observations to provide improved tropospheric ozone retrievals

6.1 Introduction

GOME-2 measurements in the Chappuis bands (from ~440 - 750nm) are not currently used to retrieve ozone information either experimentally or operationally. The potential advantages of using the bands are well known [Chance et al., 1997]: sensitivity to ozone near the Earth's surface from the traditionally used Huggins bands is limited by the typically low surface reflectance and Rayleigh / aerosol scattering. In the Chappuis range, the albedo over land is typically larger and Rayleigh scattering much reduced, so that a larger proportion of the observed photons will have passed through the lowest atmospheric layers.

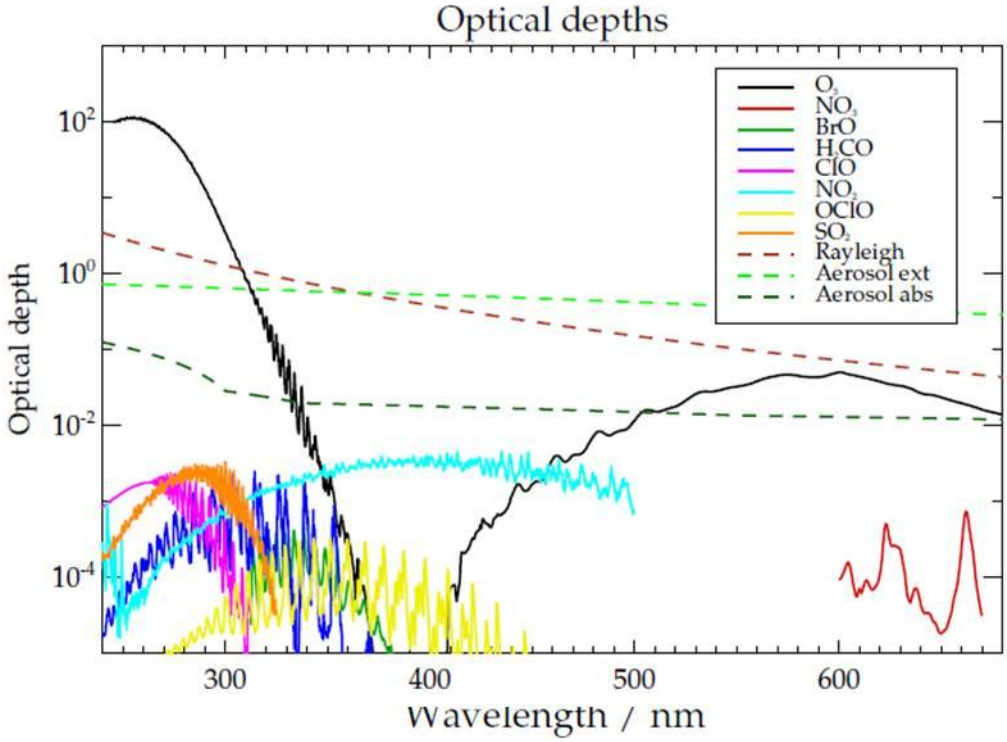

Figure 52: Optical depth as a function of wavelength for absorbing trace gases. The Huggins and Chappuis ozone bands are shown in black from 305-360nm and 410-650nm respectively.

This differential sensitivity between the two bands introduces the potential to resolve lower tropospheric ozone, provided the Chappuis bands can be fitted sufficiently accurately. However this condition is not simple to satisfy. Extracting the signal from the Chappuis bands (see Figure 52) is complicated by the fact that the amplitude of differential structures (which are exploited by DOAS techniques) are relatively low and have are relatively broad band structure compared to the features in the Huggins bands. Such features may be easily confused with a number of other effects e.g. instrumental artefacts (such as polarisation sensitivity, aliasing of spatial/spectral structure due to non-synchronous detector pixel read-out) and spectral variations in surface reflectance. In addition there are contaminating spectral features from water vapour (H_2O), oxygen dimer (O_4) and nitrogen dioxide (NO_2). Although Rayleigh scattering is reduced, the Ring effect (due to inelastic scattering by air molecules) is still significant. Inelastic scattering at the ocean surface is also important over sea, although in conditions where this is important, the information content of the Chappuis bands is less useful (as the ocean surface reflection is very low).

Here we have conducted a small study to review the potential for overcoming these difficulties such that GOME-2 Chappuis measurements can be used to provide improved information on tropospheric ozone.

The assessment is performed in two parts:

1. Profile retrieval simulations are performed to quantify the potential benefit of using the Chappuis bands for tropospheric ozone retrieval. In these simulations the information content is assessed via a full profile retrieval in which measurements from the Hartley, Huggins and Chappuis bands are inverted simultaneously. It is however noted that the Chappuis bands only provide a single piece of information on ozone, and so it would be equivalent (and more computationally convenient) to

independently retrieve the ozone column considering the Chappuis bands alone and use this column (together with errors and averaging kernel) as a "virtual measurement" in an existing UV height resolved ozone retrieval. We use these simulations to determine the precision required on the Chappuis column to provide useful additional information to a UV profile retrieval.

2. A retrieval scheme is developed to retrieve ozone column amounts from real GOME-2 Chappuis band measurements. The accuracy of retrieved columns from this scheme is compared to the requirements derived in Part 1.

6.2 Modelling surface reflectance

To satisfactorily fit the Chappuis bands, it is crucial to realistically model spectral variations in surface reflectance. Here we model surface reflectance in terms of principle components of a large set of laboratory and field measurements of a range of surface types. Spectra are obtained from two databases. The ASTER spectral library [NASA (1999), Baldridge et al., (2009)] is a compilation of over 2400 spectra of both man-made and naturally occurring materials. The USGS Spectral Library [Clark, 2007] comprises measured spectral reflectance of hundreds of minerals as a reference for the purposes of mineral identification by remote sensing. There are several versions of this database that contain different information, such as instrument-specific spectral libraries for terrestrial and planetary spectrometers as well as enhanced data for mineral grain sizes and organic compounds.

In both the retrieval simulations and the real retrievals the coefficients of the first 7 principle components of the complete set of spectra (from both spectral libraries) are fitted along with ozone and other parameters.

6.3 Retrieval simulations

The retrieval simulation scheme developed for the ESA Camelot study [Veefkind, 2009] has been extended to include Chappuis bands. Retrieval simulations are carried out for a range of surface reflectance scenarios (defined for Camelot) and for a range of assumed signal to noise ratio in the Chappuis bands. In all cases nadir viewing geometry is assumed, with a solar zenith angle of 30°. Results are also generated for two atmospheric conditions, the Camelot European and Tropical background cases. Results from two spectral ranges are shown here 410-750nm (i.e. including the entire Chappuis bands) and 450-550nm, a range selected [Richer, EGU 2012].

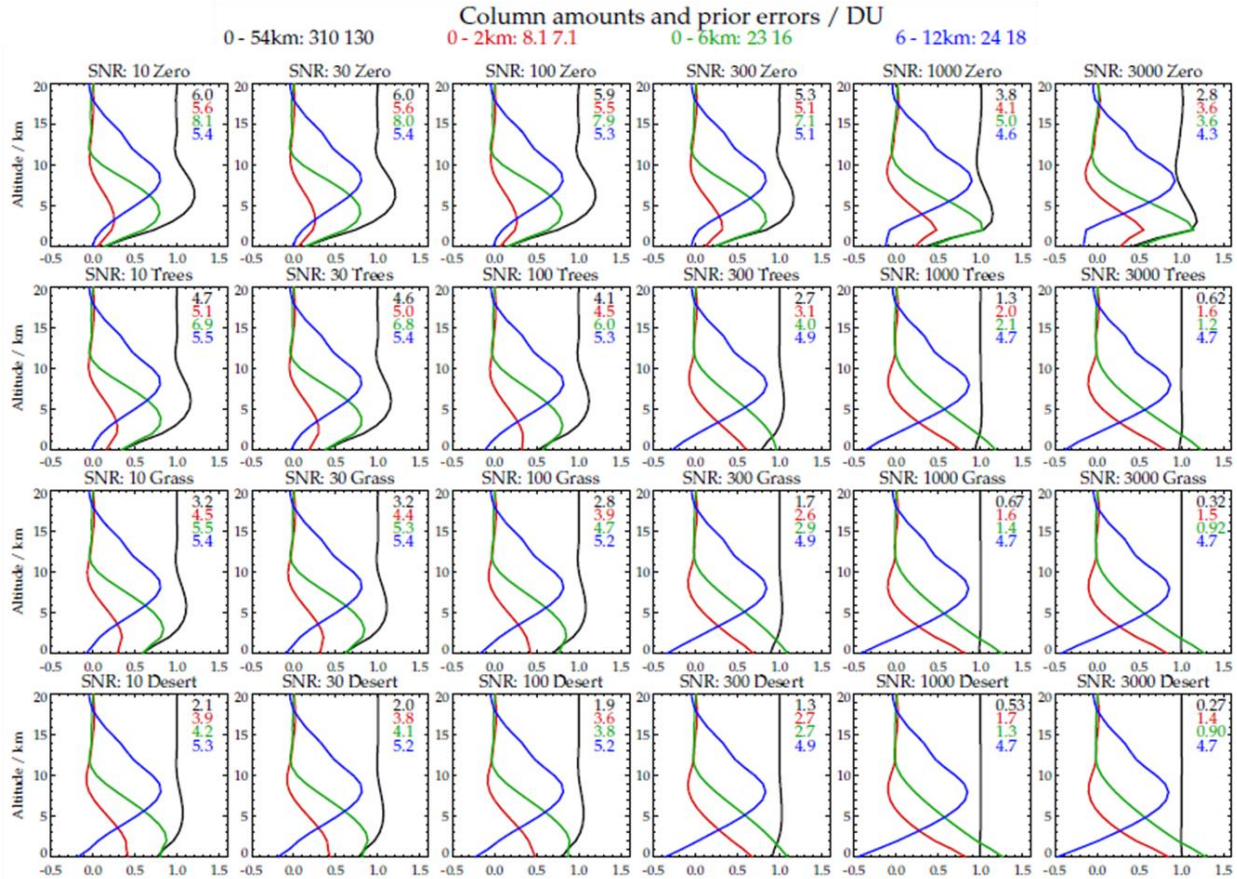

Figure 53: Simulations of averaging kernels using UV+Chappuis bands (GOME-2 channels 1, 2, 3 and 4) for a variety of Chappuis signal to noise conditions (increasing across columns) and surface types (top row no reflectance in Chappuis region, trees, grass and desert) for a European climatological ozone profile using wavelength range specified in Richter et al.,(2011). Black, red, green and blue denote sub-column averaging kernels for total column, 0-2 km, 0-6 km ad 6-12 km respectively. Coloured numbers within panels denote equivalent error on sub column in DU. Coloured header denotes sub-column prior and prior error.

Figure 53 shows averaging kernels using the full range for European Background conditions. Panels from left to right show results for increasing assumed signal to noise ratio in the Chappuis bands. Panels from top-bottom show results for different surface conditions as indicated in the caption. In all cases the standard RAL GOME-2 ozone scheme is assumed for the Hartley and Huggins bands, with noise as predicted for Sentinel 5 (comparable to the performance of GOME-2). Each panel shows averaging kernels for 4 layer amounts: Total column (0-54km), boundary layer (0-2km), lower tropospheric (0-6km) and upper tropospheric (6-12km). Kernels are shown with respect to fine scale (1km resolved) perturbations in the true profile and are normalised such that the ideal response for a perfect retrieval would be 1 in the relevant layer and 0 outside. In each panel printed figures show the estimated standard deviation (ESD, the square-root diagonal of the solution covariance matrix) for each sub column (in DU).

The capability of the Chappuis bands to enable the lower atmosphere to be more sharply resolved is clearly shown, particularly for the land surface types. With the Chappuis bands it would become possible to meaningfully retrieve a distinct boundary layer ozone column.

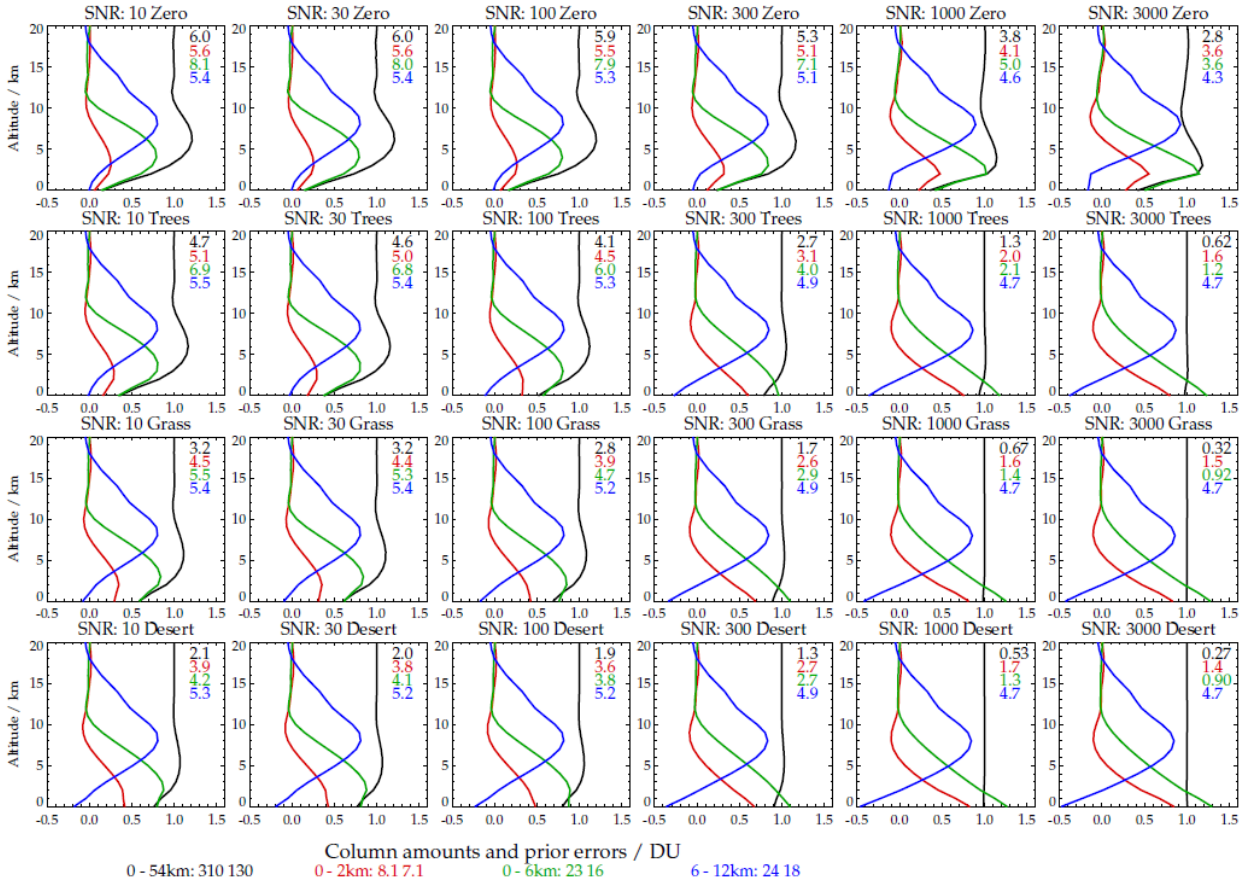

Figure 54: Simulations of averaging kernels using UV+Chappuis bands (GOME-2 channels 1, 2, 3 and 4) for a variety of Chappuis signal to noise conditions (increasing across columns) and surface types (top row no reflectance in Chappuis region, trees, grass and desert) for a European climatological ozone profile using only 450-550nm. Black, red, green and blue denote sub-column averaging kernels for total column.

Figure 54 shows analogous results for the 450-550 nm range. We now focus on results for this range as (a) it is far more likely that real retrievals can be made to work over this restricted range of GOME-2 band 3 than over both bands 3 and 4 (b) the results for the restricted range indicate good improvement can be made at plausible signal to noise values. It would seem that the Chappuis bands begin to contribute strongly to reduce the ESD of boundary layer and lower tropospheric column at about a signal to noise level of 300 for the reduced range and 100 for the full range.

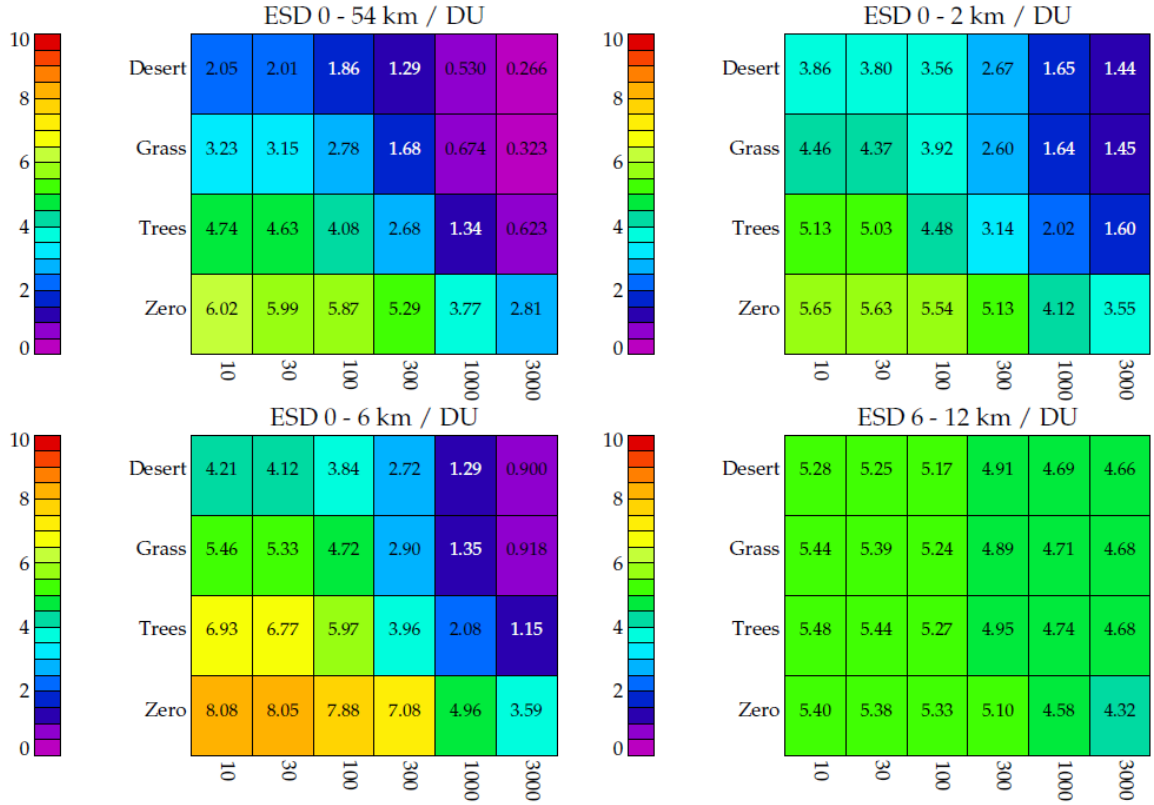

Figure 55: Simulations for sub-columns demonstrating the improvement in sub-column retrieved error for increased signal to noise and brightness of surface type for a European profile.

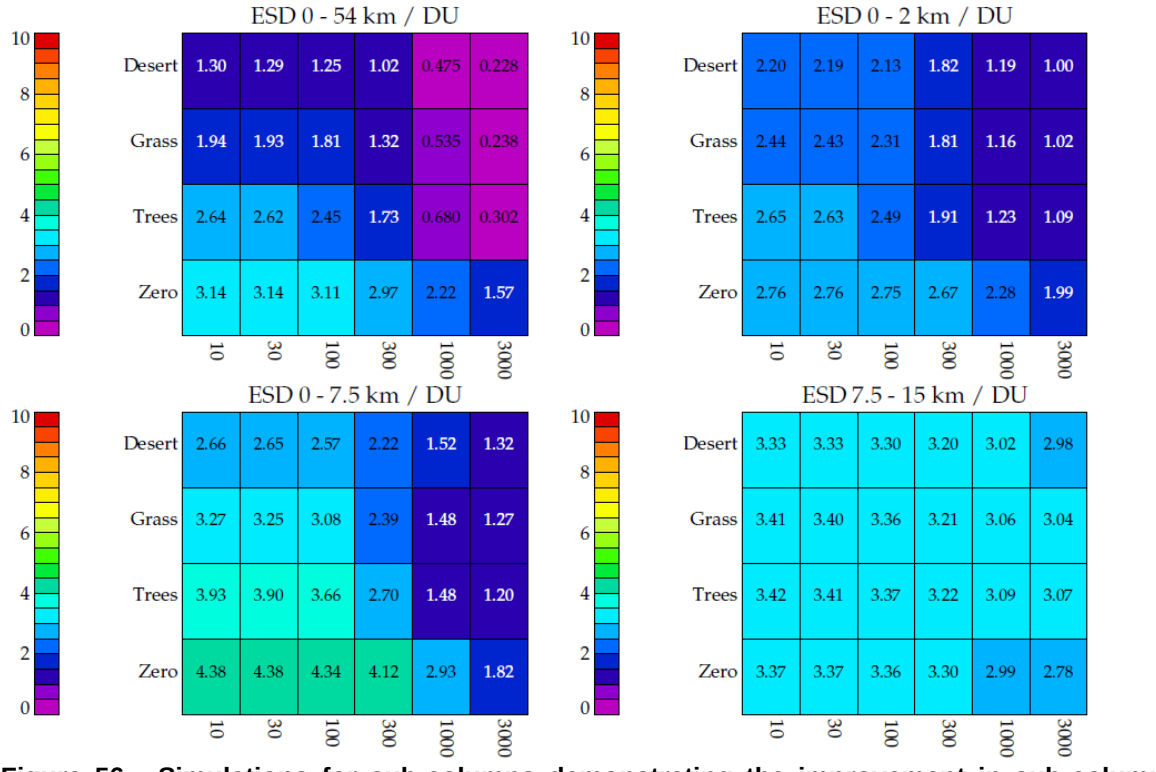

Figure 56: Simulations for sub-columns demonstrating the improvement in sub-column retrieved error for increased signal to noise and brightness of surface type for a tropical profile.

Figure 55 and Figure 56 summarise the ESDs in coloured tables for each column amount for the two atmospheric scenarios, for the restricted wavelength range.

Figure 57 shows the estimated total column ESD if only the restricted range is used and the UV bands are excluded. This indicates that the "breakthrough" signal to noise value of 300 corresponds to a Chappuis band only total column ESD of 2-4DU. I.e. a total column measurement from the Chappuis bands with a precision in this range could be expected to lead to a significant improvement in lower tropospheric ozone when used as a constraint in UV profile retrieval. A similar estimate of the required precision on Chappuis total ozone is reached analysing results analogous to those shown in Figure 57 for the full spectral range.

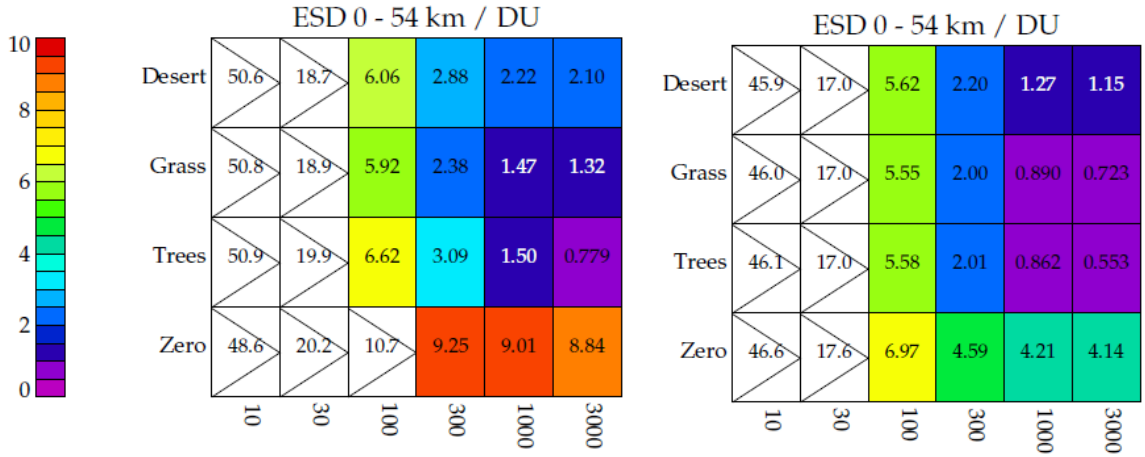

Figure 57: Estimated column ESD using only restricted wavelength range (i.e. no UV, Chappuis only) for a Eurpean (left) and tropical (right) profile.

6.4 Real retrievals

Real retrievals on GOME-2 data have been attempted. Results here are illustrated for the test day of 2 August 2008. These retrievals are mainly aimed at identifying the fit precision which can be achieved so are simple DOAS retrievals in which the measurement is the logarithm of the sun-normalised radiance. In this case, the fit is based on sun-normalised radiances for the averages of 4 neighbouring detector pixels. I.e. the GOME-2 sampling is degraded by a factor of 4 (to a resolution and sampling of 0.8nm). This is done bearing in mind that the main target ozone absorption features are relatively large and with the intention of minimising the potential for the fit to be degraded by much finer spectral features, which might be caused by wavelength calibration error, slit function errors, under-sampling etc. Sun-normalised radiance is estimated by ratioing the 4 pixel spectrally co-added radiance and irradiance spectra. After quite extensive experimentation, the following parameters are included in the fit:

- 3rd order polynomial coefficients.
- Ozone slant column (assuming Brion-Malicet cross-sections [Daumont et al., 1992; Brion et al., 1993; Malicet et al., 1995])
- O_4 slant column, assuming absorption cross sections defined in [Rozanov *et al.*, 1997]
- NO_2 slant column, assuming absorption cross sections defined in [Rozanov *et al.*, 1997]
- H_2O slant column assuming a mean absorption cross section.

Note the H_2O spectral signature cannot be simply explained by an absorption cross section, as it consists of optically thick line absorption features which are temperature and pressure dependent. Here we compute transmissions due to water vapour using the Oxford Reference Forward Model for the set of 83 profiles database of temperature and humidity profiles which have been developed by ECMWF to train the RTTOV model [http://research.metoffice.gov.uk/research/interproj/nwpsaf/rtm/]. A cross section is derived from the mean transmission spectrum, $\bar{T}(\lambda)$, as follows:

$$\bar{X}(\lambda) = \frac{-\log\left(\bar{T}(\lambda)\right)}{n_{H2O}}$$

Equation 6

where n_{H2O} is the mean total column amount of H_2O.

- To explain spectral variations in the H_2O line features we also fit scale factors for the dominant 2 singular vectors of the difference between the individual 83 transmission spectra and the mean.
- A wavelength shift of the water vapour absorption cross section is also fitted.
- Scale factor for the liquid water absorption spectrum [Pope and Fry, 1997]
- Wavelength shift of the solar spectrum with respect to the earth back-scatter spectrum (offset and linear drift in the band).
- Air molecule Ring effect scale factor (offset and linear trend across the band).
- Scale factors for the dominant 7 singular vectors of the surface spectra database (see above).

Note that all parameters are fit in a straightforward least squares manner. A third order polynomial is subtracted from all patterns (other than the fitted polynomial patterns).

All spectra patterns are defined at the full GOME-2 resolution, then convolved with the slit function key-data (derived by RAL) and then the 4 pixel co-adding is applied. The spectral patterns associated with each of these fit parameters are shown in Figure 58.

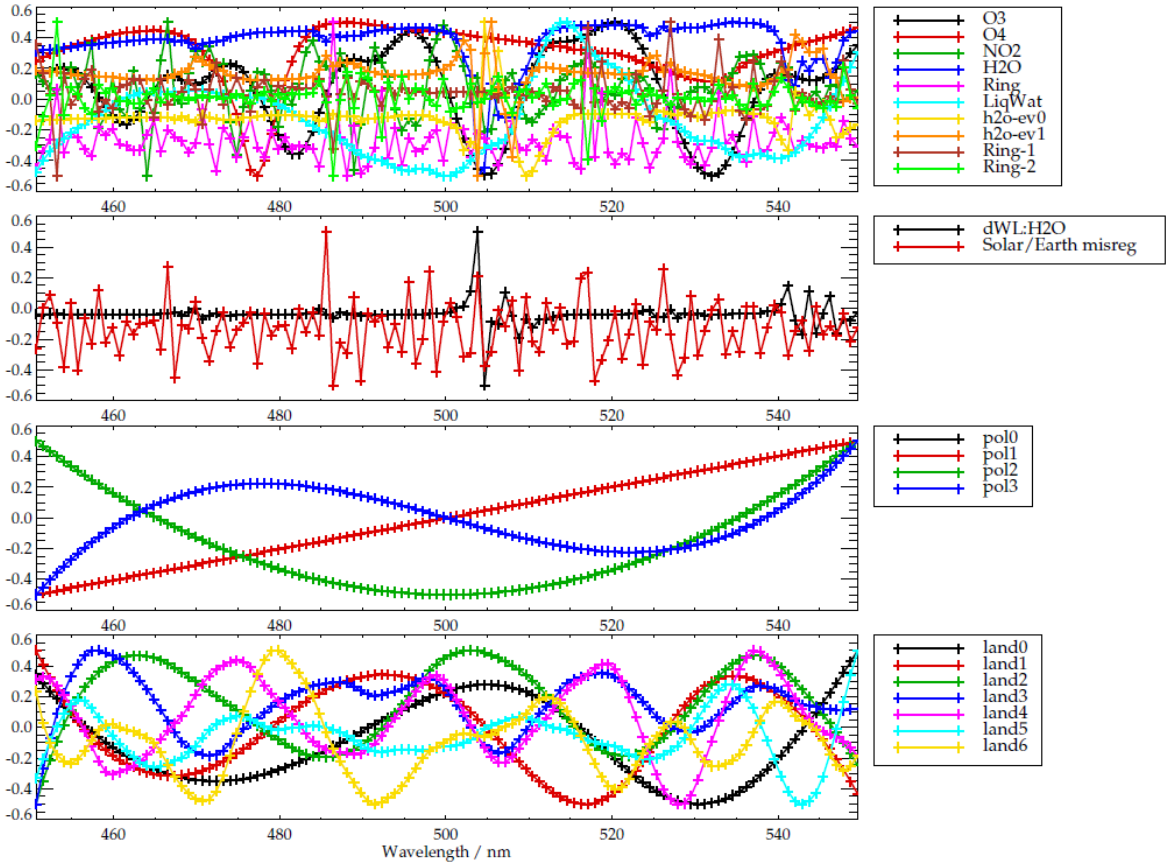

Figure 58: Spectral patterns associated with Chappuis fit parameters

Results from the fit are illustrated in Figure 59. For plotting purposes, retrieved slant columns are converted to total column using the geometric air-mass factor. In all cases only descending node data are shown (to avoid confusing structures due to overlapping orbits at high latitude).

The top panel of Figure 59 shows the sun-normalised radiance at 500nm. This clearly indicates the presence of cloud, useful for correlating with structures in other retrieved products. The centre panel shows the standard deviation of the resulting fit residual spectrum (in sun-normalised radiance units, i.e. the DOAS residual multiplied by the measured sun-normalised radiance). These are generally larger where the radiance itself is larger.

Figure 60 shows a statistical analysis of the residuals, showing the mean over land and sea from all locations, and the standard deviation of that mean at each spectral point. The bottom panel shows the scatter density of the RMS spectral residual as a function of the square-root of the mean measured reflectance. In the case that photon noise is the limiting mechanism for the fit residual, this would be expected to be a straight line. In this case it appears that the fit residuals (though small) have a systematic component with amplitude approximately proportional to the mean sun-normalised radiance. At the minimum sun-normalised radiance (0.04) the RMS fit residual is around 0.00004, i.e. a signal to noise of around 1000. For a relatively bright scene with sun-normalised radiance 0.64 (0.8^2), the RMS residual is ~0.0004, corresponding to a signal to noise of around 1600.

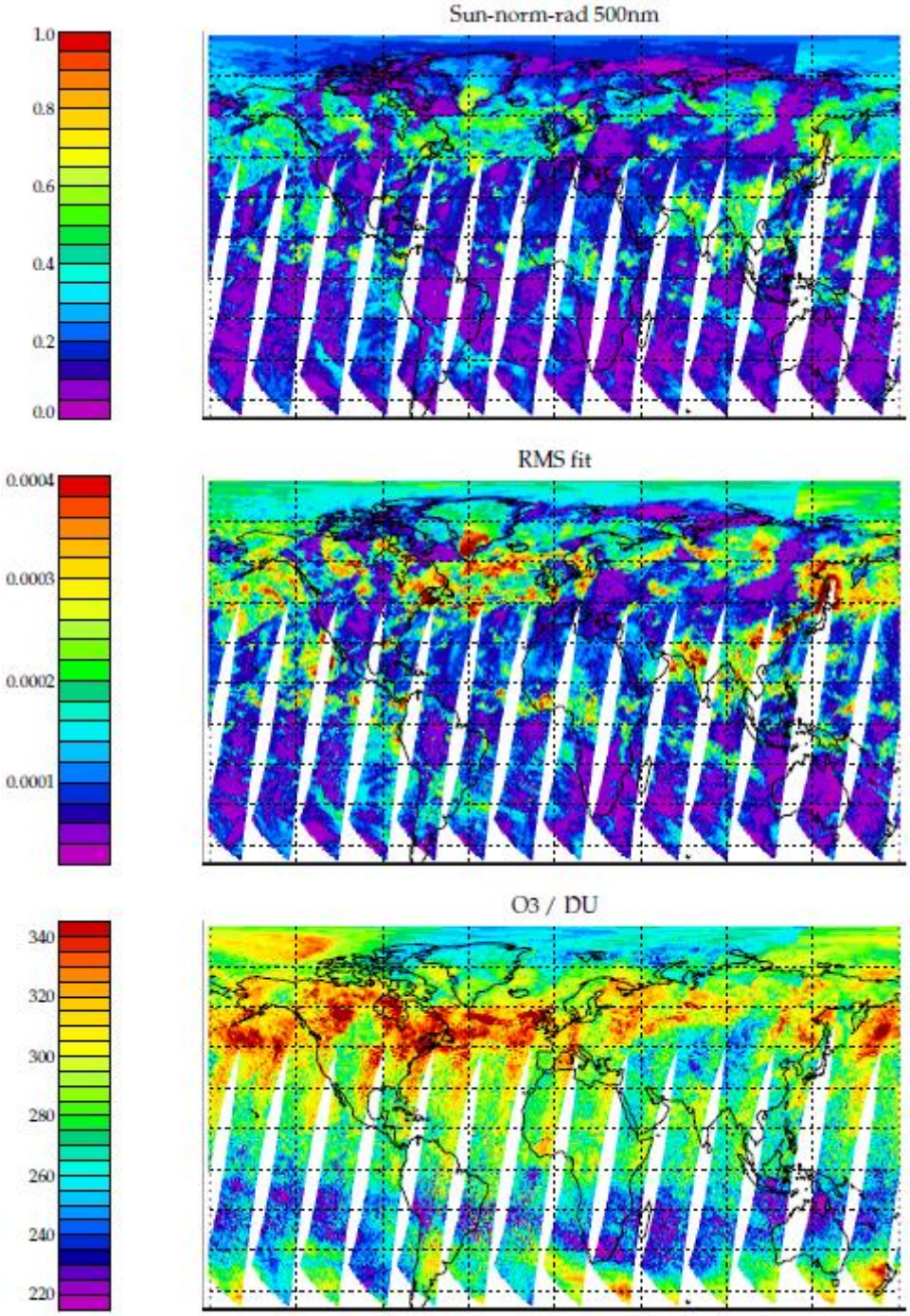

Figure 59: Sun normalised radiance at 500nm (top), RMS of fit residual in Chappuis fitting window (middle) and retrieved total column ozone just using the Chappuis bands (bottom)

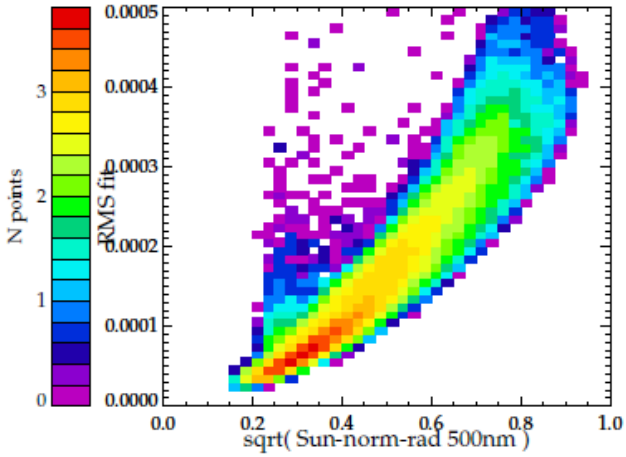

Figure 60: Relationship between the measurement noise (given as the square root of the sun normalised radiance at 500nm) and the RMS of the fit residual in the Chappuis bands.

Figures 9-16 show results for the other fit parameters. Patterns which might be expected on physical grounds are clearly present in most cases:

- O_4 is low over cloud and high altitude land surfaces (Figure 61).
- NO_2 is in very good agreement with the operational product. Features related to pollution are evident in the industrialised areas and a strong plume is observed over South Africa (Figure 61).
- Water vapour shows strong variability, is generally high in the tropics and low at the poles, is low over high cloud and high a latitude land (Figure 61).
- Ring effect is close to 1 over cloud free sea and may be particularly high on the East of the swath. It is generally much less than one over land, indicating that a large fraction of the photons are not Rayleigh scattered over land, as expected (Figure 62).
- The liquid water parameter (which is in arbitrary units here) is only significantly different from 0 over (cloud-free) sea or large lakes (Figure 62).
- The H_2O singular vector scale factors labelled h2o-ev0 and h2o-ev1 in plots generally correlate with the mean cross-section scale factor (Figure 62 and Figure 63).
- The scale factor for the gradient of the Ring scale factor across the fit window (labelled Ring-1) is low over cloud (where Ring itself in low) and significant over cloud free sea, indicating an expected variation in the relative proportion of Rayleigh scattering to the total signal across the relatively wide fit window (Figure 63).
- The second order term is quite noisy (it may not be necessary to fit it), but shows some across-track structure. The South Atlantic Anomaly is evident here (Figure 63).
- The wavelength shift of the water vapour cross section (dWL:H_2O, the unit in the plot is nm) shows structure correlated with water vapour itself (larger shift where there is more water vapour). The reason for this behaviour is not clear. On average the shift is of order -0.01nm (Figure 64).
- The solar/Earth mis-registration is of a similar magnitude, with no obvious geophysical dependency other than an along track variation from 0.01nm in the North to 0.015 nm in the South. 0.011nm at 500nm is expected because of the Doppler shift of the solar reference spectrum. Along-track dependence is not explained, but it is noted that in the Huggins bands, systematic residuals which have an amplitude which varies along the orbit have been identified in the RAL scheme (Figure 64).
- The 0th order polynomial coefficient (pol0, in natural log sun-normalised radiance units) reflects strongly cloud and surface albedo variations (Figure 64).

- The first order polynomial coefficient is strongly negative over cloud-fee sea and slightly positive over some desert regions, particularly the Sahara (Figure 65).
- The second order polynomial is small over sea, and largest over vegetated (cloud-free) land (Figure 65).
- The third order coefficient is strongest over cloud-free sea (representing the background Rayleigh reflectance) (Figure 65).
- The scale factors for the land reflectance singular vectors (land0-land6) show patterns which are not restricted to cloud-free land as might be expected. "land0" is clearly strongly related to vegetated land and "land1" to desert. However the weaker patterns are clearly used to explain spectral variations over the ocean and cloud as well as land. It is noted that if these patterns are not fitted or if fewer than 7 patterns are fitted, the quality of results degrades quite significantly over the sea or cloud as well as the land (Figure 66 and Figure 67).

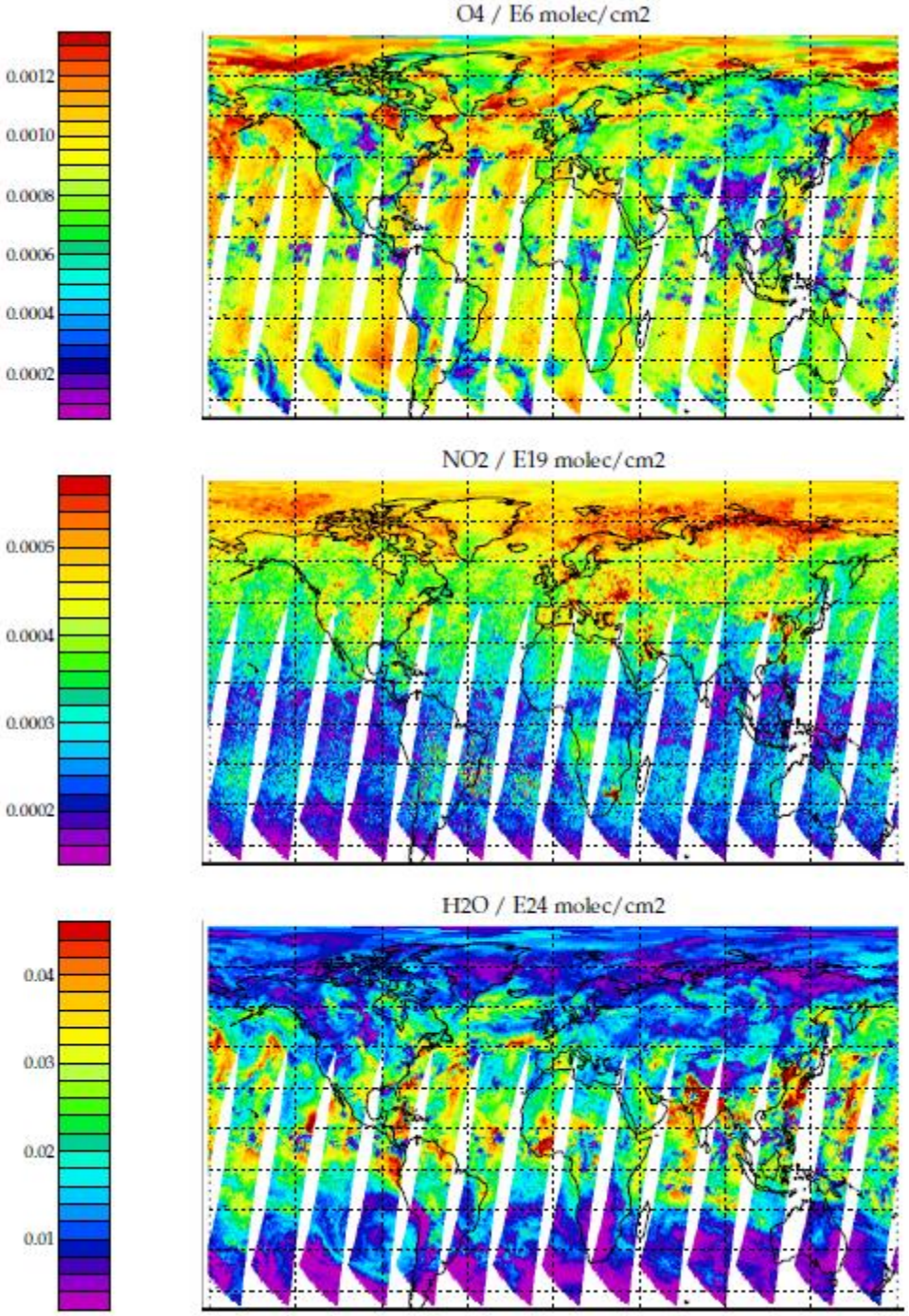

Figure 61: Retrieved fit parameters for column average concentration of O_4, NO_2 and H_2O

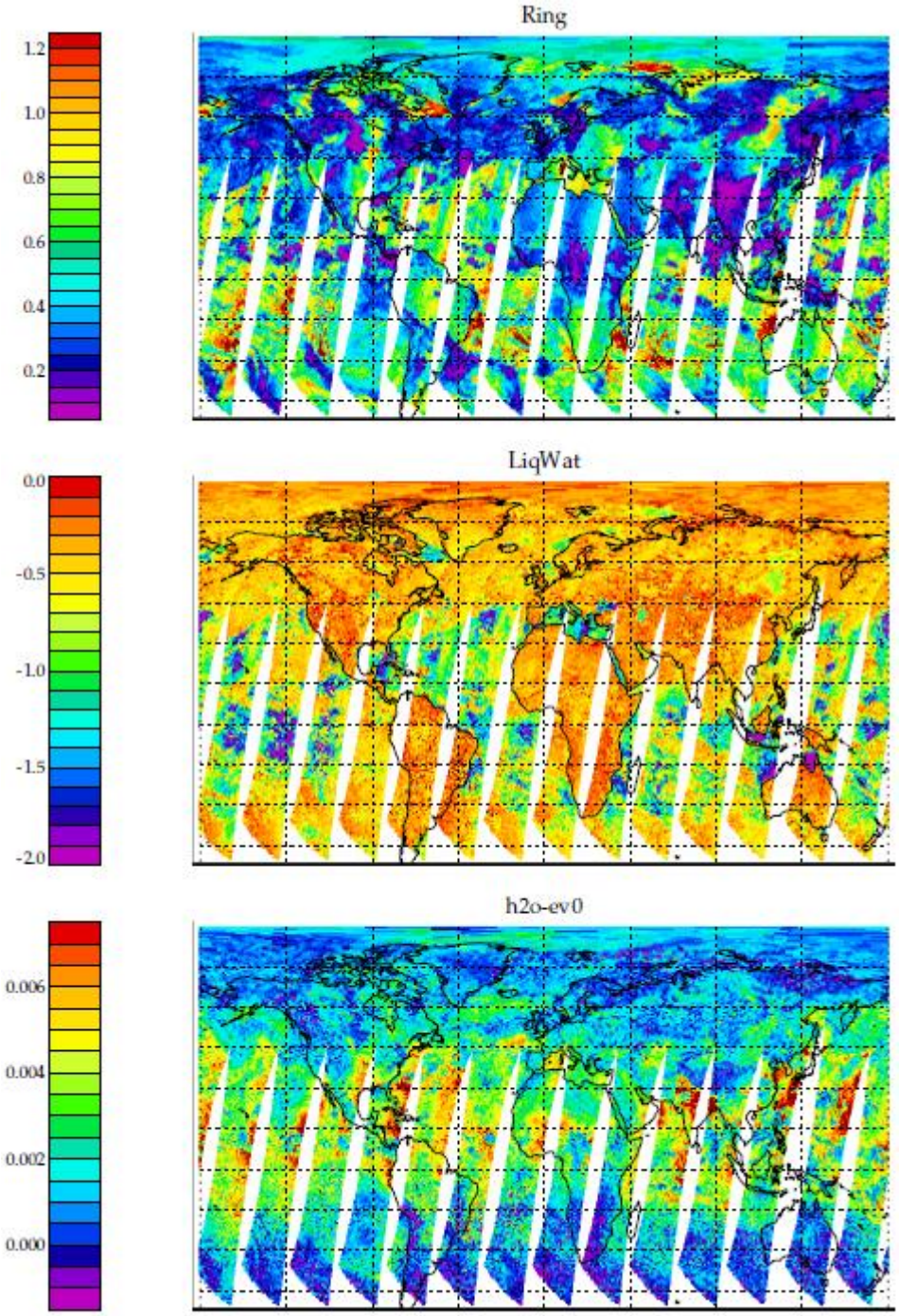

Figure 62: Retrieved fit parameters for the Ring effect, liquid water and the water vapour leading eigenvector

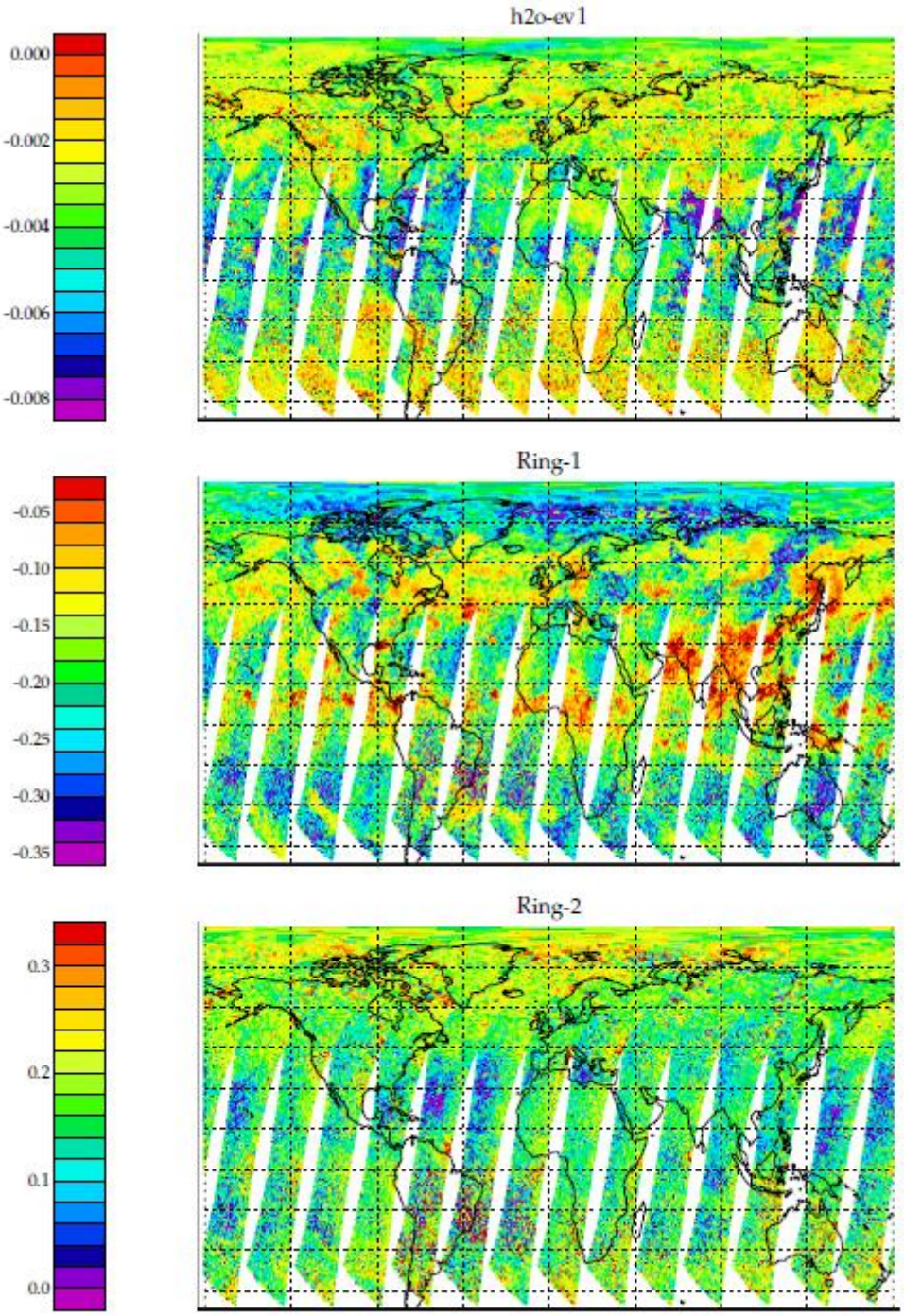

Figure 63: Retrieved fit parameters for second eigenvector for water vapour (top) and two Ring effect parameters (middle and bottom)

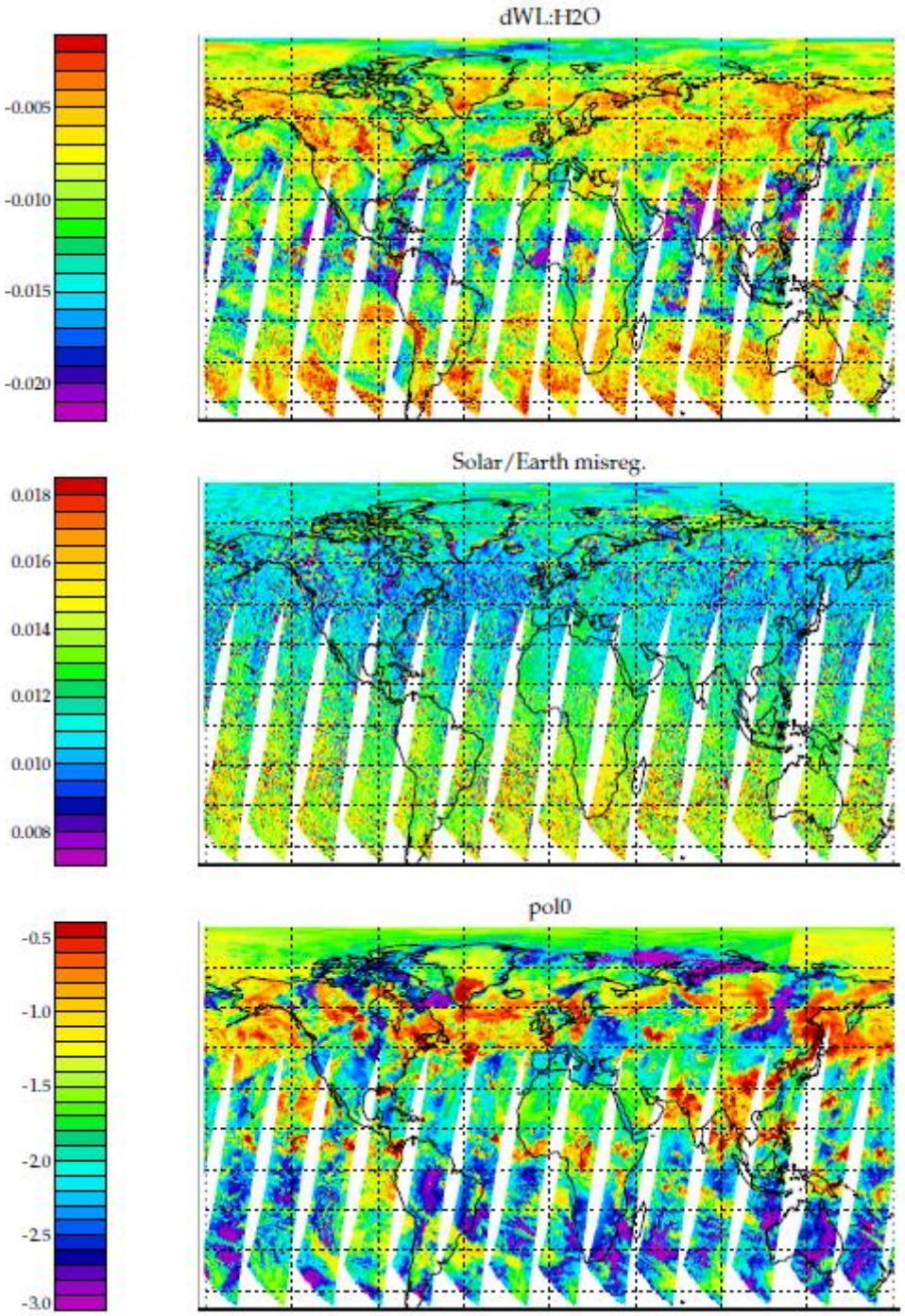

Figure 64: Retrieved fit parameters for a shift in the water vapour absorption cross section in nm (top), sun-earth mis-registration (middle) and first scattering parameter (bottom)

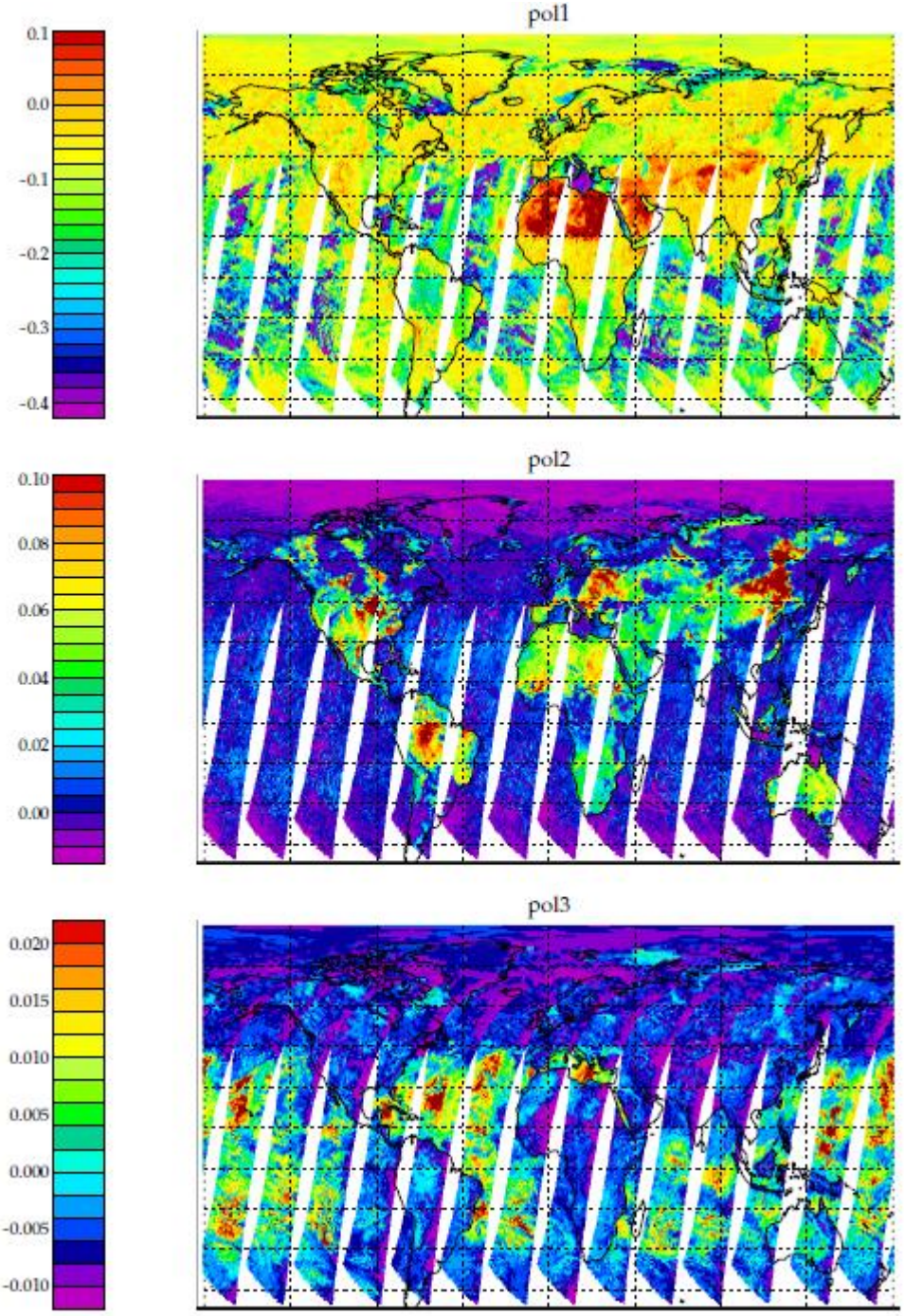

Figure 65: Three scaling factors for 3 further polynomials describing scattering processes (see text for details)

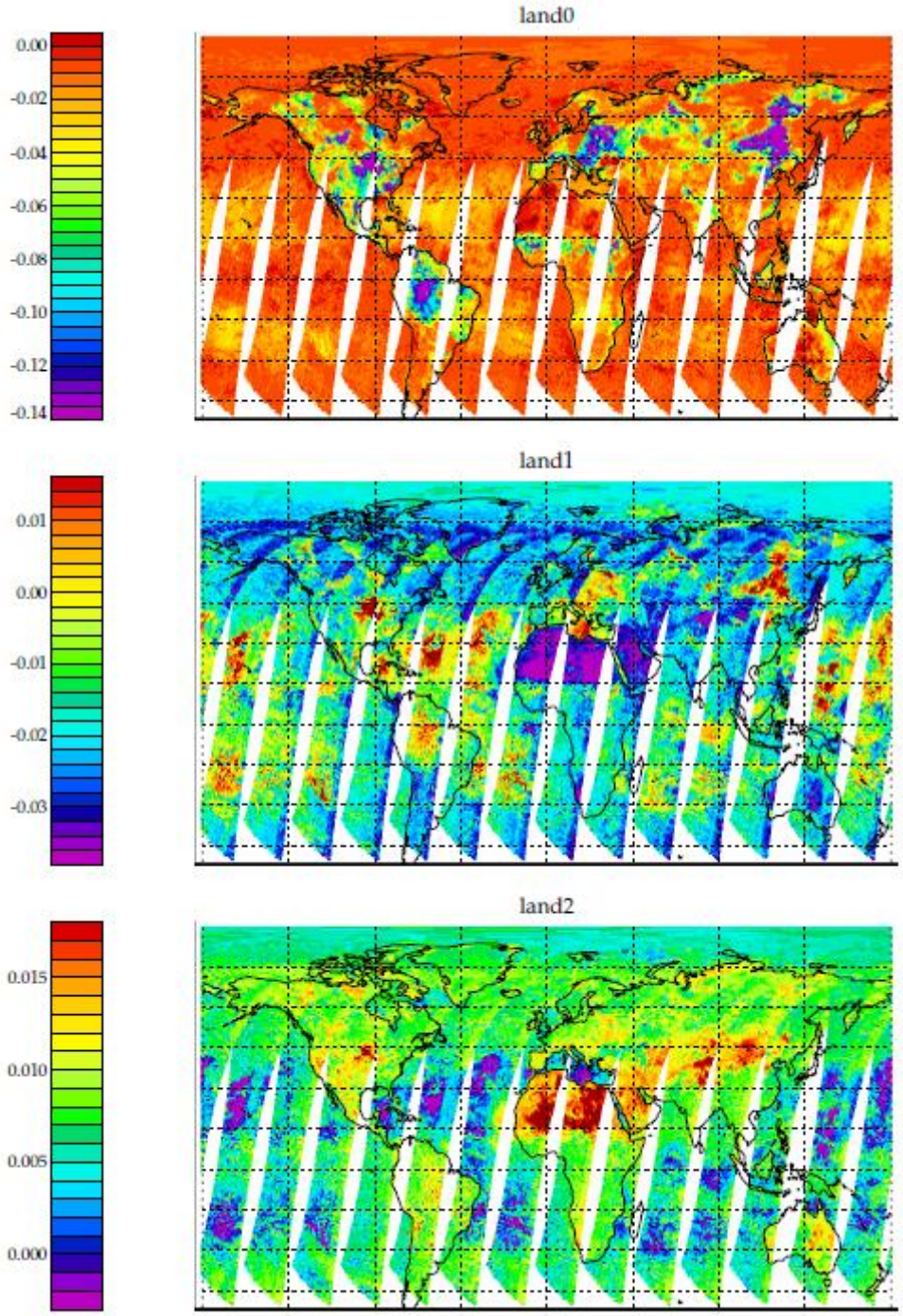

Figure 66: Retrieved scaling factors for the fit parameters for the first 3 land surface type eigenvectors

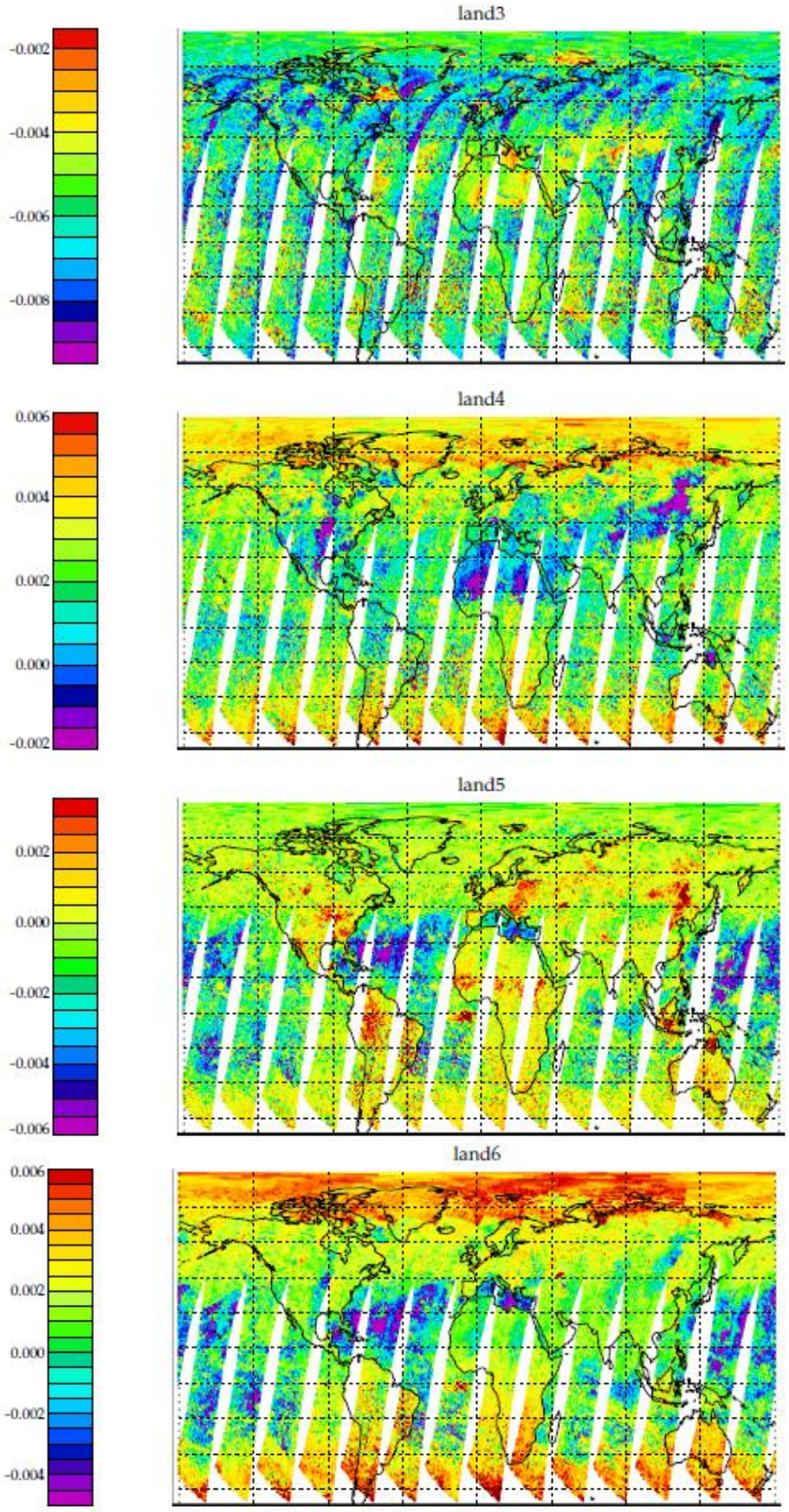

Figure 67: Retrieved scaling factors for the fit parameters for the last 4 land surface type eigenvectors

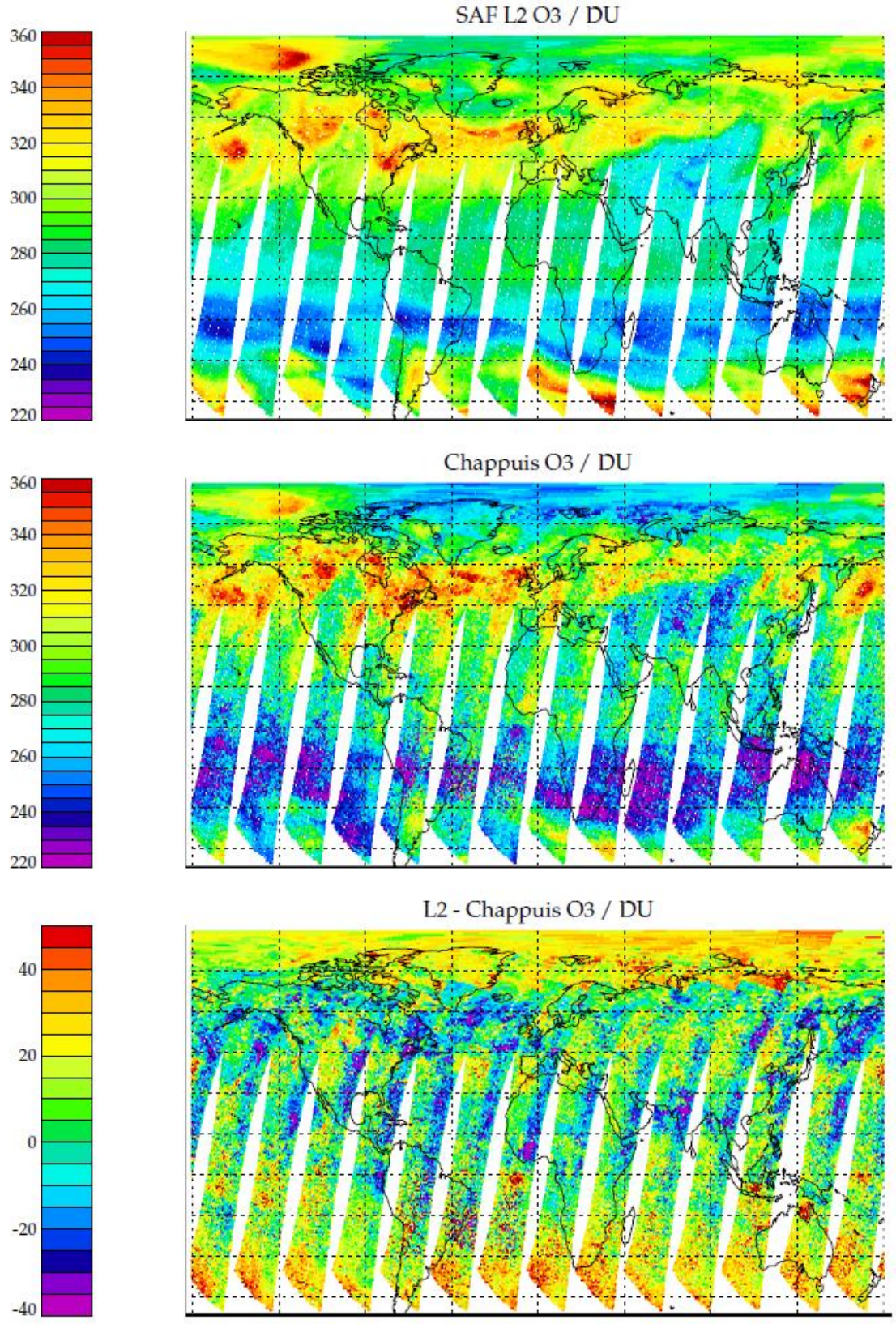

Figure 68: SAF GOME-2 Operational total column ozone product (top) in DU and total column retrieved using only GOME-2 measurements in the Chappuis band (middle) and the difference (bottom).

For comparison, the total column ozone and from the operational SAF product are shown in Figure 68. The bottom panel shows the differences between the SAF operational L2 column and the Chappuis result. Relatively large biases at latitude extremes may be caused by the use of a simple geometric air mass factor here. In mid-latitudes and tropics over land, systematic differences of order 20 DU exist over most of the swath. In the East, a stronger negative bias up to 30-40 DU is present. This across-track dependence is evident over both land and sea.

6.5 Conclusions

Retrieval simulations indicate that column measurements with a precision of 2-3 DU from the Chappuis bands would lead to substantial improvement in the tropospheric profile retrievals which are currently possible from the UV ozone bands. This capability would also clearly complement thermal infrared sounding techniques. In this short study we have attempted DOAS fitting of real GOME-2 spectra and reach results of similar quality to those reported by [Richter, 2012]. The fitting itself is very good, resulting in low RMS residuals (though not down to the noise limit at high reflectance) and produces physically highly plausible distributions of the trace gas and geophysical parameters which must be fitted together with ozone. The resulting ozone bears a good qualitative correspondence with the operational product (derived from the Huggins bands).

However differences of several 10s of DU exist with pronounced across track dependence. While discrepancies are expected for several reasons (ghost column, limitations of the geometric air-mass factor, different sensitivity to the lower troposphere), it is clear that most of this difference represents error in the Chappuis ozone.

An unsatisfactory feature of the current fits is that the singular vectors which are supposed to represent land surface reflectance structures are required to produce satisfactory results over sea and cloud. This indicates that spectral patterns exist over these surfaces which are not modelled satisfactorily. The extent to which these unknown patterns correlate with ozone (or other fitted species) is not accounted for and will lead to error.

While current retrievals are promising more work is required to bring the actual retrievals up to a quality which could enable the very significant information content of the Chappuis bands to be exploited.

6.6 Suggestions for further work

Further work is required to better understand the issues limiting the fit and which currently impact the retrieved ozone column.

Possible sources of relevant spectral features which are so far not considered include

- Ocean water Raman scattering. These could be straightforwardly modelled using known spectroscopic parameters.
- Instrument related spectral features, in particular related to polarisation.
- Relevant key-data spectra could be fitted (e.g. Eta).
- Spectral optical properties of ice and liquid cloud (though these are weak). It may be that the inclusion of ice and snow in the land-surface reflectance database partly explains the extent to which land vectors are fitted to cloudy scenes.

Given the ability of the scheme to fit the signatures associated with highly spectral dependent patterns, it may be better to fit at full resolution. A more sophisticated treatment of wavelength calibration would then be appropriate. This would entail calibrated solar irradiance by fitting to a reference spectrum, including adjustment of slit-function width, then fit shift / squeeze parameters to the reflectance spectrum alongside other parameters, as well as solar / earth spectrum wavelength mis-registration.

Progress could be perhaps be best made by focusing on retrievals over sea and cloud, without requiring the surface singular vectors to be fitted. While retrievals over land are needed for the Chappuis band to bring useful information in addition to the Huggins bands, it should simplify making progress on understanding factors limiting the fit to initially exclude issues related to land-surface reflectance.

The spectral reflectance of land surfaces should be studied by using the GOME-2 measurements themselves. This could involve statistically examining/comparing neighbouring scenes with different land surface types to identify spectral differences unique to land. A simple version of this approach was used in Richter 2012, but this could clearly be extended to derive a broader range of spectral features.

Once fit quality is improved to a point where columns are retrieved to a level of consistency with the operational column at the few Dobson Units, more consideration should be given to properly computing the air-mass factor and a test in which real retrievals are ingested into the UV profile scheme could be usefully carried out. These retrievals should then be verified against correlative data to test the improvement in the profiles brought by the Chappuis bands.

It is emphasised again that the information which could be obtained is essentially unique - no other passive technique can provide comparable information on near-surface ozone. Further work towards improving the current fit quality in this range would be extremely well justified.

7 References

Baldridge, A. M., S.J. Hook, C.I. Grove and G. Rivera. The ASTER Spectral Library Version 2.0. Remote Sensing of Environment, vol 113, pp. 711-715, 2009

Brion, J., Chakir, A., Daumont, D., and Malicet, J.: High-resolution laboratory absorption cross section of O3. Temperature effect, Chem. Phys. Lett., 213(5–6), 610–512, 1993.

Chance, K., Burrows, J et al., Satellite measurements of atmospheric ozone profiles, including tropospheric ozone, from ultraviolet/visible measurements in the nadir geometry: a potential method to retrieve tropospheric ozone, J. Quant. Spectrosc. Radiat. Transfer Vol. 51. No. 4, pp. 461476, 1997

Clark, R.N., Swayze, G.A., Wise, R., Livo, E., Hoefen, T., Kokaly, R., Sutley, S.J., USGS digital spectral library splib06a: U.S. Geological Survey, Digital Data Series 23, 2007

Daumont, M., Brion, J., Charbonnier, J., and Malicet, J.: Ozone UV spectroscopy I: Absorption cross-sections at room temperature, J. Atmos. Chem., 15, 145–155, 1992.

Henk Eskes, Peter van Velthoven, Pieter Valks and Hennie Kelder, Assimilation of GOME total ozone satellite observations in a three-dimensional tracer transport model, Q.J.R.Meteorol.Soc. 129, 1663, 2003

Kerridge, B.J. R. Siddans, B. Latter, I. Aben, C. Tanzi, W. Hartmann, J. P. Burrows, M Weber, R de Beek, V Rozanov, A Richter. GOME-2 Error Assessment Study, Phase V: Final Report, , EUMETSAT Contract EUM/CO/01/901/DK, April 2004

Malicet, C., Daumont, D., Charbonnier, J., Parisse, C., Chakir, A., and Brion, J. Ozone UV spectroscopy, II. Absorption cross-sections and temperature dependence, J. Atmos. Chem., 5 21, 263–273, 1995

McPeters, R. D., Lebow, G. J., and Logan, J. A.: Ozone climatological profiles for satellite retrieval algorithms, J. Geophys. Res., 112, D05308, doi:10.1029/2005JD006823, 2007

Meijer, Y. J., D.P.J. Swart, F.Baier, P.K.Bhartia, G.E.Bodeker, S.Casadio, K.Chance, F.Del Frate, T.Erbertseder, L.E.Flynn, S.Godin-Beekmann, G.Hansen, O.P.Hasekamp, A.Kaifel, H.M.Kelder, B.J.Kerridge, J-C. Lambert, J.Landgraf, B.Latter, X.Liu, I. S.McDermid, M.D.Müller, Y.Pachepsky, V.Rozanov, R.Siddans, S.Tellmann, R.J.van der A, R.F.van Oss, M. Weber, and C.Zehner. Evaluation of Global Ozone Monitoring Experiment (GOME) ozone profiles from nine different algorithms, *J. Geophys. Res.*, *111*, D21306, doi:10.1029/2005JD006778, 2006.

Mijling, B., O.N.E. Tuinder, R.F. van Oss en R.J. van der A, Improving ozone profile retrieval from spaceborne UV backscatter spectrometers using convergence behaviour diagnostics. Atmospheric Measurement Techniques, 2010, 3, 1555-1568, doi:10.5194/amt-3-1555-2010

Munro, R, R. Siddans, W.J. Reburn, B.J. Kerridge. Direct measurement of tropospheric ozone distributions from space. Nature, 1998, Vol.392, No.6672, pp.168-171

NASA. ASTER Spectral Library: http://speclib.jpl.nasa.gov
Reproduced from the ASTER Spectral library through the courtesy of the Jet Propulsion Laboratory, California Institute of Technology, Pasadena, California, © 1999, California Institute of Technology. ALL RIGHTS RESERVED.

Peet, J.C.A. van, R.J. van der A, A.T.J. de Laat, O.N.E. Tuinder, G. Koenig-Langlo en J. Wittig, Height resolved ozone hole structure as observed by the Global Ozone Monitoring Experiment-2. Geophys. Res. Lett., 36, doi:10.1029/2009GL038603. 2009

Pope, Robin .M and Fry, Edward.S. Absorption spectrum (380–700 nm) of pure water. II. Integrating cavity measurements. APPLIED OPTICS, Vol. 36, No. 33, 20 November 1997

N.A.D. Richards , S.R. Arnold, M.P. Chipperfield, G. Miles, A. Rap, R. Siddans, S.A. Monks, M.J. Hollaway. The Mediterranean summertime ozone maximum: A Satellite and model perspective ACPD, accepted 2012.

Richter, A., M. Begoin, A. Hilboll, and J. P. Burrows, An improved NO_2 retrieval for the GOME-2 satellite instrument. Atmos. Meas. Tech., 4, 1147–1159, 2011, www.atmos-meas-tech.net/4/1147/2011/doi:10.5194/amt-4-1147-2011

Richter, A., F. Wittrock, M. Weber, and J. P. Burrows. Evaluating the potential of GOME-2 ozone column retrievals in the Chappuis bands, EGU2012-1747 AS3.0 XY71, EGU Conference 2012.

Rodgers, C.D., Inverse Methods for Atmospheric Sounding, World Scientific, Series on Atmospheric Oceanic and Planetary Physics - Vol. 2, 2000.

Rozanov, V. V., D. Diebel, R. J. D. Spurr, and J. P. Burrows, GOMETRAN: A radiative transfer model for the satellite project GOME, the plane-parallel version, *J. Geophys. Res.*, *102*(D14), 16,683–16,695, doi:10.1029/96JD01535, 1997.

Siddans, R. Height Resolved Ozone Retrievals from the Global Ozone Monitoring Experiment, PhD Thesis, University of Reading, 2003.

Siddans, R, B.J.Kerridge, B.Latter, J.Smeets, G.Otter, S.Slijkhuis, Analysis of GOME-2 Slit-Function Measurements, EUMETSAT Contract. EUM/CO/04/1298/RM, Final Report, January 2006

Siddans, R., C Poulsen, B. Latter,A. Waterfall, B. Kerridge, S. Migliorini, A. Kaiser-Weiss, G. Bergametti, G. Foret, A. Ung. Study on the Exploitation of the SEVIRI IR 9.7µm Channel. Eumetsat Study Final Report, 2007

Veefkind, J.P (ed) CAMELOT Final Report, ESA Contract. 21533/07/NL/HE, RP-CAM-KNMI-050 Issue 1, 30 November 2009